

Electronic Theses and Dissertations, 2004-2019

2017

Development and Application of Microelectrodes to Study in situ Disinfectant Loss and Corrosion on Metal Surface

Xiangmeng Ma
University of Central Florida

 Part of the [Environmental Engineering Commons](#)
Find similar works at: <https://stars.library.ucf.edu/etd>
University of Central Florida Libraries <http://library.ucf.edu>

This Doctoral Dissertation (Open Access) is brought to you for free and open access by STARS. It has been accepted for inclusion in Electronic Theses and Dissertations, 2004-2019 by an authorized administrator of STARS. For more information, please contact STARS@ucf.edu.

STARS Citation

Ma, Xiangmeng, "Development and Application of Microelectrodes to Study in situ Disinfectant Loss and Corrosion on Metal Surface" (2017). *Electronic Theses and Dissertations, 2004-2019*. 6069.
<https://stars.library.ucf.edu/etd/6069>

DEVELOPMENT AND APPLICATION OF MICROELECTRODES TO STUDY IN SITU
DISINFECTANT LOSS AND CORROSION ON METAL SURFACE

by

XIANGMENG MA

B.S.Env.Sci., Shanghai Ocean University, 2010
M.S.Env.E., Michigan State University, 2013

A dissertation submitted in partial fulfillment of the requirements
for the degree of Doctor of Philosophy
in the Department of Civil, Environmental, and Construction Engineering
in the College of Engineering and Computer Science
at the University of Central Florida
Orlando, Florida

Fall

2017

Major Professor: Woo Hyoung Lee

©2017 Xiangmeng Ma

ABSTRACT

The primary objective of this research was to develop, fabricate, evaluate and utilize microelectrodes to metal coupons in artificial water system. In the brass experiment, it presented profiles of direct measurements of free chlorine/monochloramine, oxygen and pH to brass and cement based coupons. In monochloraminated water, brass showed a much faster corrosion process under observation. Profiles showed a less monochloramine consumption with as high as 7% greater oxygen utilization comparing to the brass in free chlorine solution, reflecting oxygen could be a major part of the corrosion initiation process. While cement showed less reactive characteristics to disinfectants and oxygen compared to the brass profiles, however, pH showed a significant rise for cement coupon under monochloramine condition. In galvanic experiment, the developed lead micro-ISE (100 μm tip diameter) showed excellent performance toward soluble lead (Pb^{2+}) with the sensitivity of $22.2 \pm 0.5 \text{ mV decade}^{-1}$ and limit of detection (LOD) of $1.22 \times 10^{-6} \text{ M}$ (0.25 mg L^{-1}). The response time was less than 10 seconds with a working pH range of 2.0 – 7.0. Using the lead micro-ISE, lead concentration microprofiles were measured from the bulk to the metal surface over time. Combined with two-dimensional (2D) pH map, this work clearly demonstrated that lead leaching at the metal surface is non-uniform and lower surface pH leads to higher lead leaching from the surface. Once significant pH variation (ΔpH : 6.0) was developed across brass-lead joint coupon, even a small pH change (ΔpH : 0.6) within the Pb/Sn alloy resulted in 4 times different surface lead concentrations ($42.93 \text{ vs. } 11.61 \text{ mg L}^{-1}$) and 5 times different fluxes ($18.5 \times 10^{-6} \text{ vs. } 3.5 \times 10^{-6} \text{ mg cm}^{-2} \text{ s}^{-1}$). Continuous surface lead leaching monitoring and surface characterization found that free chlorine is the primary contributor to lead leaching.

SUMMARY

Pipeline corrosion has been a critical issue for drinking water quality in United States. Corrosion in drinking water distribution systems (DWDS) can cause serious economic, environmental, and public safety problems from pipe damages, water loss, and water quality degradation. Many studies investigated and evaluated corrosion in DWDS with different pipeline materials under various aqueous conditions for decades. However, most of them focused on mainly bulk water monitoring using conventional water analytical methods and/or surface characterization of samples which were collected from real sites or simulated systems (e.g., pipe-loops) using electron microscopy and electrochemical techniques. Although surface characterization using atomic force microscopy (AFM) and Scanning electron microscope (SEM) can provide meaningful information, it is essentially a forensic investigation, not providing *in situ* dynamics of surface chemical reaction. Thus, it is required to develop and apply *in situ* analytical tools for better understanding of corrosion mechanism to mitigate and control effectively corrosion in DWDS.

The primary motivation of this research was to understand *in situ* dynamics of water chemistry at the interface between metal and water under various water conditions (e.g. free chlorine, monochloramine, pH, dissolved inorganic carbon, etc.) using a novel microelectrode technique. Microelectrodes have been widely used for biofilm and sediment studies; however, they were not applied for hard material due to their soft tip of the microelectrode (e.g. glass). A new technique was developed in this study and pseudo-surface chemistry (i.e. 5 μm above the metal surface) was successfully measured and the important kinetic parameters of the corrosion (e.g. flux and reaction rates) were quantitatively determined throughout the doctoral study. Various reactive

pipe materials including brass and cement, and lead-brass galvanic joints were tested and evaluated using microelectrodes in simulated DWDS.

First, brass and cement materials were tested for 120 days as representative pipe materials for DWDS to investigate the reactions of free chlorine and monochloramine at the surface of brass and cement coupons using different microelectrodes including free chlorine and monochloramine, dissolved oxygen (DO), pH and oxidation-reduction potential (ORP) microsensors. Total 4 sets of experiments were conducted on non-aged brass and cement coupons with different disinfectants (free chlorine vs. monochloramine) under two flow conditions (2 ml/min vs. stagnant) for 120 days. Bulk flowing solution contained 10 mg C L⁻¹ DIC, 100 mg Cl⁻ L⁻¹, 100 mg SO₄²⁻ L⁻¹, 2 mg Cl₂ L⁻¹ (free chlorine or monochloramine) at pH 7. Based on the measured chemical profiles, various kinetic parameters (i.e., diffusion boundary layer, flux, reaction rate, and surface concentration) were determined to provide a better understanding of relationship between disinfectant and pipe materials. At the initial stage (0 day), DO was consumed at the brass surface with both disinfectants and the oxygen reaction rate in a monochloramine solution was almost twice higher in free chlorine condition. However, free chlorine consumption (C_{surface} : 0.88 mg Cl₂ L⁻¹) was approximately three times greater than monochloramine (C_{surface} : 1.38 mg Cl₂ L⁻¹) at brass surface. After 120 days, brass coupons with both disinfectants were developed dark brown substances at the surface and disinfectants and oxygen consumption were increased at the brass surface compared to the initial stage. In cement coupons, results showed that disinfectants consumption were constant with approximately 1.5 mg Cl₂ L⁻¹ at the coupon surface with negligible oxygen consumption throughout the entire period, with slightly increased oxygen reaction (C_s : 7 mg O₂ L⁻¹) under the free chlorine condition. SEM/EDS analysis demonstrated that brass coupons in applied conditions have two distinguished area; one is filled with wavy fiber structured substances (high in zinc and

oxygen contents) at the brass coupon surface, and the other is crystal shaped structure (high in copper, oxygen and carbon contents).

As the application of microelectrodes to the metal/solid surface provided direct evidence of chemistry change at the coupon surface, galvanic joints were investigated to understand the relationship between pH and lead leaching in chlorinated water systems. During the period of the experiments, one of the major reflections on galvanic corrosion was the outbreak of Flint water crisis in Michigan due to the corrosion of lead contained pipelines. The lead concentration in household tap was found 200 times higher than the World Health Organization (WHO) standards. In the experiments, it was hypothesized that *in situ* concentration microprofiles of pH, DO, and free chlorine on different pipe materials would provide more understanding on the galvanic corrosion processes. pH microprofiles of corroding metal surfaces were measured to construct detailed *in situ* 2D spatial maps of the pH under flowing and stagnation conditions. The opposite pH trend was directly observed across the galvanic couple under flow and stagnation conditions. Water stagnation resulted in a pH at the anode (lead solder) of 1.5 pH units lower than the bulk water pH (9.0) and as much as 2.5 pH units lower than the cathode (brass). These conditions can enhance lead release at the anode, which reflects different anodic–cathodic relationships of coupled metals primarily controlled by water flow. Most importantly, this work has demonstrated the ability to make real pH measurement at the surface of corroding metals using a novel microelectrode approach. Further investigations on galvanic corrosion process was conducted based on multiple parameters changed conditions, such as different pH, chlorine concentration, and alkalinity. Multiple microelectrodes were applied to the direct measurements. Results found that Maximum pH variation of 7.5 unit ($\Delta\text{pH}=7.5$) between brass (pH 10.3) and solder surface (pH 2.8) was found at neutral condition with less than 8 hours of stagnation. The average pH variation

exceeded 4 pH unit under different stagnant conditions. However, under flow condition, especially with high pH (pH 9) or high alkalinity condition (50 mg C L^{-1}), the pH was more evenly distributed with their buffer pH. And no obvious surface oxygen ($< 0.3 \text{ mg L}^{-1}$) decrease was found. Data also showed that with addition of 3.0 mg P L^{-1} of orthophosphate as corrosion inhibitor, the pH diversity on coupon surface was greatly decreased under both flow and stagnant condition. Results were presented using 2D mapping technique in liquid-metal interfacial micro-environment. Also, surface characterization techniques were used to provide co-relation between water chemistry and coupon surface morphology.

In the final stage of galvanic corrosion experiments, a novel method using a micro-ion-selective electrode (micro-ISE) technique was developed for *in situ* lead monitoring at water-metal interface of a brass-leaded solder galvanic joint in a simulated chlorinated drinking water environment. The developed lead micro-ISE ($100 \text{ }\mu\text{m}$ tip diameter) showed excellent performance toward soluble lead (Pb^{2+}) with the sensitivity of $22.2 \pm 0.5 \text{ mV decade}^{-1}$ and limit of detection (LOD) of $1.22 \times 10^{-6} \text{ M}$ (0.25 mg L^{-1}). The response time was less than 10 seconds with a working pH range of 2.0–7.0. Using the lead micro-ISE, lead concentration microprofiles were measured from the bulk to the metal surface over time. Combined with two-dimensional (2D) pH mapping, this work clearly demonstrated that lead build-up across the lead anode surface was substantial, non-uniform, and dependent on local surface pH. A large pH gradient (ΔpH : 6.0) developed across the brass and leaded-tin solder joint coupon. Local pH decreases were observed above the leaded solder to a pH as low as 4.0 indicating it was anodic relative to the brass. The low pH above the leaded solder supported elevated lead levels where even small local pH differences of 0.6 (ΔpH : 0.6) resulted in four times different surface lead concentrations ($42.9 \text{ vs. } 11.6 \text{ mg L}^{-1}$) and five times different fluxes ($18.5 \times 10^{-6} \text{ vs. } 3.5 \times 10^{-6} \text{ mg cm}^{-2} \text{ s}^{-1}$).

Overall, the research addressed key technical challenges associated with understanding the metal corrosion at multiple analytical scales through the combined use of microelectrode techniques, microscopic observations, other surface characterization techniques, and kinetic modeling, confirming what others have previously speculated or indicated by alternate "macro" methods.

ACKNOWLEDGMENTS

First, I appreciate everything happened in the last four years of my Ph.D. program here at the University of Central Florida. Not only it helped my academic career, also it shaped my strong personality into someone I mean to be.

I feel deeply honored and grateful to have Dr. Woo Hyoung Lee as my advisor for the last four years. He showed me countless support, guidance, and being professional through my steps to become a qualified Ph.D. Along the way, I made millions of mistakes, and Dr. Lee's forgiveness ease me through the darkest time. This later gave me full confidence in research, especially towards the last year of my program. Dr. Lee also gave me great advices in manuscript preparation, which improved my writing and phrasing much better comparing when I just arrived school. I'm always chasing the high standards and excellency Dr. Lee has in his mind.

I express my thanks to all my committee members: Dr. Steven Duranceau, Dr. Anwar Sadmani, and Dr. Karin Chumbimuni-Torres. I'm grateful for them being on my committee and attend my defense. Their guidance and suggestions improve my thesis and future work.

I also would like to thank my research group and friends: Jared Church, Xiaochen Wang, Farris Munshi, and Dr. Hwang. They always show me their professional attitude and critical thinking along the way, which inspired me greatly, and their help in my research will be something I never forget.

Finally, I dedicate this work to my parents: Yinxian Sheng and Youjun Ma, and my girlfriend Jiaxun Wei. They showed me endless support and love, especially my girlfriend, countless travel between China and U.S. made this relationship special and unbreakable.

TABLE OF CONTENTS

LIST OF FIGURES	xiii
LIST OF TABLES	xviii
CHAPTER ONE: INTRODUCTION.....	1
1.1. Abiotic reaction in brass and cement materials.....	3
1.2. Galvanic corrosion mechanisms in brass-lead joints	4
CHAPTER 2: LITERATURE REVIEW	6
2.1. Brass in DWDS: surface chemical reaction and corrosion mechanisms	6
2.2. Copper in DWDS: surface chemical reaction and corrosion mechanisms.....	7
2.3. Cement in DWDS: surface chemical reaction and corrosion mechanisms	9
2.4. Brass–lead galvanic joints in plumbing systems: surface chemical reaction and corrosion mechanisms	10
CHAPTER 3: MICROELECTRODE-BASED TEMPORAL INVESTIGATION OF THE IMPACTS OF CHLORINE AND MONOCHLORAMINE ON BRASS AND CEMENT.....	14
3.1. Introduction	14
3.2. Materials and Methods.....	17
3.3. Results and Discussion.....	20
3.4. Conclusion.....	30
CHAPTER 4. IN-SITU 2D MAPS OF PH SHIFTS ACROSS BRASS-LEAD GALVANIC JOINTS USING MICROELECTRODES	31

4.1. Introduction	31
4.2. Materials and Methods	34
4.3. Results and Discussion.....	40
4.4. Conclusion.....	47
CHAPTER 5: THE AFFECT OF ALKALINITY, FLOW, AND BULK pH ON INTERFACIAL MICROENVIRONMENT OF BRASS-LEAD GALVANIC COUPONS IN SYNTHETIC DRINKING WATER.....	
	49
5.1. Introduction	49
5.2. Materials and Methods.....	52
5.3. Results and Discussion.....	56
CHAPTER 6: IN-SITU MONITORING OF Pb^{2+} LEACHING FROM THE GALVANIC JOINT SURFACE IN A SIMULATED CHLORINATED DRINKING WATER.....	
	69
6.1. Introduction	69
6.2. Materials and Methods.....	71
6.3. Results and Discussion.....	75
CHAPTER 7. SUMMARY.....	88
CHAPTER 8. FUTURE WORK	90
8.1. Phosphate sensor development.....	90
8.2. Chloride to sulfate mass ratio (CSMR) experiment.....	90

APPENDIX A: SOLUTION PREPARATION, MICROELECTRODES FABRICATION, AND CALCULATION	91
APPENDIX B: A SAMPLE CODE FOR PYTHON FIGURES.....	94
REFERENCES	100

LIST OF FIGURES

Figure 1: Pourbaix diagram for copper in sodium solution.	8
Figure 2. Operation setups & Microelectrode profiling setups.....	18
Figure 3. Horizontal view of coupons for multiple purposes.	19
Figure 4. Surface changes on brass coupons over 120 days through microscope observations. ...	21
Figure 5. Surface changes on cement coupons over 120 days through microscope observations	21
Figure 6. Long-term chemical profiles for brass coupon from day 0 to day 120 under flow and RMT conditions. (a) & (b) Free chlorine and oxygen profiles of brass in chlorinated condition; (c) & (d) Monochloramine and oxygen profiles of brass in chloraminated solution (pH 7, chlorine residuals 2 mg L ⁻¹ , oxygen 8.5 mg L ⁻¹).....	24
Figure 7. Long-term chemical profiles for cement coupon from day 0 to day 120 under flow and RMT conditions. (a) & (b) Free chlorine and oxygen profiles of cement coupon in chlorinated condition; (c) & (d) Monochloramine and oxygen profiles of cement coupon in chloraminated solution (pH 7, chlorine residuals 2 mg L ⁻¹ , oxygen 8.5 mg L ⁻¹).	25
Figure 8. Free chlorine (or monochloramine) and oxygen consumption with reactive surface for brass and cement coupons over 120 days. (a) free chlorine consumption and (b) oxygen consumption (FC: free chlorine, Mono: Monochloramine).....	26
Figure 9. High selective zinc leaching area and zinc compounds forming area SEM images and EDS results of brass coupon in free chlorine solution at day 60 and 120.	27
Figure 10. High selective zinc leaching area and zinc compounds forming area SEM images and EDS results of brass coupon in monochloramine solution at day 60.	27

Figure 11. Long-term SEM images of cement coupon in free chlorine and monochloramine solutions under flow and stagnant condition (500 times magnification).....	28
Figure 12. Weight losses of brass and cement in free chlorine and monochloramine under stagnation.....	29
Figure 13. Schematic diagram of the simulated water distribution system for aged brass and galvanic coupons preparation.	36
Figure 14. pH 2D contour mapping experimental setup. (a) microprofiling setup, (b) flow cell system for microelectrode profile measurements.	37
Figure 15. Optical microscopic images of brass coupons and galvanic coupon in a microprofiling flow cell. (a) 80 days aged brass coupon. (b) 200 days aged brass coupon. (c) 14 days aged brass-lead galvanic connection coupon.....	39
Figure 16. 2D pH contour map of 80 days aged brass coupon. (a) 2D map grid with scale, (b) with flow (2 ml/min). (c) under stagnation. The pH in the bulk solution was 9.0.....	40
Figure 17. 2D pH contour map of 200 days aged brass coupon. (a) 2D map grid with scale, (b) with flow (2 ml/min). (c) under stagnation. The pH in the bulk solution was 9.0.....	41
Figure 18. Measured representative 1D pH microprofiles of brass coupons. (a) pH microprofiles of 80 days aged brass coupon with and without flow. (b) pH microprofiles of 200 days aged brass coupon with and without flow. The pH in the bulk solution was 9.0. Two locations per one coupon (Figure 16) were measured and an average value with error bar was presented for each pH profile.....	41
Figure 19. 2D pH contour map of 14 days aged brass/lead solder joint coupon. (a) 2D map grid with scale for flow condition, (b) 2D map with flow (2 ml/min), (c) 2D map grid with scale for stagnant condition, and (d) 2D map under stagnation. The pH in the bulk solution was 9.0.	44

Figure 20. Measured representative 1D pH microprofiles of 14 days aged brass/lead solder joint coupon. (a) pH microprofiles under flow condition (2 ml/min) and (b) pH microprofiles under stagnation. The pH in the bulk solution was 9.0..... 45

Figure 21. Galvanic joint coupons and microprofiling. (a) Vertical view of an epoxy specimen mounted galvanic joint coupon with scale specification, (b) Smoothness of the coupon by horizontal view, and (c) In-situ pH microprofiling near the coupon surface (100 μm from the surface) using microelectrodes. 53

Figure 22. 2D mapping of pH on galvanic coupons surface under different flow, DIC, and free chlorine concentration (pH 7, 100 mg Cl⁻ L⁻¹, 100 mg SO₄²⁻ L⁻¹)..... 56

Figure 23. 2D mapping of free chlorine concentration on galvanic coupons surface under different flow, DIC, and free chlorine concentration (pH 7, 100 mg Cl⁻ L⁻¹, 100 mg SO₄²⁻ L⁻¹). 57

Figure 24. 2D mapping of pH on galvanic coupons surface under different flow, DIC, and free chlorine concentration (pH 9, 100 mg Cl⁻ L⁻¹, 100 mg SO₄²⁻ L⁻¹). 58

Figure 25. 2D mapping of free chlorine concentration on galvanic coupons surface under different flow, DIC, and free chlorine concentration (pH 9, 100 mg Cl⁻ L⁻¹, 100 mg SO₄²⁻ L⁻¹). 59

Figure 26. 2D pH mapping of (a) consecutive stagnation after initial flow condition vs. (b) stagnation without flow under pH 7, free chlorine 2 mg Cl₂ L⁻¹, and DIC 10 mg C L⁻¹. 63

Figure 27. Surface characterization of galvanized coupon (after two hours of flow under pH 7, free chlorine 2 mg Cl₂ L⁻¹, and DIC 10 mg C L⁻¹, 100 mg Cl⁻ L⁻¹, 100 mg SO₄²⁻ L⁻¹). (a) Observation of corroded coupon and location for surface characterization; (b) SEM image of the selected location with magnification (×22); (c) Backscattered electrons (BSE) image of location with magnification (×22); (d) Magnification (×100) of BSE image of selected location in Figure 7c; (e) and element distribution using EDS. 65

Figure 28. Cross-sectional 2D mapping view of pH profiles under stagnation (pH 9, free chlorine 2 mg Cl ₂ L ⁻¹ , DIC 50 mg C L ⁻¹), with comparison among commercialized pH sensor tip size and this research pH tip size.	66
Figure 29. A finished Pb ²⁺ micro-ISE with a tip size of 100 μm and membrane length of 200 μm. (nickel for scale).	72
Figure 30. A specifically designed brass-lead galvanic coupon (2×1 cm) imbedded using a cold epoxy specimen mounting technique.	73
Figure 31. (a) 2D map grid (total 96 points: 8×12) with scale on the brass-lead galvanic coupon (2×1 cm) and (b) a schematic of microprofiling using a Pb ²⁺ micro-ISE in a flow cell.	74
Figure 32. Calibration curves of a developed Pb micro-ISE with different Pb ²⁺ concentrations. Pb(NO ₃) ₂ was used for preparing Pb standard solutions and NaNO ₃ was used for testing ion interference (pH 4.8, 23 °C). The lead concentrations in the x-axis are the measured lead concentration by AAS.	76
Figure 33. (a) pC-pH diagram simulated using MINEQL software and (b) measured data using a Pb ²⁺ micro-ISE. 10 ⁻⁵ M Pb ²⁺ in DI water was used for both the simulation and the experiment.	77
Figure 34. (a) In situ Pb ²⁺ concentration microprofiling of a lead-brass galvanic joint coupon with three profiling locations, (b) Pb ²⁺ concentration and pH microprofiles on location 1 and location 3 after 1 hour of stagnation, and (c) Pb ²⁺ concentration microprofiles on location 1 and 2 after 2 hours of stagnation (pH 7, 23 °C, 2.0 mg Cl ₂ L ⁻¹ , 100 mg Cl ⁻ L ⁻¹ , 100 mg SO ₄ ²⁻ L ⁻¹ , and DIC 10 mg C L ⁻¹).	78
Figure 35. 2D mapping of pH on the galvanic coupon surface (50 μm above the surface) under stagnation (pH 7, 23 °C, stagnation, free chlorine 2 mg L ⁻¹ , 100 mg L ⁻¹ of Cl ⁻ and SO ₄ ²⁻ , and DIC 10 mg C L ⁻¹).	81

Figure 36. Continuous real-time monitoring of Pb^{2+} leaching from the lead surface (50 μm above the surface) and comparison of Pb^{2+} concentrations between lead joint surface and bulk. Another spike of a feed solution after 15 hours was performed (pH 7, 23 °C, stagnation, free chlorine 2 $mg L^{-1}$, 100 $mg L^{-1}$ of Cl^{-} and SO_4^{2-} , and DIC 10 $mg C L^{-1}$). 83

Figure 37. Metal surface characterization using Raman spectroscopy. (a) Optical images of (left) the part and (right) the brass, lead joint and region made of white deposit characterized with Raman spectroscopy. (b) Average Raman spectra obtained in each region described in (a) with bands corresponding to Pb_3O_4 (125 cm^{-1}), PbO (185 cm^{-1}), $PbCO_3$ (230 cm^{-1}), SO_4^{2-} (980 cm^{-1}) and CO_3^{-} (1050 cm^{-1}). 84

Figure 38. Spatio-temporal microprofiling of in situ Pb^{2+} measurements at the brass-lead galvanic coupon surface (pH 7, 23 °C, 2.0 $mg Cl_2 L^{-1}$, 100 $mg Cl^{-} L^{-1}$, 100 $mg SO_4^{2-} L^{-1}$, and DIC 10 $mg C L^{-1}$). 85

Figure 39. Experiment setups for microprofile system..... 93

LIST OF TABLES

Table 1. Summary of Pb detecting main methods in drinking water.....	12
Table 2. Experiment operating conditions for microelectrode profiles.	18
Table 3. Galvanic series of selected metals and alloys and standard electrode potential (electromotive force series).....	32
Table 4. Summary of the surface pH changes on brass coupons and a galvanic solder coupon. .	42
Table 5. Experimental conditions for microprofiling and 2D mapping of galvanic joint coupons in synthetic drinking water.....	53
Table 6. Pb ²⁺ concentration comparison between AAS method and Pb ²⁺ micro-ISE method	76
Table 7. Quantification of Pb leaching from microprofiles after 1 hr and 2 hrs.....	85
Table 8. Monitoring of Pb ²⁺ concentration, pH, and free chlorine concentration in the experimental solution over 24 hours.....	86

CHAPTER ONE: INTRODUCTION

This research was focused on the fundamental mechanisms at the early stages of corrosion on the surface of different metal pipe materials, via *in-situ* investigations of water chemistry changes using microelectrodes in simulated drinking water distribution systems. The metal corrosion symptoms may include a localized corrosion in the presence of water disinfectants (e.g., free chlorine and chloramines). Copper, brass, ductile iron, cements and galvanic joints are typical common pipe materials used for drinking water distribution systems. This research addressed the key technical challenges associated with understanding the metal corrosion at multiple time length scales through the combined use of microelectrode techniques, microscopic observations, and kinetic modeling.

The need to understand, assess, and reduce corrosion in drinking water is more urgent than ever due to the aging drinking water pipeline system around the country at the moment. Corrosion is a major cause of failure in water, oil, and energy infrastructure throughout the world, causing billions of dollars in losses annually. Particularly, corrosion and degradation of drinking water plumbing materials significantly deteriorates drinking water quality and causes a failure to supply safe water to the public. As a result of the Lead and Copper Rule,¹ many water utilities in the U.S. have evaluated corrosion control strategies. A better understanding of the fundamental mechanisms contributing to the rates and magnitude of corrosion at the surface of pipe materials can lead to improved corrosion control strategies, reduction of the costs for distribution system maintenance and conservation of drinking water quality. Although new drinking water utilities and households now use polyvinyl chloride (PVC) or concrete-lined pipes, cast or ductile iron pipes are still 56.6 % based on the recent pipe inventory survey. PVC and polyethylene pipe are 17.7 %

of the pipe inventory survey . For the customer service line, about 56.3% of materials are copper pipes and 8% are galvanized line.^{2, 3} Among the most common causes of main breaks, internal corrosion contributed to 25%, leading to pipe leaks and water quality changes.⁴ In the early stage of my research, brass and cement were used as two representative reactive pipe materials which are susceptible to corrosion in drinking water distribution systems. Brass-lead joints were used as a representative galvanic joint which can be found in household plumbing systems in the following stage experiment. Although corrosion has been studied intensively and conceptual theories on the surface chemistry of corroding metals are available, actual measurements of chemical profiles that permit correlation between water chemistry and corroding metals at water-metal interfaces have not been made, limiting our fundamental understanding of corrosion mechanisms in microenvironments. Majority of existing studies focused on macroscopic investigation of the corroding materials and the knowledge gained is thus often case-specific and non-transferrable. Nano/microscale understanding of the fundamental mechanisms contributing to the rates and magnitude of corrosion at the surface of pipe materials can induce and enable unprecedented improvements in the prevention and mitigation of metal corrosion in drinking water environments, reduction of the costs for distribution system maintenance and conservation of drinking water quality. The utilization of microelectrode to quantify chemical changes can greatly improve the fundamental understanding of water chemistry at the metal surface level.

The main objective of my research is to measure various chemical profiles directly using microelectrodes to investigate *in-situ* chemical reactions on the surface of metals used in drinking water distribution systems. The chemical profiles to be measured in this research include free chlorine (or monochloramine), DO (DO) concentrations, pH, and oxidation-reduction potential (ORP) microprofiles. The specific objectives are 1) to evaluate the disinfectant loss and evaluate

corrosion mechanisms of brass and cement materials, 2) to investigate corrosion across the surface of brass-lead galvanic joints in a micro-environment, 3) to extend chemical constituents effect on the galvanic corrosion with higher dose of dissolved inorganic carbon (DIC) and free chlorine concentration, and 4) the development of lead microelectrode for quantification of galvanic corrosion study.

1.1. Abiotic reaction in brass and cement materials

Corrosion in drinking water distribution systems (DWDS) can cause serious economic, environmental, and public safety problems from pipe damages, water loss, and water quality degradation. Over the past decades, corrosion mechanisms have been studied by monitoring bulk water quality changes and performing forensic studies of pipe-loops like surface characterization using electron microscopy.⁵⁻⁹ Even though metal surface chemistry has been analyzed using atomic force microscopy (AFM) and scanning electron microscope (SEM) characterization, the samples need to be scarified and further analysis (or temporal analysis) is not possible. *In-situ* liquid-solid water chemistry dynamics between chlorinated (or chloraminated) water and pipe materials over time has rarely been studied due to the limitation of techniques. The approach presented here is to provide a better understanding of the reactions of free chlorine (or chloramines) at the surface of brass and cement by applying microelectrodes to measure *in-situ* free chlorine (or monochloramine), DO concentration, pH and oxidation-reduction potential (ORP or redox) microprofiles from bulk water to the proximity of material surface (e.g., 50 μm above the surface). The obtained chemical profiles were interpreted to determine kinetic parameters and cross-evaluated with SEM/EDS results, which can provide detail information on micro-scale corrosion process and diffusion-reaction kinetics of reactive pipe materials with chlorine (or chloramines)

and oxygen. The use of microelectrode techniques for investigating the *in-situ* reaction elucidate related corrosion mechanisms is the main novelty of this research.

1.2. Galvanic corrosion mechanisms in brass-lead joints

One form of corrosion, galvanic corrosion, results when two dissimilar metals are in electrical contact in water where one of the metals corrodes preferentially to the other. The impact of galvanic corrosion is an important issue that affects the quality of potable water by releasing metals of concern. Lead (Pb) solder has been widely used as a galvanic joint for connecting home plumbing materials such as brass and iron. It accelerates the process of lead-containing particles releasing to the potable water with probable cause of construction disturbances or destabilization of corrosion byproducts at the galvanic connection with other new metal materials. Therefore, these joints have often caused the level of lead in aged drinking water service lines to reach regulatory noncompliance. In 1991, the LCR was released by the U.S. Environmental Protection Agency (EPA) which required a lead action level lower than $15 \mu\text{g L}^{-1}$ and partial replacement of utility-owned lead service lines. However, the replacement of some lead service lines has been suspended for various reasons (e.g., high lead level in children's blood found in DC area).¹⁰ The recent Flint water crisis brought national attention to the problem of lead leaching from aging pipes into the water supply. The average of lead concentration in the initial victim's house is over $2,000 \mu\text{g L}^{-1}$, 200 times more than the WHO standards ($10 \mu\text{g L}^{-1}$ for adults) over 20 minutes of water usage.¹¹ Studies have shown the main problem in Flint drinking water incident is the classic "red water" and extremely high lead concentration, which can be induced by the changing of water source and aged pipeline system¹² and also have shown that corrosive water sources and a lack of corrosion inhibitors in distribution systems may be the main causes.¹³

The issue for the Pb leaching in drinking water is mainly occurred during the water transportation and household plumbing stages due to galvanic/general corrosion on lead material, including lead pipes, tin coating, lead solder joints and fittings ¹⁴. In the case of water transportation pipeline perspective, before the Safe Drinking Water Act established in 1986, lead pipelines were used as a common drinking water transporting material, and according to Rosario-Ortiz et al., 22% of the pipelines in US are over 50 years old, which exceeds the average pipe failure age (47) ¹⁵. Although, Pb service line replacement was applied, studies showed that situations with partial Pb service line replacement could stimulate the Pb leaching in the drinking water ¹⁶⁻¹⁸. Also, upstream pipeline corrosion not only can affect the water quality of the specific area, with scales detachment, it can affect downstream and even household water quality as well due to the deposit corrosion ¹⁹. Due to various reasons (pH, disinfectant, alkalinity, etc.), galvanic corrosion can lead to household pipeline leaks and lead leaching. This urges progress in Pb monitoring and control in drinking water system.

Many studies regarding to galvanic interactions with water chemistry changes have been conducted with bulk monitoring and microscopic investigations, the corrosion mechanisms are still unclear. Detail research on chemistry changes between water-metal surfaces have not been done in the galvanic corrosion initiation. In this study, a microelectrode system was applied to investigate *in-situ* chemical reaction between bulk water and metal surface with high spatial and temporal resolutions. Various *in-situ* two-dimensional (2D) spatial images (e.g., pH, DO, and free chlorine concentration distribution) across metal surfaces including galvanic corrosion will be constructed along with 1D chemical profile measurements and SEM and Energy Dispersive X-ray Spectroscopy (EDS) surface characterization.

CHAPTER 2: LITERATURE REVIEW

2.1. Brass in DWDS: surface chemical reaction and corrosion mechanisms

In drinking water distribution system, brass as a copper-zinc alloy has been widely as tap valves, heating components, various fittings, and other fixtures.²⁰ Even though the addition of zinc and other impurities, such as aluminum, silica, iron, lead and tin, greatly increased the resistance of corrosion for brass in drinking water, corrosion still occurs over time in different water environment.²¹ Previous studies have showed fundamental knowledge of brass corrosion mechanisms in drinking water. The main mechanisms of brass corrosion are due to dezincification and passive film formation. In dezincification process, it characterized by dealloying zinc from the brass material can result in pipe leakage, fitting failures and pitting problems.²² During the dezincification process, at the anode end, zinc was oxidized to zinc ions with cathode reaction of oxygen or other oxidants in the water gaining electrons.²³ While passive film formation at the brass surface normally coupled with copper oxidation at the brass surface as an electron donor, and oxygen or chlorine species as electron acceptors. The key possible electrochemical half reactions related to dezincification mainly are listed below (1-5) ²³:



Dezincification process with leaching of lead can create a low pH environment for the pipeline surface, where localized pitting can be formed.²³ However, at higher pH water environment, according to literature review, a white particulate film (or block named “meringue”)

can be formed on brass surface.²⁴ The formation of meringue is mainly due to the low zinc solubility with the production of zinc carbonate and causing blocking problems in brass fittings in the plumbing system.²³

2.2. Copper in DWDS: surface chemical reaction and corrosion mechanisms

Copper corrosion is the result of the loss of solid copper metal to solution. This occurs when electrons are lost by the base metal, and the solid phase is transformed into soluble, dissolved cuprous (Cu^+) and/or cupric (Cu^{2+}) ions. During metal corrosion in drinking water, chemical oxidation occurs at anodes where electrons are released and alternately chemical reduction (the gain of the electrons) occurs at cathodes.²⁵ In relatively new plumbing system, pure copper on pipe walls are exposed to the water environment and can be easily oxidized to cupric hydroxide ($\text{Cu}(\text{OH})_2$) which maintains high levels of soluble copper in potable water^{26, 27} and in cases can contribute to human stomach problems from ingesting elevated soluble copper.²⁸ For this reason, copper concentrations in drinking water are regulated by the USEPA LCR (USEPA, 1991) with action level at 1.3 mg L^{-1} . For example, according to a copper Pourbaix diagram presented in Figure 1,²⁹ in saturated water without chlorine residual (or other oxidants) copper will spontaneously react with DO and form cupric ion according to the following balanced redox reaction (1)³⁰:



Localized, or pitting, corrosion is a major cause of household copper drinking water pipe failure and, as a result, the subject of many studies on the relationship between pitting corrosion and water quality.²⁵ Pitting corrosion describes the case where corrosion is localized and copper metal is lost at small, fixed anode points. Eventually, this attack penetrates the pipe wall. The

relatively large surrounding surface of the pipe surface serves as the cathode. Since the electron acceptors in drinking water are chlorine (or other disinfectant residual) and/or oxygen, the rate of corrosion is sensitive to the concentrations of both of these oxidizing agents. Pitting corrosion on the surface of copper pipes is a very complex phenomenon that involves many initiating factors including pH, temperature, oxygen, alkalinity, chloride, sulfate, phosphate, and organic matter, also operating conditions as stagnation time and pipe age.²⁵

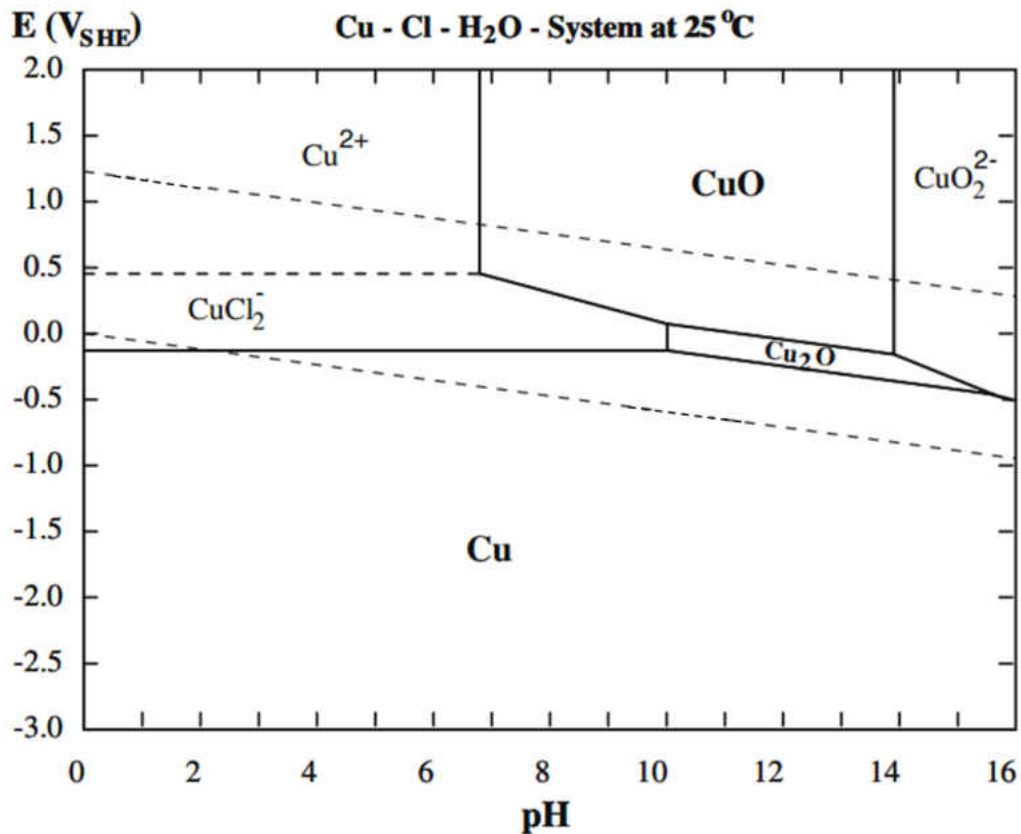


Figure 1: Pourbaix diagram for copper in sodium solution.

Copper pitting is normally considered as a two-step process including an initiation and a propagation process. The initiation process is not well understood, but is considered greatly depending on physical and chemical parameters, such as pH and oxygen.^{23, 31} However, for the

propagation process, it is generally believed to be proceeded with cathodic and anodic reactions in the presence of oxygen and free chlorine (2-4):



In the anodic area of the copper pipe, the pit water pH becomes extremely low due to the Lewis acidity of released cupric ions, and in some cases the acidic environment will promote the corrosion of pit.²³

2.3. Cement in DWDS: surface chemical reaction and corrosion mechanisms

Cement/concrete pipeline is mainly used in the drinking water transportation process as another important material.³² In field practice, newly installed ductile iron pipelines is typically lined with cement-mortar to protect iron materials from corrosion process.³³ Cement (primarily Portland cement) contains calcium silicates, calcium aluminate, iron calcium aluminate, and gypsum, which can harden the cement through multiple reactions. While most drinking water corrosion studies focused on the metal corrosion, little research has been done on the cement materials. However, the degradation of cement material can greatly affect the quality of drinking water downstream and promoting the corrosion in the pipeline system.³² During the water transportation stage, if the water in the cement pipeline has low pH and low alkalinity, it could promotes the dissolution of the cement material, which directly affect the integrity of the cement pipeline; when the water in the cement pipeline has relatively high pH and high alkalinity, it could lead to the aggregation of the cement material, which could lead to large scales formed at the

materials surface leading to pipeline blocking.^{33, 34} Furthermore, the corrosion process of the cement material can indirectly affect other chemical reactions, such as copper corrosion and lead leaching.³² These research results helped greatly to understand the fundamental knowledge of cement material behavior in drinking water systems.³⁵⁻³⁷ In the study of cement material for my research, it mainly focused on the investigation on the chemical profiles at the cement surface, which showed both great novelty and direct evidence for chemical reactions compared to the conventional experiments (weight change and surface characterization). This laid importance foundation for general corrosion studies, and the effect of the results can be further interpreted for other material studies.

2.4. Brass–lead galvanic joints in plumbing systems: surface chemical reaction and corrosion mechanisms

Galvanic corrosion has been a major issue in drinking water quality for the last decade. The general concept of galvanic corrosion is when two dissimilar metals are in electrical contact in water where one of the metals corrodes preferentially to the other. It can result in the metal concentration elevation the consumer's drinking water. In my research, experiments were focused on lead leaching from the galvanic corrosion process. Lead (Pb) in drinking water can cause various health problems, such as kidney failure and damage to nervous systems, especially among children. Even though risks due to Pb exposure have been widely studied for many years, outbreaks of Pb in drinking water remain to be a serious issue over the last decade, such as Washington and Flint water crisis³⁸⁻⁴⁰. According to EPA reports, over 2000 water utilities across the control have exceeds the Pb MCLs ($15 \mu\text{g L}^{-1}$) over the past four years, and Florida is among the most contaminated states⁴¹.

Aside from the pure lead pipeline installed before 1986, lead was mainly leached from lead service lines and leaded solder joints, which can be accelerated by the galvanic connection with other metal materials,⁴²⁻⁴⁴ where lead (Pb) serves as an anode (location of oxidation) and lead ions (Pb²⁺) are released and the cathodic metal (brass) protected from a galvanic reaction (10-11).⁴⁵



Although general theories regarding galvanic interactions leading to lead release have been described, and experimental and microscopic support has been reported,⁴²⁻⁴⁵ detail *in-situ* water quality measurements at the surface of galvanic connections have not been performed. Specifically, no direct measurements of water-metal interface chemistry on a micro-scale environment have been conducted, and thus a practical link between bulk water chemistry and the metal surface dynamics has not been well established. Therefore, an obvious need to better understand the surface chemical dynamics of galvanic couples leading to enhanced metal release is apparent. Conventional analytical approaches of Pb detection normally involves with expensive or high demanding methods, including inductively coupled plasma-atomic emission spectroscopy (ICP-AES), inductively coupled plasma-mass spectrometry (ICP-MS), continuous flow-cold vapor-atomic absorption spectrometry (CV-AAS), and total carbon and total sulfur by combustion¹⁹. In last decade, numerous scientists have reported innovation methods for *in-situ* and *ex-situ* Pb monitoring (Table 1). As for industries and family, samples are normally collected and send it to the lab for analysis.

Table 1. Summary of Pb detecting main methods in drinking water

Methods	Detection limit	Materials	Limitation	Reference
Colorimetric	3 nM (0.625 ppb)	Gold nanoparticles and DNAzyme	pH adjustment required (Acidic)	46
Selective catalytic DNA biosensor	10 nM (1.3 ppb)	Deoxyribozyme based	Fluorescence quenching	47
Stripping voltammetry	Varies from 0.3 ppb – 12 ppb	Bismuth, carbon, gold, antimony, boehmite@SiO ₂ /Fe ₃ O ₄ , and boron-doped diamond	Long accumulation time, toxic chemical release	48, 49
Dispersive liquid–liquid microextraction (DLLME) and flame atomic absorption spectrometry (FAAS)	0.5 ppb	Diethyldithiophosphoric acid (DDTP), carbon tetrachloride and methanol	Special equipment required	50
Potentiometric	70 ppb	PVC based membrane	pH adjustment required (≤ 7)	51, 52

Industries lead leaching control strategies in drinking water varies due to the water source, facility location, and suggestions from the commercial chemical company. The common procedures include cathodic and anodic protection, metal pipe pretreatment and coating, and chemical additions to the drinking water.

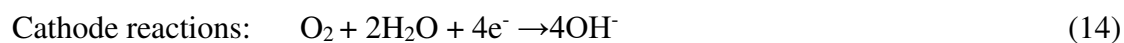
Cathodic/Anodic protection and metal pipe coating are normally done by the piping industry, while the chemical addition is performed by the water treatment plant. As for residents, different filters are suggested by the Disease Control and Prevention that can be applied to the house, such as reverse osmosis, distillation, and carbon filters, which are designed to remove lead. Also, it is recommended to test the water at the tap regularly. The main idea of applying chemicals as corrosion inhibitor to drinking water is to form a protective scale over the metal surface. These

scales are commonly recognized as inorganic precipitates. The formation of the passive film (Scale) can act as a diffusion barrier and reduce the corrosion rate ⁵³. The available corrosion control treatment methods include pH/Alkalinity/DIC adjustment, phosphate-based inhibitors addition, and silicate inhibitors addition, which can be used to control the Pb leaching ⁵⁴. However, different water quality needs different approaches and dosages, parameters including pH, metal ions, alkalinity, and disinfectants. These parameters are widely studied by researchers. For example, different disinfectants usage can change Pb leaching in drinking water. Xie and Giammar reported in 2011, with 1 mg L⁻¹ of free chlorine presented in the drinking water, lead release was decreased, and Edwards and Dudi (2004), also illustrated more Pb leaching in drinking water when switching free chlorine to monochloramine as disinfectants ^{55, 56}.

CHAPTER 3: MICROELECTRODE-BASED TEMPORAL INVESTIGATION OF THE IMPACTS OF CHLORINE AND MONOCHLORAMINE ON BRASS AND CEMENT

3.1. Introduction

Brass as a copper-zinc alloy has been widely used in drinking water distribution systems, mainly in house plumbing, such as tap valves, heating components, various fittings, and other fixtures.²⁰ The addition of zinc greatly improves the brass mechanical properties and made brass more cost effective compared to copper tubing. In addition, impurities incorporation of aluminum, silica, iron, lead, and tin can increase corrosion resistance to brass in drinking water conditions.²¹ As brass has often been installed in the household plumbing systems, many studies have been done to investigate the chemistry reaction of the brass material and water environment. The main mechanisms of brass corrosion are due to dezincification and thin film formation. Dezincification characterized by dealloying zinc from the brass material can result in pipe leakage, fitting failures and pitting problems.²² The key possible electrochemical half reactions related to dezincification mainly are listed below²³:



Due to the selective leaching process of zinc at low pH, the brass pitting can be localized.²³ However, at high pH, a white particulate film (or block named “meringue”) can be formed on brass surface.²⁴ The formation of meringue is mainly due to the low zinc solubility with the production of zinc carbonate and causing blocking problems in brass fittings in the plumbing system.²³

Cement/concrete is another important material used for drinking water distribution pipelines.³² In field practice, newly installed ductile iron pipelines is typically lined with cement-mortar to protect iron materials from corrosion process.³³ Cement (primarily Portland cement) contains calcium silicates, calcium aluminate, iron calcium aluminate, and gypsum, which can harden the cement through multiple reactions. For last two decades, numerous research had investigated the relationship among water chemistry, concrete materials, and iron materials. In 1996, American Water Works Association Research Foundation and DVGW-Technologiezentrum Wasser (AwwaRF and TZW) reported that calcium related compounds from the cement can dissolve into the drinking water based on the saturation point and their solubility, which can significantly increase the pH of the water, therefore affecting the drinking water environment aspects, such as corrosion control chemicals, disinfection by-products (DBPs) formation, and scaling.³³ Other researchers later tested and found that metal impurities can also leach into the drinking water.^{57, 58} In 2007, Trussel and Morgan proved that calcium silicate dissolution in the water can greatly affect the integrity of cement-lined pipes.³⁴ In 2012, Parks et al. investigated how zinc and orthophosphate to prevent chemicals from leaching and scaling in cement materials at different alkalinity, pH, and hardness.³² And a lot more research have been done relating to this subject.³⁵⁻³⁷

Understanding water chemistry changes on pipe materials can help to understand the mechanisms of pipe corrosion processes, however, for both brass and cement materials studies,

most of them were focused on using electrochemical methods (corrosion potentials, current, and noise), metal leaching to the water environment, weight changes and other technologies and limiting information can be gained from these methods.^{5, 20, 34, 36, 37, 59, 60} Little research has been conducted on the simulation of corrosion for both materials, especially on a micro-level of study. One key point of investigating the corrosion process is to study the chemistry changes over the material surface at certain time length, such as disinfectants concentration, oxygen level, and pH of the water environment. Even though microelectrode technique has been extensively used in the biomedical field and bioscience field since late 1960s,⁶¹⁻⁶³ only a few studies used the microelectrodes for investigating corrosion of reactive materials.⁶⁴⁻⁶⁶ With the acknowledgement of these information can help us better to gain a more profound understanding regarding to the corrosion process of brass and cement in the distribution systems. This study has three specific objectives to present:

- Gain detail information about surface water chemistry changes by direct measurements of pH, oxygen and free chlorine (or monochloramine) using microelectrodes on material surface.
- Understand reactions of brass and cement materials with different chemicals in the bulk water over time.
- Evaluate the effect of pH, chlorine species and oxygen on brass and cement materials surface characterization over time.

3.2. Materials and Methods

CDA 443 brass slides (UNS C44300, admiralty brass, density 8.52 g/cm³, Metal Samples Co., Munford, AL) and concrete coated slides (BST 503-12, BioSurface Technologies Corp., Bozeman, MT) were used for abiotic corrosion tests. A brass slide was cut into small pieces of coupons (1.5 × 1.2 cm) and cleaned by following G31-72⁶⁷ and D2688-83⁶⁸, two American Society for Testing and Materials (ASTM) coupon wash procedures. Concrete coupon was cut into two similar size pieces (size not measured), and then gently flushing and immersing in DI water for 5 minutes to eliminate any impurity contamination from other sources.³²

Total four sets of flow cells were constructed and operated for abiotic tests (Figure 2. Ex 1: brass coupon with free chlorine, Ex 2: brass coupon with monochloramine, Ex 3: cement coupon with free chlorine, and Ex 4: cement coupon with monochloramine). In each test set (Figure 2), 4 coupons were placed in a special designed transparent acrylic flow cell followed by a reduced-mass-transfer (RMT) cell with two coupons in it. The feeding solution of artificial tap water was prepared with composition of 100 mg Cl⁻ L⁻¹, 100 mg SO₄²⁻ L⁻¹, 10 mg C L⁻¹ dissolved inorganic carbon (DIC), and 2.0 mg Cl₂ L⁻¹ at 23 °C (Table 2). pH was adjusted to 7.0 by adding 1 M HCl or 1M NaOH. A calculated amount of NaHCO₃, NaSO₄, and NaCl (Fisher Scientific, Fair Lawn, NJ) were added into 20L feeding tank with DI water to match background SO₄²⁻, Cl⁻, and DIC. The artificial tap water was air-saturated by bubbling air for 15 min before pH adjustment and free chlorine (or monochloramine) addition. Free chlorine solutions were prepared by diluting 6% sodium hypochlorite (Fisher Scientific, Fair Lawn, NJ) to 10,000 mg Cl₂ L⁻¹ as stock solution, and then diluted to the target concentration in the bulk test water solution for the experiments. Monochloramine solutions were prepared with the same stock solution, with addition of ammonia at a Cl₂: N ratio of 4 by weight at pH 8.0 and adjusted back to 7 for the operation control.⁶⁹ The

artificial tap water was then fed into the flow cell at 2 ml/min of flow rate using a peristaltic pump (Masterflex, Cole-Parmer Instrument Company, Court Vernon Hills, IL).

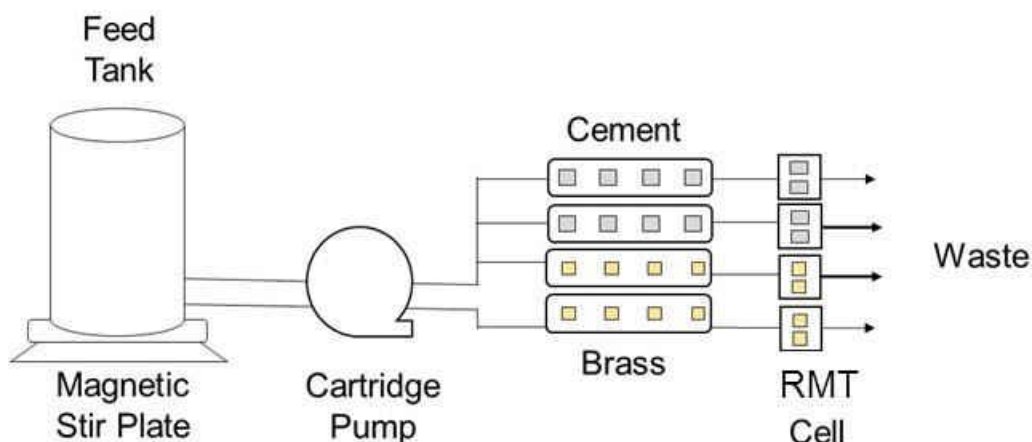


Figure 2. Operation setups & Microelectrode profiling setups.

Table 2. Experiment operating conditions for microelectrode profiles.

Operating parameters	Detail information
Flow speed	2 ml/min
pH condition	7.0
Background ions concentrations	0.83 mM NaHCO ₃ , 100 mg SO ₄ ²⁻ L ⁻¹ , and 100 mg Cl ⁻ L ⁻¹ .
Disinfectant concentration	2.0 mg Cl ₂ L ⁻¹ (free chlorine/chloramines)
Oxygen concentration	Saturated
Temperature	Room (~23 °C)
Light condition	Dark

Free chlorine (or monochloramine), pH, and oxygen were measured directly using microelectrodes for each coupon. pH microelectrode (pH-10, 10 μm tip diameter, UNISENSE A/S, Denmark) and oxygen microelectrode (Ox-10, 10 μm tip diameter, UNISENSE A/S, Denmark) were used for pH and oxygen microprofile measurements, respectively. Free chlorine and monochloramine microelectrodes were fabricated in the lab.^{70, 71} The tip diameter of free chlorine

and monochloramine microelectrodes were controlled at 10 μm , and calibrated with level of confidence at 99%. Microelectrodes used in this research were pre- and post-calibrated.

Microprofiles were then conducted at Day 0, and 60 under flow condition along with day 120 under both flow and RMT conditions. For microprofile measurements, the working microelectrode was connected with an Ag/AgCl reference milli-electrode (MI-401, Microelectrodes Inc., Bedford, NH) and the microelectrode tip was positioned by controlling a 3D micromanipulator (UNISENSE A/S, Denmark) under a microscope (World Precision Instruments, Sarasota, FL) inside the Faraday cage. The microprofiles were then step-size measured from bulk solution to coupon surface at 50 μm intervals. A guide microelectrode was used during profile measurements to identify the coupon surface.⁷² The electrical signals (pA or mV) were recorded using a multimeter (UNISENSE A/S, Denmark), a data acquisition system, and a software program (SensorTrace Pro 3.0, UNISENSE A/S, Denmark). Two random locations were selected for the microprofile experiments and duplicate measurements were conducted for each parameter at each location. SEM/EDS experiments for each coupon were also conducted on the following day (Figure 3).

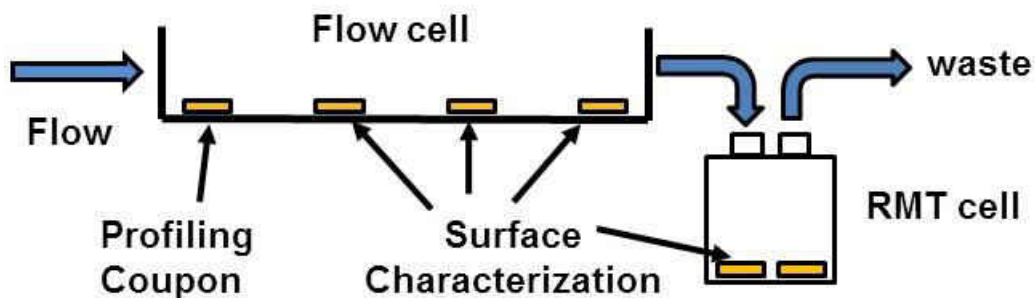


Figure 3. Horizontal view of coupons for multiple purposes.

3.3. Results and Discussion

3.3.1. Surface changes over 120 days for brass and cement coupons

During the profiling experiments, coupon surfaces were monitored under the microscope for both observation and micro-electrode positioning control purposes. At Day 0, the initial profiling stage, brass coupon in monochloramine solution had dark substances appeared on the surface after one-hour pretreatment during the microprofiling experiment, while in free chlorine solution, the brass coupon remained a shining yellow color throughout the whole process (Figure 4, Day 0). Similarly, during the entire experiment operation period, it appeared that the dark substances coverage of brass coupons in monochloramine solution were much faster compared to the ones in free chlorine solution under flow condition. This observation is in the agreement with the previous brass corrosion studies.^{5, 7, 60, 73} However, in RMT cell (Figure 4, RMT Day 120), the results were opposite to the free chlorine condition, brass with uniformed dark matters in free chlorine solution was observed, and in monochloramine solution, brass surface was covered of dark brown material mottled with original yellow color. Surface changes on cement coupons were more similar in either solutions. Both coupons started to have yellow substances developed on the surface around Day 60, and cement coupon under free chlorine condition had a larger overlapping area and darker color (Figure 5), similar situation for concrete coupons in RMT cells.

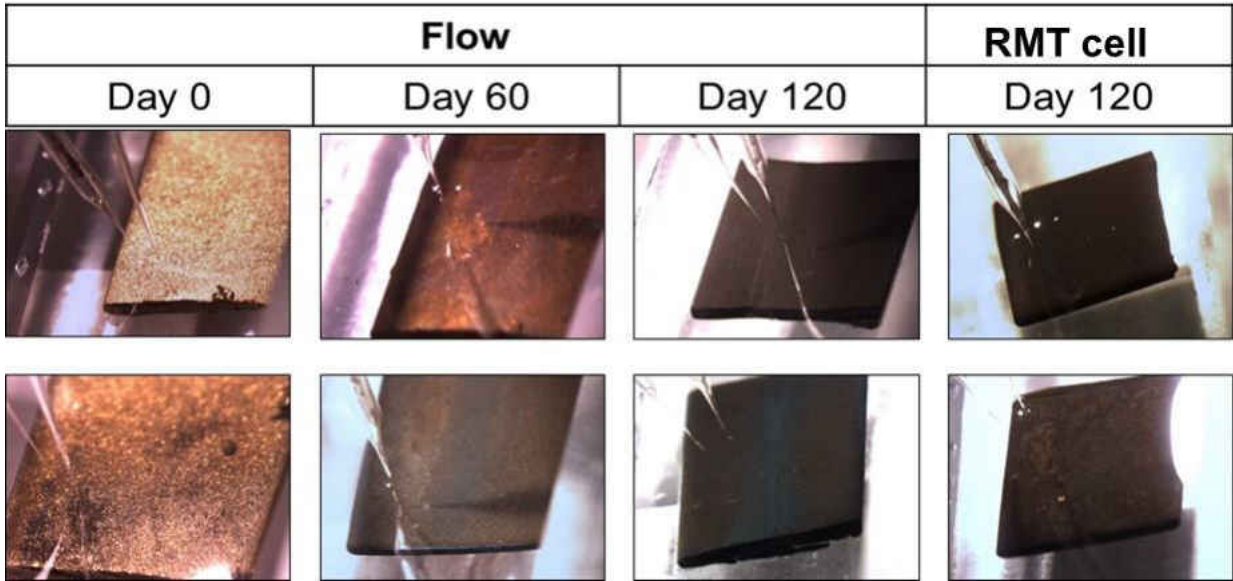


Figure 4. Surface changes on brass coupons over 120 days through microscope observations.

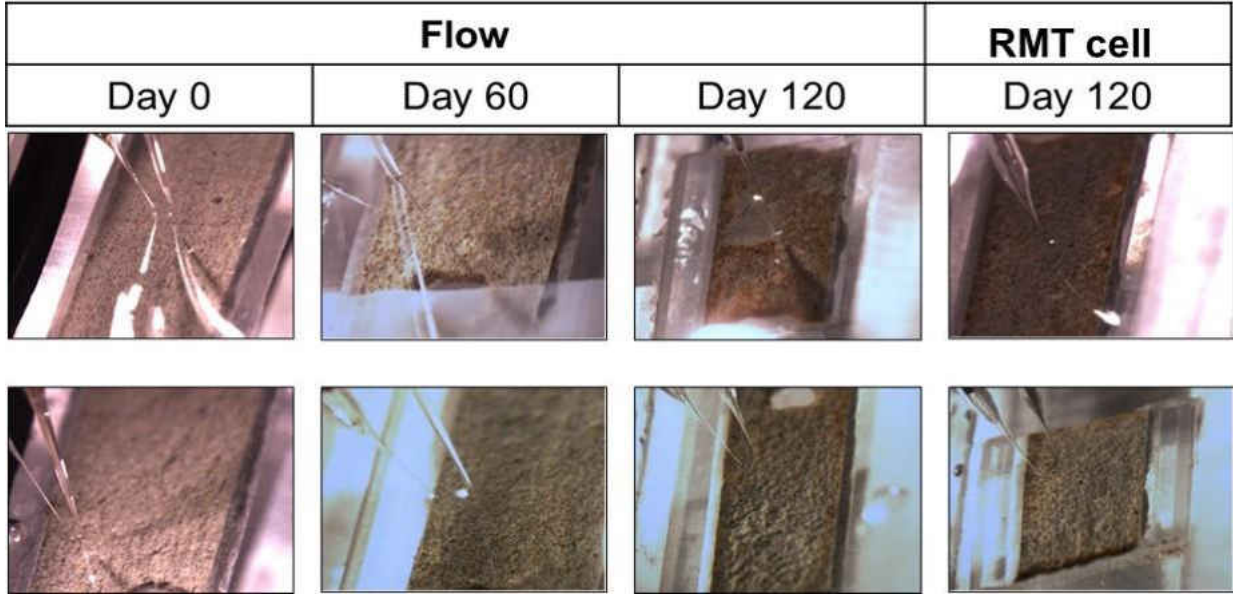


Figure 5. Surface changes on cement coupons over 120 days through microscope observations

3.3.2. Water chemistry profiles and consumptions on brass and cement coupons

Microprofiling experiments were conducted on coupons at day 0, 60, and 120 under flow and reduced-mass-transfer (RMT) conditions. For brass in free chlorine solution (Figure 6a), profiles

showed constant decrease of free chlorine concentration at surface with time. At day 120, the concentration of free chlorine at brass surface reached about $0.28 \pm 0.09 \text{ mg Cl}_2 \text{ L}^{-1}$ under flow condition. Similar trend was found in oxygen profiles for brass in free chlorine solution (Figure 6b), even though the differences between each stage were less obvious. Brass coupon in RMT cell appeared to be much less reactive to free chlorine than in flow condition, the free chlorine concentration at the brass surface ($1.45 \pm 0.04 \text{ mg Cl}_2 \text{ L}^{-1}$) were higher compared to day 0, indicating only small portion of free chlorine were consumed at the reaction of RMT cell, indicating much less free chlorine was consumed at the brass surface in RMT cell. However, unexpected oxygen decreasing in RMT condition was measured. The oxygen concentration reduced 35% ($5.21 \pm 0.64 \text{ mg L}^{-1}$) at brass surface compared to the bulk concentration (Figure 6b). The reactions between brass and free chlorine were much more significant influenced by the flow, while oxygen appeared to be the significant factor for brass reaction under RMT condition.

Monochloramine was known as a much more stable disinfectants in the drinking water, and a less reactive disinfectant compared to free chlorine.⁷⁴ Profiles of monochloramine at the brass surface showed relatively similar results at day 0, 60 and RMT conditions. Monochloramine remaining concentrations in these stages were able to maintain above 55%. However, at day 120 under flow condition, monochloramine concentration experienced a dramatic decrease at the brass surface with concentration of $0.33 \pm 0.18 \text{ mg Cl}_2 \text{ L}^{-1}$ left, similar to free chlorine result at the same stage. What distinguish from free chlorine was that, under monochloramine condition, profiles showed a much important role of oxygen in both flow and RMT conditions. Lower concentration of oxygen was measured on brass surface in monochloramine condition compared to free chlorine condition, indicating that oxygen might be the key factor for brass corrosion in monochloramine condition. One interesting observation was discovered from the results, at day 60, oxygen

reactivity on brass surface for both conditions reduced to the minimum level, less than 4% of oxygen were consumed at this stage (Figure 6d). Despite the differences in profiles of brass in free chlorine and monochloramine solutions over 120 days' time period, resemblance in disinfectants and oxygen consumption at day 120 under flow and RMT conditions cannot be denied (Figure 6). Both free chlorine and monochloramine showed up to 80% consumption at the surface under flow condition, while merely 20% of which were found under RMT condition. Oxygen, on the other hand, gave an opposite conclusion, almost 20% more oxygen consumptions were measured in both free chlorine and monochloramine solutions under RMT conditions, which showed that free chlorine and monochloramine was much more reactive under flow condition, and oxygen can be the main reactant for brass under RMT condition.

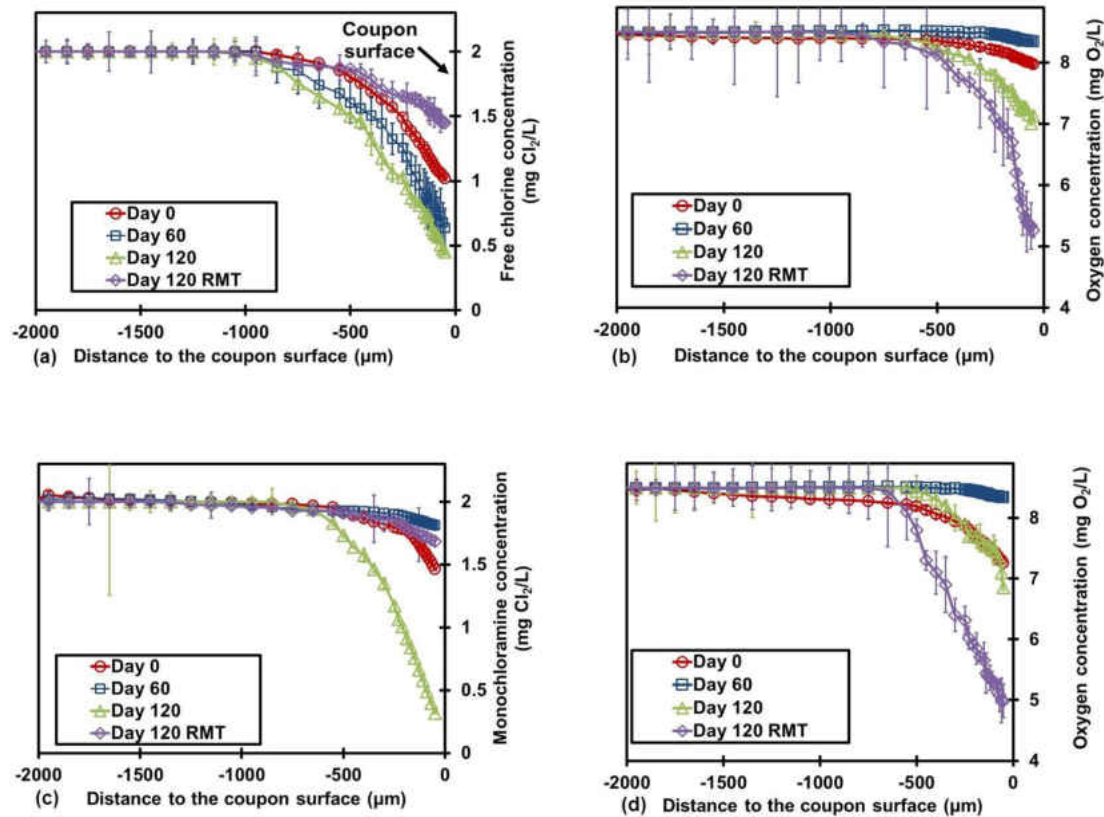


Figure 6. Long-term chemical profiles for brass coupon from day 0 to day 120 under flow and RMT conditions. (a) & (b) Free chlorine and oxygen profiles of brass in chlorinated condition; (c) & (d) Monochloramine and oxygen profiles of brass in chloraminated solution (pH 7, chlorine residuals 2 mg L^{-1} , oxygen 8.5 mg L^{-1}).

Free chlorine profiles on cement coupon showed that the reactivity at day 0, 60, and RMT stages were quite similar due to the surface concentration measured. However, it was observed that free chlorine was greatly declined to $0.67 \pm 0.06 \text{ mg Cl}_2 \text{ L}^{-1}$ at day 120 under flow condition. This was probably occurred due to the increased dissolution of lime from the cement material,³² or the reaction between free chlorine and the yellow substances developed on the cement coupon after 60 days. Comparable profiles were also found on oxygen concentrations on cement coupon in free chlorine solution. At day 0 and 60, unnoticeable decrease of oxygen concentrations was measured $50 \text{ }\mu\text{m}$ above the surface. While at day 120, under both flow and RMT conditions,

oxygen concentrations showed a dramatic drop. Again, this decreasing showed that oxygen played an important role under RMT conditions, which was similar to the oxygen in brass profiles. As for cement in monochloramine solution (Figure 7c&d), profiles for both monochloramine and oxygen were completely opposite from results obtained in free chlorine for cement materials. The monochloramine concentration was much lower at the cement coupon surface at day 120 under flow condition ($0.46 \pm 0.05 \text{ mg Cl}_2 \text{ L}^{-1}$), indicating the reaction of monochloramine at surface was much more severe than free chlorine, while the oxygen concentration under flow and RMT were merely decreased about 0.9 mg L^{-1} .

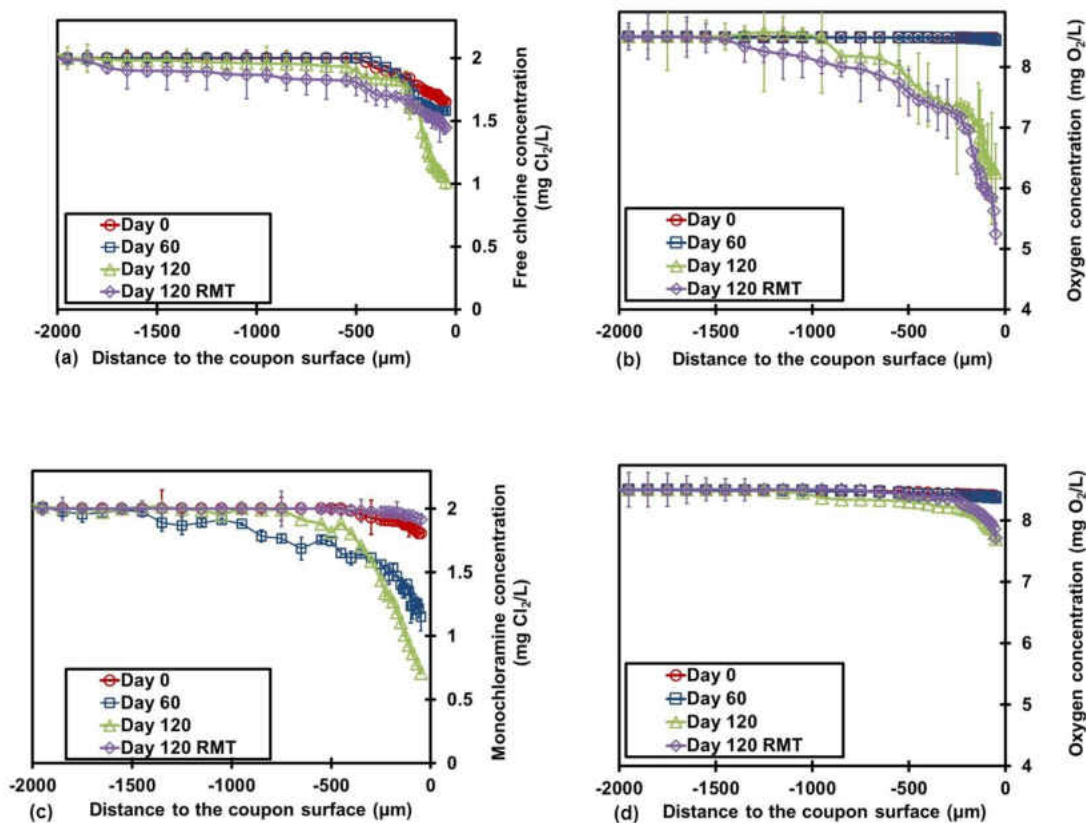


Figure 7. Long-term chemical profiles for cement coupon from day 0 to day 120 under flow and RMT conditions. (a) & (b) Free chlorine and oxygen profiles of cement coupon in chlorinated condition; (c) & (d) Monochloramine and oxygen profiles of cement coupon in chloraminated solution (pH 7, chlorine residuals 2 mg L^{-1} , oxygen 8.5 mg L^{-1}).

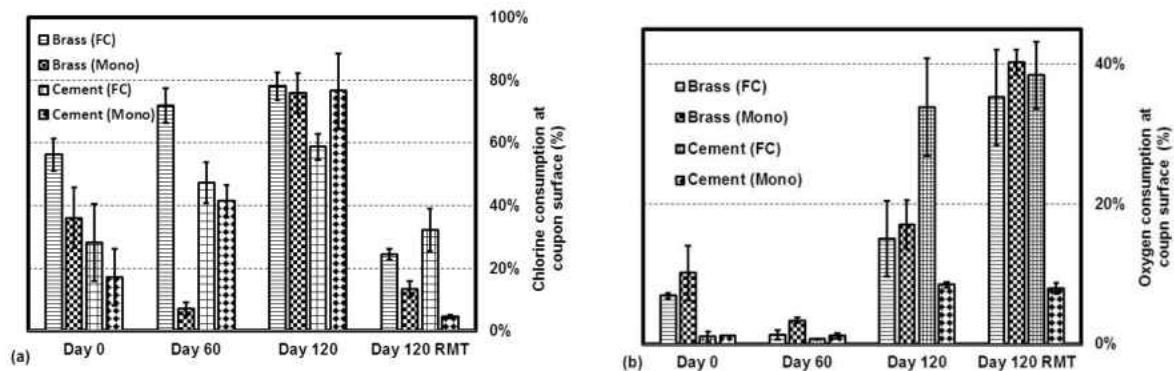


Figure 8. Free chlorine (or monochloramine) and oxygen consumption with reactive surface for brass and cement coupons over 120 days. (a) free chlorine consumption and (b) oxygen consumption (FC: free chlorine, Mono: Monochloramine).

3.3.3. Surface characterization of brass and cement coupons

When brass and cement coupons were conducted in profiling experiments for different parameters, surface characterizations (SEM/EDS analysis) were also performed with same time line. At Day 0, brass coupons in both conditions showed relative smooth surface with minor scratch on the surface. After 60 days, brass in free chlorine conditions formed “valley” areas with high zinc contents (40.73%) according to the EDS results (Figure 9). Similar high zinc area was also found on day 120 under flow and RMT condition, and after 5000 times magnification, fiber structured zinc compounds were developed at the coupon surface without any copper detection. This could be the re-deposition of zinc carbonate compounds.²³ Similar formation was found on brass surface in monochloramine condition, however, few places with high zinc compounds were found in monochloramine brass coupon and none were found in RMT conditions for brass in monochloramine, which could be the increased dezincification process on brass surface in the monochloramine condition.

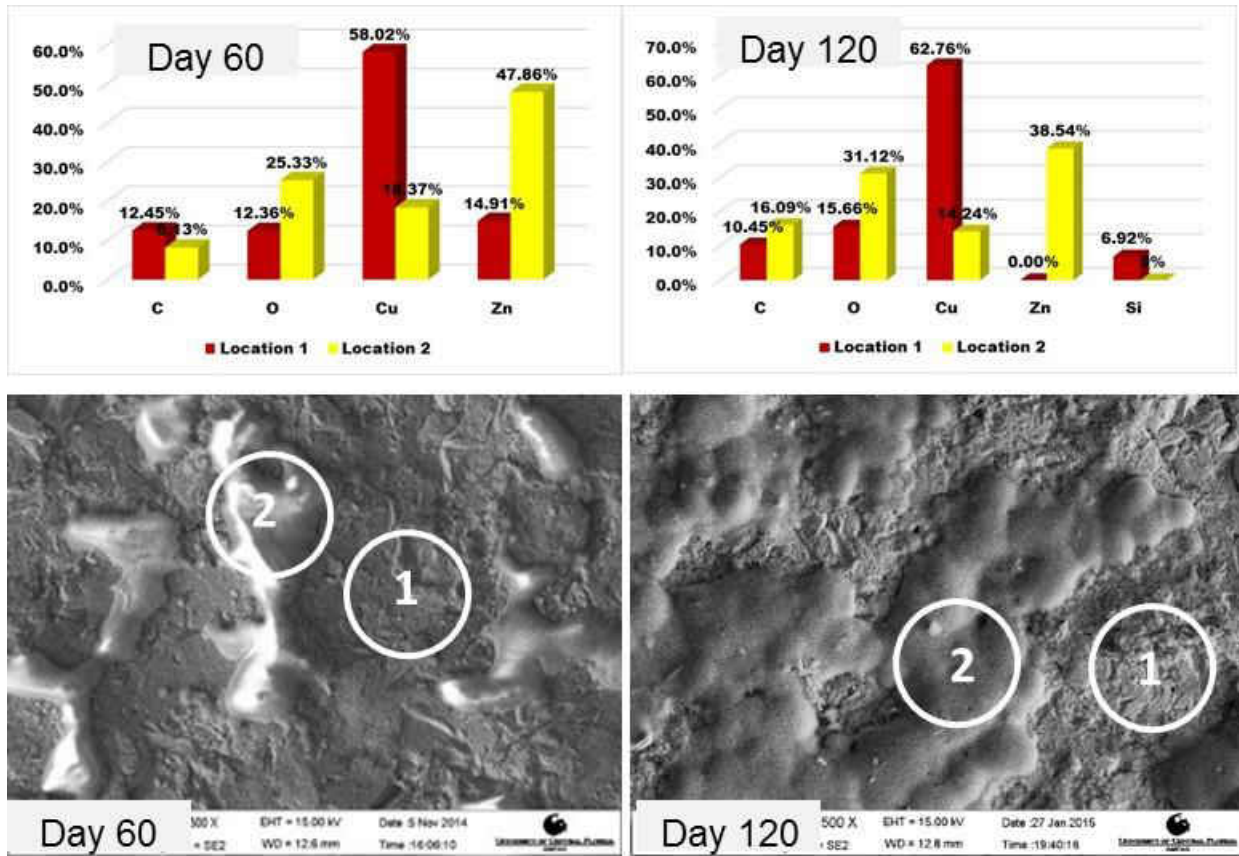


Figure 9. High selective zinc leaching area and zinc compounds forming area SEM images and EDS results of brass coupon in free chlorine solution at day 60 and 120.

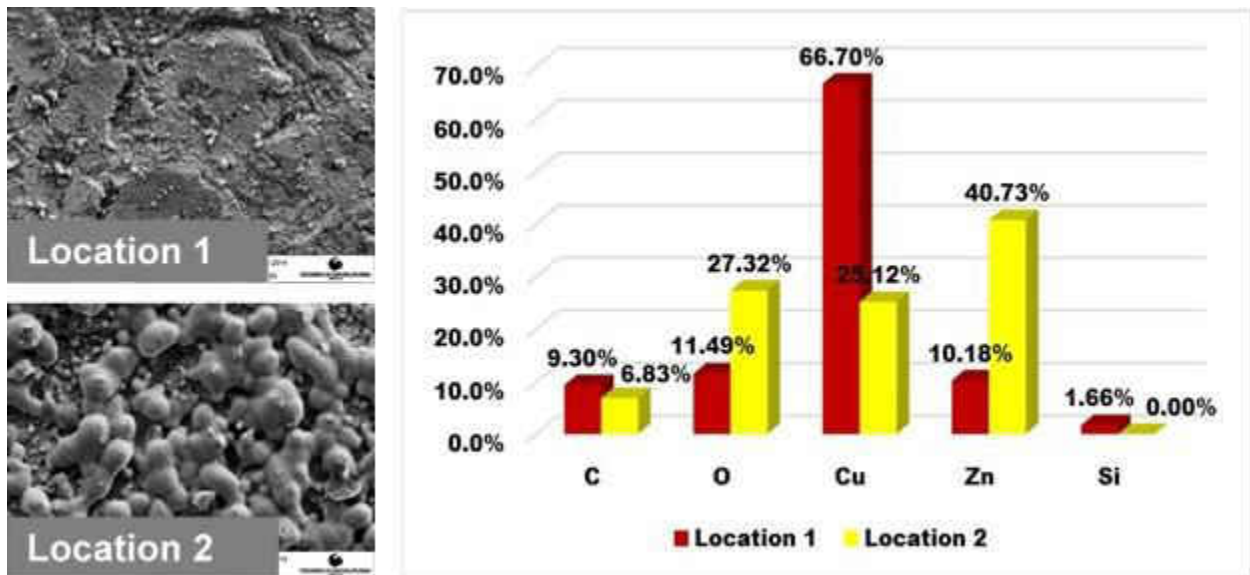


Figure 10. High selective zinc leaching area and zinc compounds forming area SEM images and EDS results of brass coupon in monochloramine solution at day 60.

SEM images of cement coupon in both solutions were comparably alike (Figure 11). At initial stage (Day 0), cubical shaped cement materials were closely attached to the coupon surface. After 60 days, under both free chlorine and monochloramine conditions, large silicon stones were appeared on under the SEM images. And fully exposure of silicon stones was found in Day 120 under flow and RMT conditions for both solutions. This dissolution of cement materials observation validated the previous mechanism of cement behavior in drinking water system pipelines.³²

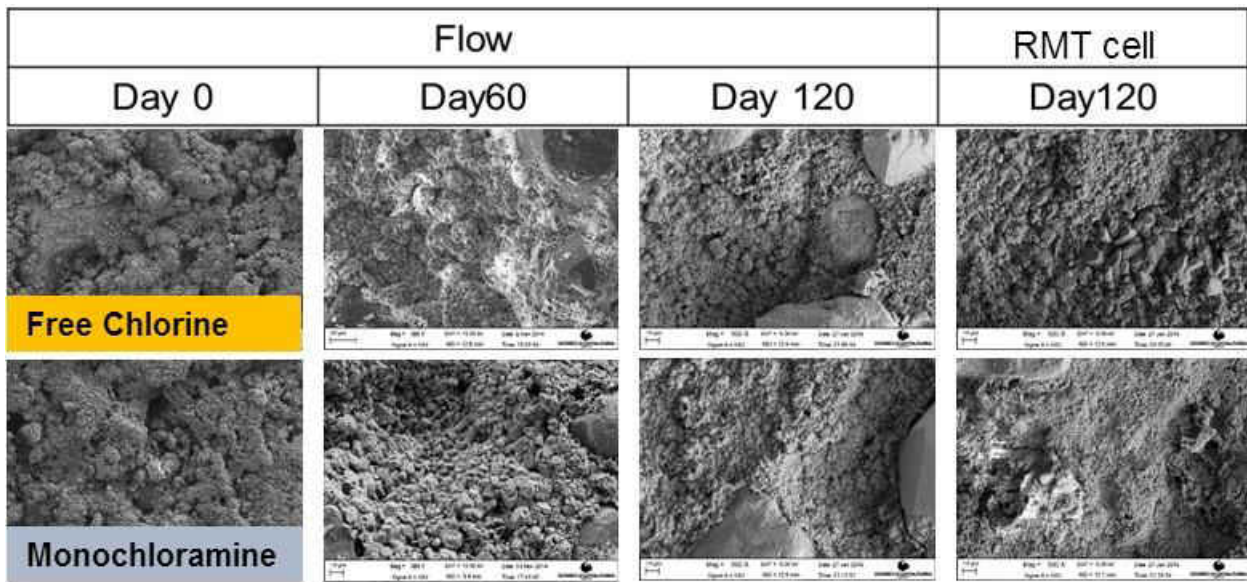


Figure 11. Long-term SEM images of cement coupon in free chlorine and monochloramine solutions under flow and stagnant condition (500 times magnification).

3.3.4. Weight losses of brass and cement coupons in RMT condition

The weight loss of brass was controlled under averaging 5% (Figure 12). The difference between brass in free chlorine and monochloramine might due to the higher dezincification rate showed in the EDS results, and continuously re-deposit of zinc compounds on brass surface in free chlorine solution resulted in half less weight loss. Higher weight loss was also found in cement coupon in monochloramine condition. It appeared that the dissolution rate of cement materials was much faster in monochloramine solution rather than in free chlorine solution. The larger formation of yellow substance on cement coupon surface probably attributed to this result. Further study is needed to determine the yellow substance. The high rate of cement material loss could result in the penetration of chloride ion into the cement-lined steel, causing further corrosion in the drinking water system.⁷⁵

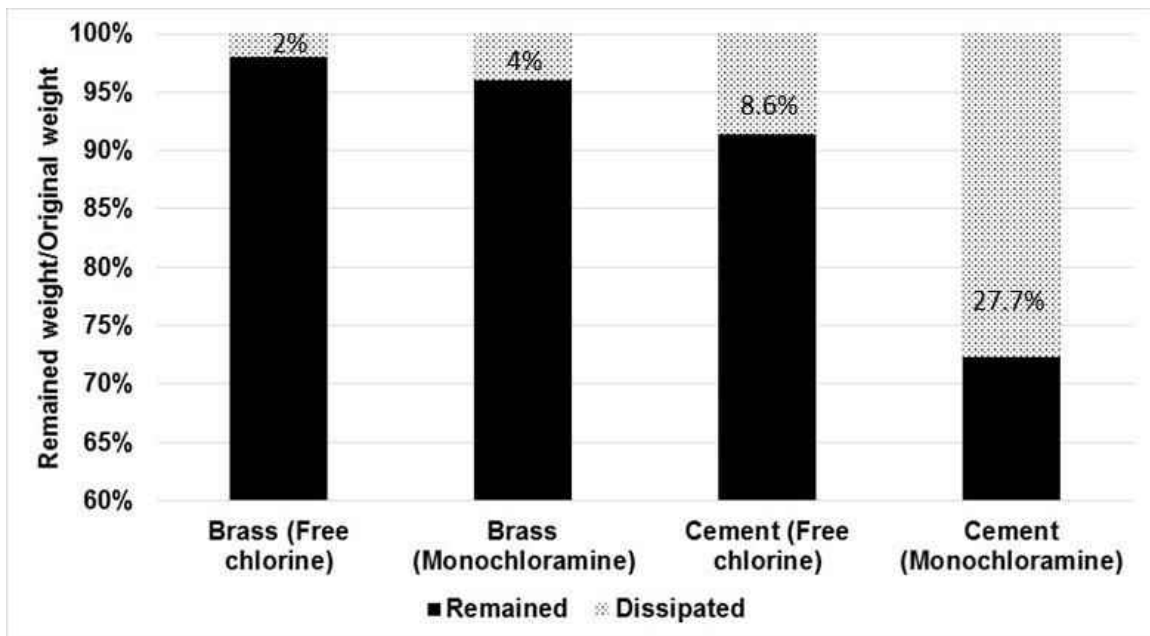


Figure 12. Weight losses of brass and cement in free chlorine and monochloramine under stagnation.

3.4. Conclusion

Brass and cement reactions with disinfectants and oxygen in abiotic artificial water environment were closely examined on micro-level in the present study, which provides a more detailed understanding between water chemistry and surface characteristic changes of brass and cement in corrosion studies. In this applied water type, free chlorine and monochloramine served a significant role for both brass and cement corrosions under flow condition, and both of which showed great reactivity during the experiments. In the reduced-mass-transfer cell, the oxygen availability appears to be the essential factor to the corrosion processes with high consumption rate at the coupon surface. On brass coupons, selective leaching of zinc gets extremely serious at certain areas over time, especially under monochloramine condition, while under free chlorine condition, re-deposit of zinc compounds can be easily found on the surface under artificial water. According to previous review, cement behavior in both solutions were similar to the dissipating process of cement material with elevation the pH of the surrounding water environment. These results provide detailed information of key parameters change over the material surface, and can be used to assist the further study on the abiotic corrosion and biotic corrosion studies for brass and cement materials in the future.

CHAPTER 4. IN-SITU 2D MAPS OF PH SHIFTS ACROSS BRASS-LEAD GALVANIC JOINTS USING MICROELECTRODES

4.1. Introduction

Corrosion in drinking water distribution systems can cause serious economic, environmental and public safety problems from pipe damage, water loss and water quality degradation. One form of corrosion, galvanic corrosion, results when two dissimilar metals are in electrical contact in water where one of the metals corrodes preferentially to the other. The impact of galvanic corrosion on metal release is an important issue that affects the quality of potable water. The practice of partial lead (Pb) service line replacement and the associated possible increased risk of lead release into drinking water has been a concern.^{10, 42, 76} Lead-containing particles are being released due to disturbances associated with construction, destabilization of corrosion by-products on the remaining lead pipe, and galvanic corrosion at the connection between the remaining lead pipe and new service material such as copper. These are many causes for elevated lead release following partial lead service line replacement. Lead leaching from lead service lines and leaded solder joints can be accelerated by the galvanic connection (Table 3) with other metal materials⁴²⁻⁴⁴ including brass and copper, where lead (Pb) serves as an anode (location of oxidation) where lead ions (Pb^{2+}) are released and the cathodic metal (brass) protected from a galvanic reaction (17-18).⁴⁵



Table 3. Galvanic series of selected metals and alloys and standard electrode potential (electromotive force series).

Galvanic series of selected metals and alloys in seawater		Electrode reaction	Standard electrode potential (V-SHE* @25 °C)
Cathodic (noble, least likely to corrode) ↑ Brasses ↓ Anodic (active, most likely to corrode)	Gold	$Au^{2+} + 2e^{-} \leftrightarrow Au$	1.50
	Silver	$Ag^{2+} + 2e^{-} \leftrightarrow Ag$	0.80
	Copper	$Cu^{2+} + 2e^{-} \leftrightarrow Cu$	0.337
	Tin	$Sn^{2+} + 2e^{-} \leftrightarrow Sn$	-0.136
	Lead	$Pb^{2+} + 2e^{-} \leftrightarrow Pb$	-0.126
	Lead-tin solders		
Zinc	$Zn^{2+} + 2e^{-} \leftrightarrow Zn$	-0.763	
Magnesium	$Mg^{2+} + 2e^{-} \leftrightarrow Mg$	-2.37	

Although general theories regarding galvanic interactions leading to lead release have been described, and experimental and microscopic support has been reported,⁴²⁻⁴⁵ detail *in-situ* water quality measurements at the surface of galvanic connections have not been performed. Specifically, no direct measurements of micro-environment water chemistry at metal surface have been conducted, and thus a practical link between bulk water chemistry and the metal surface dynamics has not been well established. Therefore, an obvious need to better understand the surface chemical dynamics of galvanic couples leading to enhanced metal release is apparent. In order to provide

effective mitigating solutions for reducing metal release associated with galvanic corrosion and complying with the lead and copper rule (LCR),⁷⁷ *in-situ* water-metal interaction of galvanic joints must be better understood. Many studies have been conducted to evaluate the impact of water quality parameters on brass corrosion, for example, pH, temperature, DO (DO), free chlorine (or monochloramine), chloride, corrosion inhibitors and others.⁵⁻⁹ Electrochemical measurements (e.g., current density), visual observation, weight loss, metal release and surface characterization are also commonly used as analytical methods for studying corrosion in water. Arnold and Edwards (2012)⁷⁸ demonstrated a mass balance of lead release by measuring electrochemical potential (E_{corr} vs. Ag/AgCl) of metal and investigating lead release from galvanic connections in different water patterns, disinfectants, and corrosion inhibitor. Nguyen et al. (2010)⁹ evaluated the relationship between chloride to sulfate mass ratio (CSMR) and the associated galvanic current using an electrochemical method, surface characterization and microelectrode techniques.

These methods provide fundamental understandings of brass corrosion; however, they have been limited to bulk monitoring. Direct measurements in the proximity of the very surface is required for better understanding of corrosive microenvironment to develop appropriate control corrosion strategies (e.g., lead leaching control). Some of studies used electrode (or microelectrode) technique;^{9, 78} however, most of them used a macro electrode (e.g., a standard hydrogen electrode (SHE) electrode) which is not able to provide a localized chemical information. pH microelectrodes (Microelectrode Inc.) were also used to investigate pH changes,⁹ however, a relative big tip diameter (0.8 mm) was limited to measure one dimensional (1D) profile (e.g., 1D pH and chloride profiles along with pipe distance) in a bulk of copper joint macrocell. Although pH is one of the most important parameters for elucidating corrosion mechanism, the measurement was limited only to the bulk and no two-dimensional (2D) surface contour map of pHs on a metal

surface (or galvanic couple) has not been constructed due to the lack of microelectrode technique to measure chemical profiles in the proximity of the very surface. In order to better understand conditions at galvanic connections that lead to enhanced metal release and provide remedial strategies, the localized corrosion reaction at water-metal interfaces must be better understood.

The objective of this work is to develop a new experimental methodology to measure *in situ* pH changes from the bulk to the proximity to metal surfaces and construct 2D maps across a galvanic joint, providing a direct evidence of micro-environment's chemistry dynamics for better understanding of galvanic corrosion mechanisms. Brass was selected as a representative material for a galvanic connection with a lead-tin solder. Brass is a copper-zinc alloy that often contains relatively small amounts of lead and has been widely used in drinking water distribution systems, especially in premise plumbing components including faucets, valves and other types of connectors.^{7, 60, 79} Brass coupons alone were also used for constructing a 2D pH contour map to establish a baseline. Two different flow conditions (flow vs. stagnation) were compared to evaluate the effect of flow on pH at the metal surfaces. Although it is well known that galvanic corrosion can result in the localized change of pH, the present work found a novel phenomenon that flow and stagnation may result in an opposite trend for the change of pH. The results of this study provide a direct evidence of pH shifts on the metal surface across a galvanic joint which have been hypothesized for many years.^{3, 18, 26-29}

4.2. Materials and Methods

4.2.1. Metal Coupons Preparation

New brass CDA 443 coupons (UNS C44300, admiralty brass, density 8.52 g/cm³, Metal Samples Co., Munford, AL) with 1.6 mm thick×12 mm wide×140 mm long were cut into

small sections (1.6 mm thick×12 mm wide×14 mm long). The sections of brass coupons were cleaned using a combination of two American Society for Testing and Materials (ASTM) coupon wash procedures: G31-72⁶⁷ and D2688-83.⁶⁸ Four sections were immersed in a specifically designed Teflon flow cell (Brass 1) with a flow at 2 ml/min of a synthetic chlorinated water (Figure 13). For the first 120 days, a test water with a pH 7.0, 100 mg Cl⁻ L⁻¹, 100 mg SO₄²⁻ L⁻¹, 10 mg C L⁻¹ dissolved inorganic carbon (DIC), 2.0 mg Cl₂ L⁻¹ free chlorine at 23 °C was fed through the flow cell. After 120 days, free chlorine concentration was increased to 4.0 mg Cl₂ L⁻¹ and pH was adjusted to pH 9.0 to provide a corrosive environment in order to accelerate brass corrosion.^{5, 43, 80} At the same time (at 120 days of Brass 1), another four sections of brass coupon were immersed in a separate flow cell (Brass 2) under the same water conditions (pH 9.0 and 4.0 mg Cl₂ L⁻¹). Then, after 80 days of aggressive water environment, each brass coupon was taken from each flow cell and 1D pH microprofiles and 2D pH contour maps were measured for each coupon (i.e., 200-day aged coupon for Brass 1 and 80 day aged coupon for Brass 2). For preparation of the test water, reagent grade chemicals (NaHCO₃, NaSO₄, and NaCl) (Fisher Scientific, Fair Lawn, NJ) were added into a 20 L carboy with DI water. Free chlorine solutions were prepared by diluting 6% sodium hypochlorite (Fisher Scientific, Fair Lawn, NJ) to 10,000 mg Cl₂ L⁻¹ as stock solution, then diluted to the target concentration in the bulk test water solution for the experiments. HCl and NaOH were used for pH adjustments. The bulk water was air-saturated before the pH adjustment and free chlorine addition. Flow cells were operated in the dark by covering them with aluminum foil.

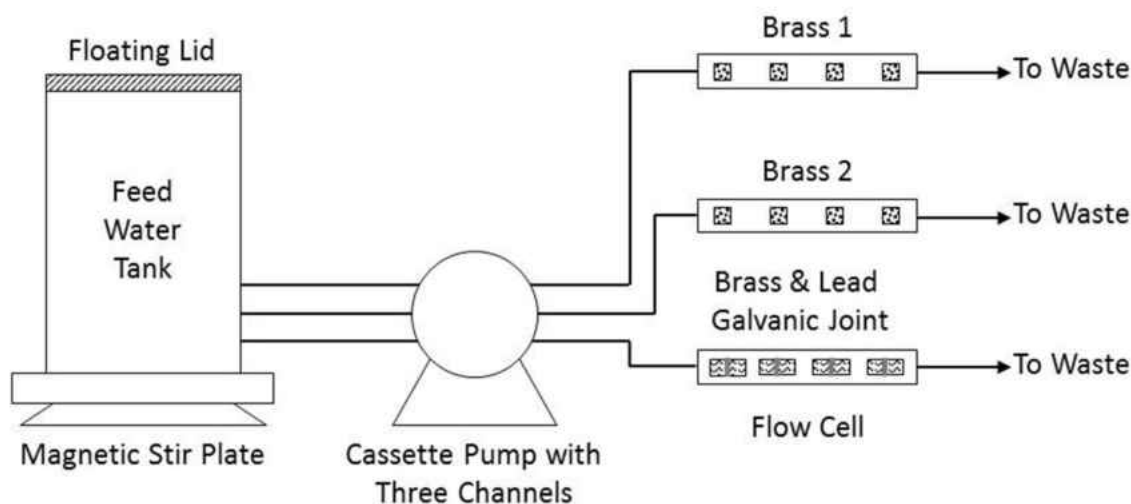


Figure 13. Schematic diagram of the simulated water distribution system for aged brass and galvanic coupons preparation.

After cleaning (see Section 2.1.1 ASTM brass cleaning procedures), two small pieces of brass coupon (CDA 443, admiralty brass, Metal Samples Co., Munford, AL) were connected to each other with a 3-mm in length and 8-mm in width 50:50 Pb-Sn solder (38110, Forney) to create a simulated brass-lead soldered galvanic joint coupon (8-mm in width and 25-mm in length). The fresh galvanic coupon was placed in a flow cell (Figure 13) under the same aggressive water condition as brass coupons (pH 9.0, 100 mg $\text{Cl}^- \text{L}^{-1}$, 100 mg $\text{SO}_4^{2-} \text{L}^{-1}$, 10 mg $\text{C} \text{L}^{-1}$ DIC, 4.0 mg $\text{Cl}_2 \text{L}^{-1}$ free chlorine, and 23 °C) for two weeks. The galvanic joint coupon was then taken for pH profile measurements and 2D pH contour mapping. The flow cell was also operated in the dark by covering it with aluminum foil.

4.2.2. Microprofile measurements and pH contour mapping

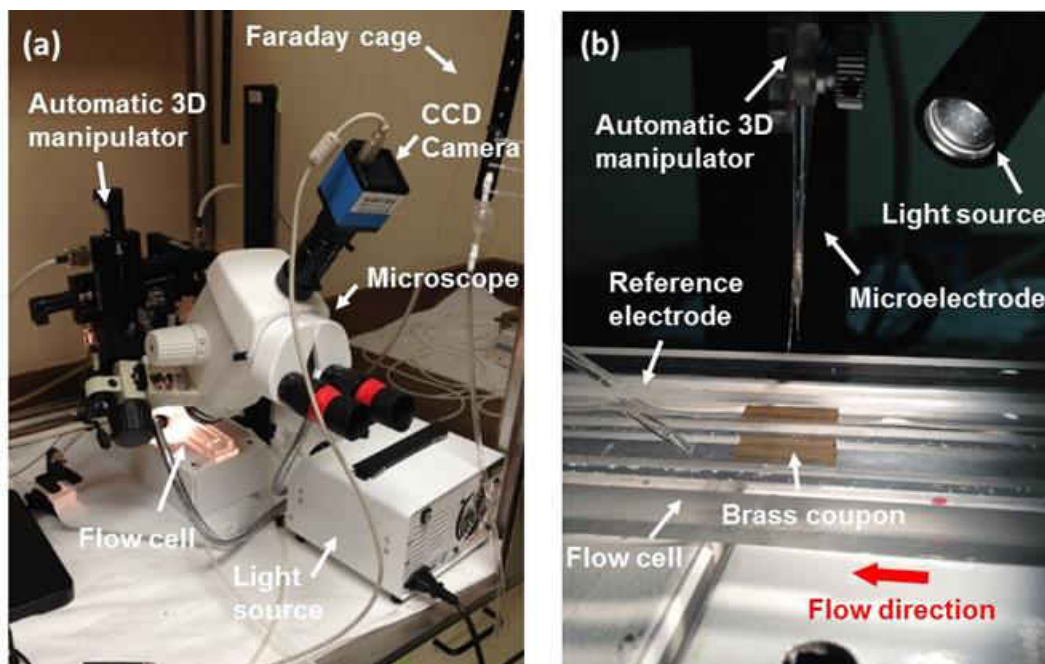


Figure 14. pH 2D contour mapping experimental setup. (a) microprofiling setup, (b) flow cell system for microelectrode profile measurements.

pH microprofiles were measured using a pH microelectrode⁷⁰ and an automatic 3D micromanipulator (World Precision Instruments, Sarasota, FL) (Figure 14). The pH microelectrode used in this work has been widely used and its performance has been validated previously.⁸¹⁻⁸³ Each coupon taken from each flow cell was moved to a transparent acrylic flow cell which was filled with the same test water (i.e., pH 9.0, 100 mg Cl⁻ L⁻¹, 100 mg SO₄²⁻ L⁻¹, 10 mg C L⁻¹ DIC, and 4.0 mg Cl₂ L⁻¹ free chlorine). The coupon was then acclimated under the same water condition for one hour before profile measurements. The pH microelectrode was connected with an Ag/AgCl reference milli-electrode (MI-401, Microelectrodes Inc., Bedford, NH) and the sensor tip was positioned by controlling a 3D manipulator (UNISENSE A/S, Denmark) under a microscope (World Precision Instruments, Sarasota, FL). The microprofiles were then measured from the bulk to 100 μm above the metal surface. After positioning a pH microelectrode, 10-30

seconds was spent to stabilize the pH readings initially. Then, pH (as mV vs. Ag/AgCl) was measured by moving the tip of the sensor (3 sec), waiting before the signal recording (3 sec), and recording the signal (3 sec). 1D profiles were measured triplicate (or duplicate) to ensure that the measured pH microprofile is representative and reproducible. Under flow condition, flow was controlled at 2ml/min, the flow effect on the pH measurements was very minimal and negligible. Pre- and post-calibration were conducted for every pH profile measurement. The metal coupon surface was initially identified with a used microelectrode. The electrode signals were monitored and recorded using a multimeter (UNISENSE A/S, Denmark), a data acquisition system and a software program (SensorTrace Pro 3.0, UNISENSE A/S, Denmark). Microelectrode profile measurements using a control coupon (e.g., polycarbonate slides) were conducted and validated previously.^{84, 85}

For the 2D pH map, pH was measured at 100 μm above the metal surface with a certain grid. For the 80-day aged brass coupon, a total of 25 points (5 \times 5) were measured over the coupon surface of 6,400 μm (W) \times 7,200 μm (L) with a distance interval of 1,600 μm (W) and 1,800 μm (L). For the 200-day aged brass coupon 2D pH map, 25 points (5 \times 5) were measured over the coupon surface of 4,000 μm (W) \times 7,200 (L) with a distance interval of 1,000 μm (W) and 1,800 μm (L). Triplicated data was recorded in each point for 2D mapping. Triplicates for the pH measurements indicate three profiles measurements at one point before moving to a next point. 1D pH microprofiles were measured from the bulk (2,000 μm above the metal surface) with a 50 μm interval, and at least two random locations were selected to investigate the heterogeneity of measured pH profiles (Figure 15). Each measurement was replicated at least once. The total duration for obtaining a 2D pH contour map of a single brass coupon was 1.5 to 2.5 hours. For the galvanic solder coupon measurement, 30 points (3 \times 10) were selected over the coupon surface of

4,000 μm (W) \times 18,000 (L) with an interval 2,000 μm (W) and 2,000 μm (L) under flow condition, and 65 points (5 \times 13) were selected over the coupon surface of 4,800 μm (W) \times 24,000 (L) with an interval of 1,200 μm (W) and 2,000 μm (L) under stagnant condition. Triplicated data was also recorded in each point for 2D mapping. Three different locations (brass | solder | brass) were selected for 1D pH microprofile measurement (Figure 15). Each measurement was replicated at least once. The total duration for obtaining a 2D pH contour map of a galvanic coupon was 3 to 4 hours. After surface pH scanning with the pH microelectrode, 2D maps were constructed using a programming language (Python 2.7.10, Python software). Free chlorine concentrations in the bulk solution in a flow cell were measured before and after the experiments by a colorimetric test kit (Hach-8021) and a DR 5000 spectrophotometer (Hach Co.). Weight loss of the galvanic solder coupon was measured on a weekly basis. The pH microelectrode was pre- and post-calibrated during the profiles to make sure that the pH changes are not from the electrode signal drift.

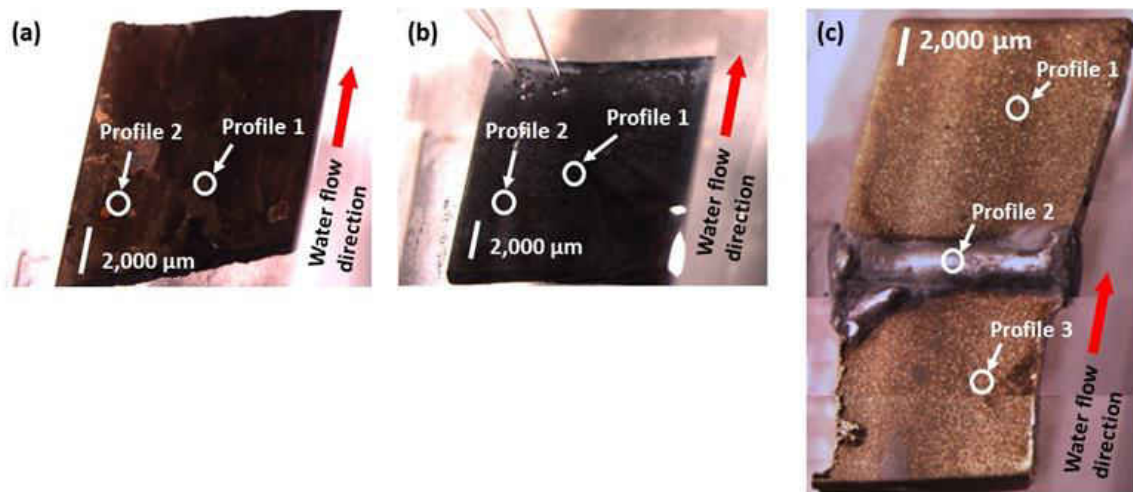


Figure 15. Optical microscopic images of brass coupons and galvanic coupon in a microprofiling flow cell. (a) 80 days aged brass coupon. (b) 200 days aged brass coupon. (c) 14 days aged brass-lead galvanic connection coupon.

4.3. Results and Discussion

4.3.1. 2D pH shift on aged brass coupons

After 80 and 200 days of flow cell operation, the colors of both brass coupon surfaces turned from their original bright yellow to dark brown, reflecting the development of corrosion by-products on the surface (Figure 15a and b), which has been reported in previous brass corrosion studies.^{5, 7, 60, 73} The 200-day brass coupon showed more homogenous dark brown corrosion by-products formation across the surface than the 80-day coupon.

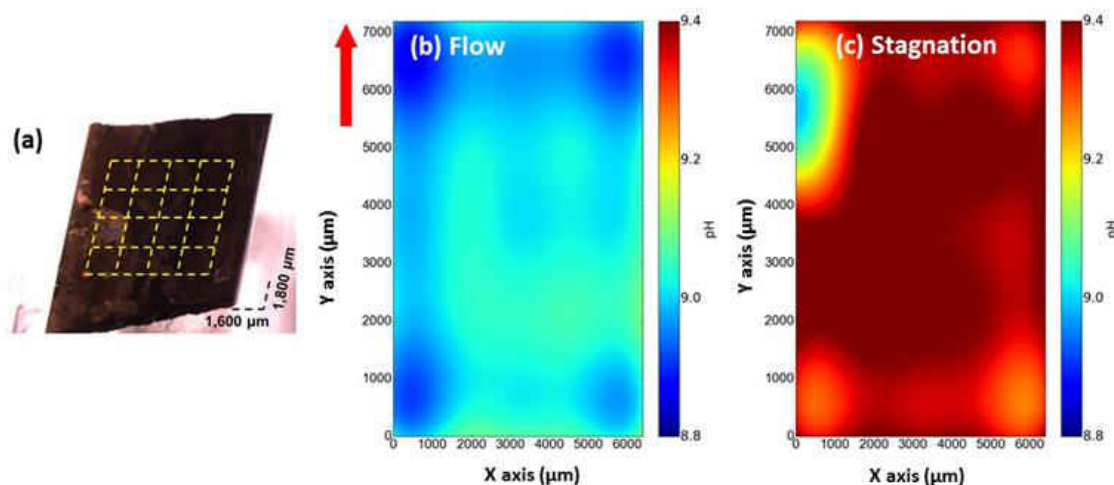


Figure 16. 2D pH contour map of 80 days aged brass coupon. (a) 2D map grid with scale, (b) with flow (2 ml/min). (c) under stagnation. The pH in the bulk solution was 9.0.

2D pH surface profiles above the brass coupons showed that the water flow influenced the pH across the coupon surface (Figure 16 and 17). During flow, the pH near surface averaged pH 9.0 and was relatively uniform across the surface for coupons after 80 and 200 days (Table 4, Figure 16b and 17b), which was the same as the bulk pH. However, under the stagnation of 1.5 to 2.5 hours, the pH varied from 9.0 (min.) to 9.5 (max.) with an average of 9.4 ± 0.08 across the 80-day brass coupon surface (Figure 16c) and from 9.1 (min.) to 9.4 (max.) with an average of

9.2±0.08 across the brass coupon surface after 200 days (Figure 17c). Water stagnation increased the pH at the brass surface as compared to the bulk water. In addition, the pH across the surface was much more variable. During the stagnation test, free chlorine residual was maintained at 3.8 and 3.1 mg Cl₂ L⁻¹ for 80- and 200-day brass coupons, respectively. This indicates pH may continue to change with time. Water stagnation showed a wider range of pH distributions across the surface compared to flow condition, indicating that even in a small area, brass coupons can be polarized and thus corrosion proceeds non-uniformly.⁶⁰

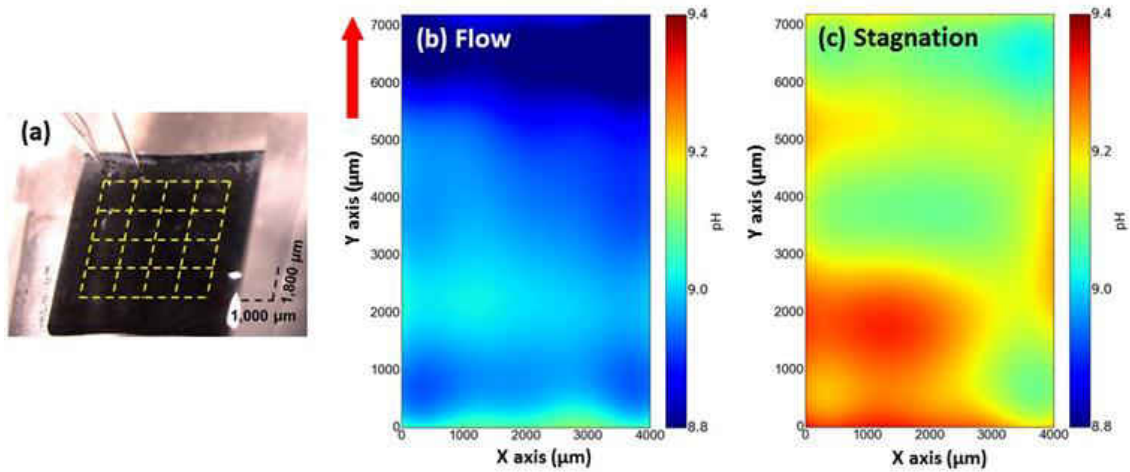


Figure 17. 2D pH contour map of 200 days aged brass coupon. (a) 2D map grid with scale, (b) with flow (2 ml/min). (c) under stagnation. The pH in the bulk solution was 9.0.

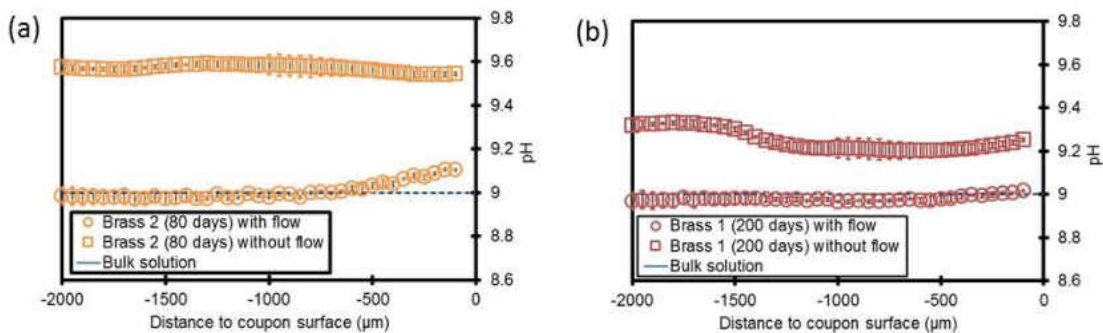


Figure 18. Measured representative 1D pH microprofiles of brass coupons. (a) pH microprofiles of 80 days aged brass coupon with and without flow. (b) pH microprofiles of 200 days aged brass coupon with and without flow. The pH in the bulk solution was 9.0. Two locations per one coupon (Figure 16) were measured and an average value with error bar was presented for each pH profile.

Table 4. Summary of the surface pH changes on brass coupons and a galvanic solder coupon.

Metal Coupons	Flow condition		Stagnation	
	Ave. pH	Δ pH	Ave. pH	Δ pH
Aged brass (80 days)	9.0 ± 0.03		9.4 ± 0.08	
	<i>max.</i> : 9.1	0.1	<i>max.</i> : 9.5	0.5
	<i>min.</i> : 9.0		<i>min.</i> : 9.0	
Aged brass (200 days)	9.0 ± 0.08		9.2 ± 0.08	
	<i>max.</i> : 9.1	0.3	<i>max.</i> : 9.4	0.3
	<i>min.</i> : 8.8		<i>min.</i> : 9.1	
Brass-lead galvanic connection (14 days)	9.1 ± 0.12		8.9 ± 0.51	
	<i>max.</i> : 9.4	0.4	<i>max.</i> : 10.0	2.1
	<i>min.</i> : 8.9		<i>min.</i> : 7.9	

1D pH profiles (Figure 18) confirmed that the pH under flow conditions did not change. The pH was very close to the bulk water pH (200-day brass) or slightly increased to pH 9.1 (80-day brass). The water flow influenced surface pH near the brass surface within a diffusion boundary layer (DBL) of 600 to 800 μ m thickness from the metal surface. Water stagnation greatly affected pH. The pH increased to as high as 9.5 (80 day-aged brass) and 9.3 (200 day-aged brass) as compared to the initial pH of 9.0 during the stagnation. For both flow and stagnation, the 80-day brass coupon showed slightly higher pH at the surface compared to the 200-day brass coupon, indicating higher reactivity of the newer brass surface in chlorinated water. For the 200-day aged brass coupon, dark brown deposits covered the entire surface, which may have contributed to the

lower pH surface change during stagnation (Figure 18) as compared to the 80-day aged brass coupon. In contrast, corrosion by-products on the surface of the 80-day brass coupon were non-homogenous and poorly established, which may have resulted in relatively higher cathodic reactions⁵ along with higher pH across the surface under stagnation (Figure 16c). An interesting observation for the 200-day aged coupon is that, as shown in Figure 15b which was taken after the experiment, white compounds were formed at the end of the brass coupon following a flow direction. On the other hand, with 80-day aged brass coupon, there were no similar findings. It seems that the formation of zinc meringue corrosion by-products⁵ may be initiated after the completion of the surface oxidation (i.e., 200-day aged coupon with entire color change to dark brown).

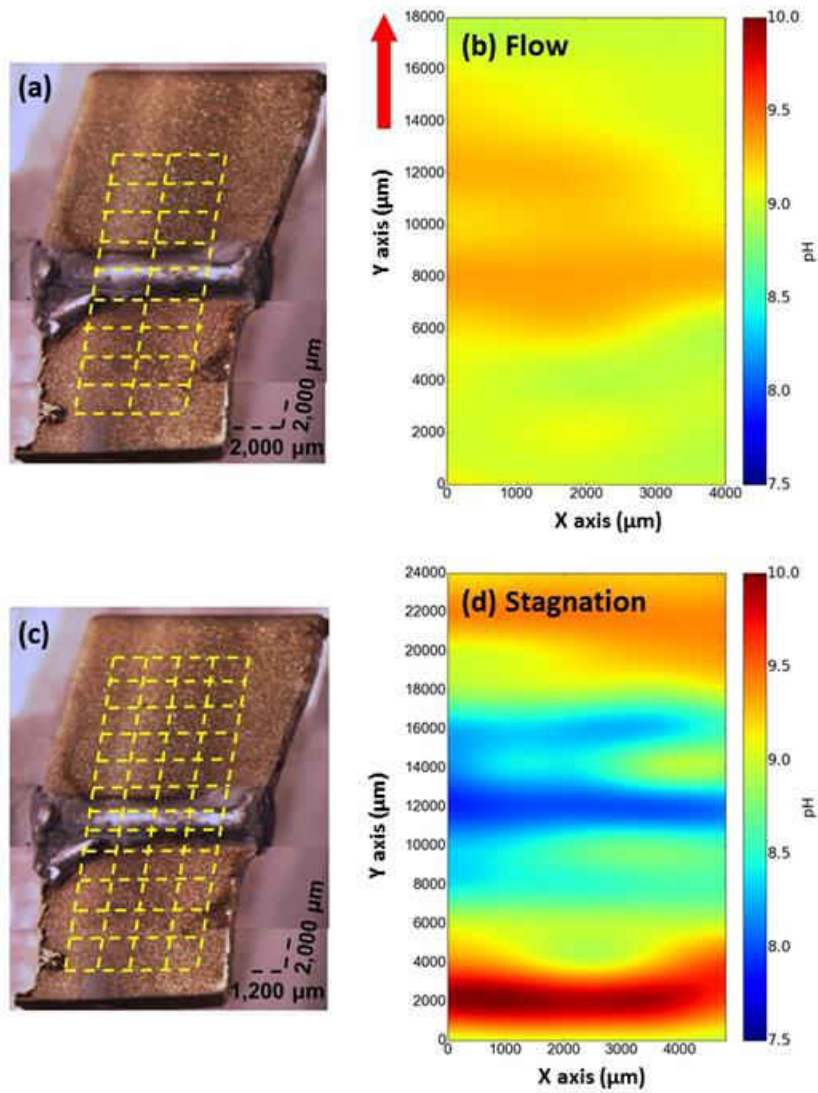


Figure 19. 2D pH contour map of 14 days aged brass/lead solder joint coupon. (a) 2D map grid with scale for flow condition, (b) 2D map with flow (2 ml/min), (c) 2D map grid with scale for stagnant condition, and (d) 2D map under stagnation. The pH in the bulk solution was 9.0.

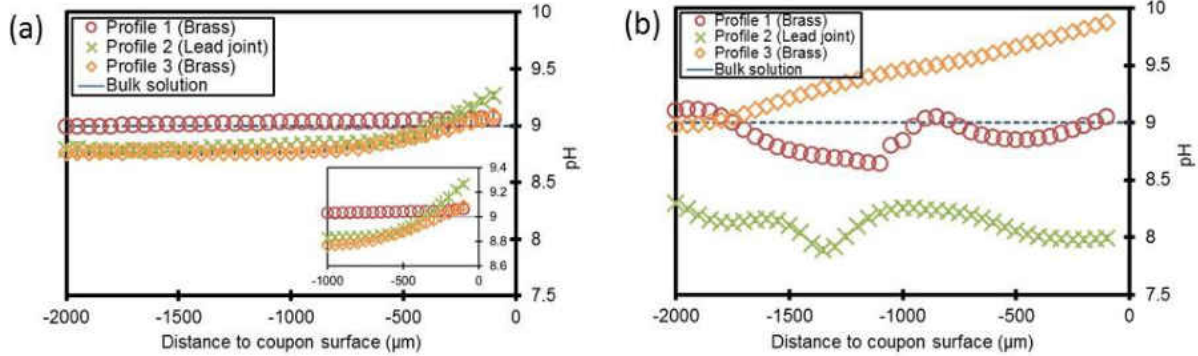


Figure 20. Measured representative 1D pH microprofiles of 14 days aged brass/lead solder joint coupon. (a) pH microprofiles under flow condition (2 ml/min) and (b) pH microprofiles under stagnation. The pH in the bulk solution was 9.0.

4.3.2. 2D pH shift on a brass-lead soldered joint coupon

Many studies showed lead leaching from solder by analyzing bulk solutions^{9, 86, 87}; however, only a conceptual description of the anodic and cathodic reactions has been provided and no direct measurements have been conducted. In this experiment, the brass-lead joint coupon was harvested after two weeks under flow condition. During this period, white colloidal particles were observed on and near the joint area. Surface characterization using SEM/EDS of the particles was failed due to the interference of other salt precipitates; however, the white deposits, mostly observed on the solder area, resemble lead (Pb) and tin (Sn) colloidal particles associated with the solder based on similar findings illustrated in previous investigations.^{43, 88} The feeding solution was gently flushed for five minutes over the coupon surface before profile measurements in order to avoid any interference from the particulate deposits.^{89, 90} The 2D pH map (Figure 19) clearly demonstrated the pH increase in lead joint (solder) under flow condition. While the pH at both brass ends was the same as the bulk pH, the pH increased from both brass ends to the joint “layer by layer,” reaching its maximum value of pH 9.4 at the left end of the lead connection. This pH

increase at lead surface under flow condition can be explained by the following: (1) micro-galvanic deposition corrosion,^{42, 91, 92} where zinc (Zn^{2+}) and cupric ions (Cu^{2+}) are released from the upstream and deposited on the lead surface forming micro-galvanic cells. This cathodic reaction occurred on the deposited copper causes a pH increase at the lead surface, releasing lead⁴²; (2) Free chlorine can reduce lead solubility with oxygen by forming hydrocerussite ($Pb_3(CO_3)_2(OH)_2$) or Pb (IV) oxides, increasing pH at the surface.^{55, 80, 93} The measured pH profiles in this work provided a direct evidence to these two theories. 4.2 mg (0.11%) weight loss was measured after exposing the coupon to the bulk water at a flow of 2 ml/min continuously for seven days, indicating the possible zinc and/or copper ions release. However, when water flow stopped and stagnant water contacted brass and lead solder (simulated soldered joint), the 2D pH surface showed a different phase as opposed to the pH shift under flow condition. Under stagnation, a corrosion cell was formed between metals in solder (Pb and Sn) and the brass, resulting in a relatively corrosive microenvironment at the solder surface which may contribute to rapid lead release.^{42, 91} The different surface pH dynamics between flow and stagnation were quantitatively determined for a galvanic solder coupon (Table 3). After three to four hours of stagnation, the lead surface became anodic with a pH drop to 7.9, while the pH on brass increased up to 10.0. The pH difference between cathodic area (brass) and anodic area (lead) was 2.1, and the average pH across the galvanic connection was 8.9 ± 0.51 .

1D pH profiles (Figure 20) measured at three different locations showed that under flow condition, the pH profile on the brass coupon was similar to the bulk water pH, while the pH on the lead joint increased from the bulk pH of 8.8 to 9.3 (ΔpH : 0.5). However, under stagnation, the pH on lead joint showed an opposite aspect. During the stagnation, the bulk pH dropped to 8.6; however, the pH on the brass increased up to 9.9, while the pH at the galvanic connection location

dropped further to 8.0 near the lead surface (Figure 20b). This observation along with 2D pH surface demonstrated that 1) under water stagnation, the galvanic connection significantly promoted a cathodic reaction at the brass contributing to pH increase, and 2) lead ions released at the joint could contribute to the formation of soluble complexes or insoluble precipitates that contain OH^- , Cl^- and SO_4^{2-} .⁹ The chlorine residual was $2.4 \text{ mg Cl}_2 \text{ L}^{-1}$ after the experiment. DeSantis *et al.*⁴⁴ showed deep corrosion of brass or copper piping immediately adjacent to soldered joint and summarized brass/copper materials behaving anodically when coupled with lead, contrary to conventional wisdom of commonly referenced galvanic series tables and standard electro-potential series. In this study, it was obvious that the 2D pH surface under stagnation was completely opposite to the 2D pH surface under flow condition, indicating that the water flow condition may be one of the most significant parameters controlling anodic-cathodic relationships of coupled metals in addition to water chemistry. It appeared that under flowing condition, micro-galvanic deposition corrosion^{42, 91, 92} or the formation of hydrocerussite ($\text{Pb}_3(\text{CO}_3)_2(\text{OH})_2$) or Pb (IV) oxides^{55, 80, 93} would be the dominant reaction, whereas under stagnation, galvanic corrosion releasing lead ion⁴² would be the main cause.

4.4. Conclusion

This work is the first to construct, by direct measurement, the 2D pH map to demonstrate large pH variation across a galvanic couple. The observations reflect galvanic interactions between lead solder-brass joints under stagnant water conditions. Under continuous flow conditions, surface pH was relatively uniform and close to the bulk water pH. However, under stagnation the surface pH varied by as much as 2.1 pH units. In the case of brass-solder connections, pH scanning images under flow and stagnation showed opposite pH changes over the solder surface, which

could be the possible different mechanisms of the lead corrosion process under flow and stagnant conditions. pH was notably lower at the solder surface while the brass surface pH was much higher. The galvanic connection between brass and lead/tin solder appeared to “protect” brass, but the corrosion of solder may be accelerated under stagnation. The differences in pH on the surface likely reflected anodic and cathodic regions across metals.

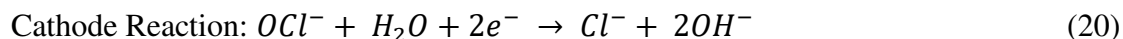
As practical implications from the study, pH in the bulk solution of aged brass pipelines may be identical with the pH near the metal surface, indicating that bulk monitoring would provide meaningful information on interfacial processes between aged brass and water. However, when it comes to the brass-lead galvanic joint under stagnation, the bulk pH monitoring as a corrosion assessment would not provide any information regarding the magnitude of corrosion at the interface of galvanic joints. In addition, this work demonstrated a new experimental method to directly measure pH in the proximity of the metal surface, which has never been successfully conducted previously. This measurement provides a direct evidence of localized metal corrosion mechanisms in a micro-environment, confirming what others have previously speculated or indicated by alternate "macro" methods.^{3,17,26-28} Future work will seek to collect more spatiotemporal microprofile data with regard to longer-term corrosion processes under various water conditions along with other important chemical profiles such as free chlorine (or monochloramine), oxygen, redox potential, lead, zinc, and phosphate as a corrosion inhibitor. The extension of the localized water chemistry measurements using microelectrodes will lead to better understanding of the corrosion mechanisms and validate existing theories.

CHAPTER 5: THE AFFECT OF ALKALINITY, FLOW, AND BULK PH ON INTERFACIAL MICROENVIRONMENT OF BRASS-LEAD GALVANIC COUPONS IN SYNTHETIC DRINKING WATER

5.1. Introduction

In DWDS, corrosion can cause pipeline damage, water leakage, and water quality degradation, which will eventually lead to distribution system structure integrity failure, national economic loss, and public health issues.⁹⁴ Corrosion process in DWDS is generally impacted by numerous factors, such as pH, alkalinity, hardness, DO, chlorine residual, chloride, temperature, corrosion inhibitor, and bacterial.⁹⁵ For the last couple of years, Flint water crisis became national news, and raise great attention of lead leaching in drinking water. This water crisis showed how water chemistry change can enormously affect the water quality, especially for lead in the DWDS.⁹⁶ In early February, the New York Times reported that in states of Ohio, Mississippi, North Carolina, and South Carolina, the lead concentration was exceeding the EPA action level by LCR.⁹⁶ Since 1987, the Safe Water Drinking Act (SWDA) established the regulation for the pipeline, prohibiting the use of any non-lead-free pipe, fitting, solder, or flux to water system that has direct contact to human beings.⁹⁷ However, before the SWDA, lead was considered as a common material for the plumbing system due to its longer life time over iron (35 years to 16 years) and its flexibility.⁹⁸ Even today, there are still great amounts of lead pipes and fittings serving at service line, especially in old homes. In corrosion mechanisms, galvanic corrosion is considered as one of the major reasons for the elevating lead concentration in the drinking water. The fundamental understanding of the galvanic corrosion is when two dissimilar metals directly connected together, the reactive end will be sacrificed while the noble end is being protected

through the reaction in drinking water.⁹⁹ The general concepts and theories galvanic corrosion process with lead is well studied through the years.^{18, 44, 99-101}



In the anode reaction, lead (Pb) can be oxidized to lead ions (Pb^{2+}/Pb^{4+}), creating a strong Lewis acid, which can lead to local pH drop at the lead surface with aggressive water environment.⁹⁹ While in the cathodic reaction, as can be seen from the equation (2) and (3), oxygen and chlorine species can both serve as the oxidizing reagents in the galvanic corrosion. However, as the pH increases in the solution, the oxidizing ability of oxygen decreased more than twice much faster compared to chlorine species theoretically.¹⁰² These reactions can be accelerated in a very short time under stagnation process.^{9, 94}

In previous studies, both field tests and laboratory examinations were performed with standard sampling methods, such as bulk water sampling with inductively coupled plasma mass spectrometry (ICP-MS) analysis, weight loss measurement, electrochemical methods (e.g., potential and current density), and surface characterization.^{10, 42-44, 76} These results illustrated the fundamental relationship between water chemistry and lead leaching process in the drinking water, such as evaluation of pH effect, chlorine residual effect, corrosion inhibitors, and chloride-to-sulfate ratio (CSMR), which generated insightful reviews between water quality control and galvanic corrosions.⁴²⁻⁴⁴ In these studies, the bulk solution monitoring, and sample collecting were main studying objects, and reviews were general and extensive. Even though interfacial studies of different parameters have been progressed through last 3 decades, the investigation of water chemistry in water-metal interface related to galvanic corrosion is limited.^{9, 103, 104} Lee et al. used

multiple microelectrodes to measure the free chlorine and monochlorine profiles penetrating through the biofilm in drinking water system, while comparing to the activity of the bacteria.¹⁰⁵ Church et al. (2015) successfully measured direct pH drop and monochloramine concentration decrease in a field pitting copper sample under stagnant condition using microelectrodes.¹⁰⁶

Another important perspective of galvanic corrosion studied in this research is deposit corrosion study. Hu et al. (2012) found that high concentration of dissolved copper ion can induce the lead release in the drinking water with formation of micro-galvanic cell at the lead pipe surface.¹⁰⁷ Later, Clark et al. (2015) proved this theory with more complete examination of surface characterization.¹⁰⁸ These results showed detail information about the morphology of metal surface during galvanic corrosion.

The objective of this work is to extend previous work (Chapter 4),⁹⁴ and aimed to perform extensive and profound experiments using multiple microelectrodes to evaluate the effect of flow, pH, alkalinity, oxygen, and free chlorine residual on the re-constructed galvanic connected coupon based on micro-environment. Experiments are conducted in various conditions, and real time *in situ* readings of pH and chlorine residual concentrations were obtained as the main assessment of the targeting environment. Thus, direct visual outcomes can be provided as the evidence for galvanic corrosion theory, as well as the actual surface chemistry change in the galvanic corrosion process. Also, using SEM observation, backscattered Electron (BSE) images and EDS can provide co-relation between water chemistry and coupon surface morphology. With the aid of microelectrodes, the interfacial chemistry between water and metal surface can be further studied as the fundamental knowledge for the galvanic corrosion.

5.2. Materials and Methods

5.2.1. Metal coupon preparation and condition

Metal materials used in this research were CDA 443 brass coupons (UNS C44300, admiralty brass, density $8.52 \text{ g}\cdot\text{cm}^{-3}$, Metal Samples Co., Munford, AL) and 50:50 Pb-Sn solder (38110, Forney). Brass coupons were cut into small fragments (1.6 mm thick \times 12 mm wide \times 14 mm long) and cleaned using a combination of two American Society for Testing and Materials (ASTM) coupon wash procedures: G31-72 and D2688-83.^{67,68} Then lead-tin was soldered in between two pieces of brass coupon and then applied with cold epoxy specimen mounting technique to provide a smooth even surface after polishing with 800 grit sandpaper (Figure 21a & 1b). Coupons were preserved in the sealed box before applying them to synthetic drinking water. During the experiment, these galvanic connected coupons were placed in an acrylic glass flow cell under 2 ml/min for measurements under different conditions such as pH, free chlorine residual, and dissolved inorganic carbon (DIC) (Table 5). After 2D mapping and microprofiling experiments under flow, a continuous stagnant condition was applied for 2 hours before the stagnation measurements. During the artificial water preparation, reagent grade chemicals (NaHCO_3 , Na_2SO_4 , and NaCl) (Fisher Scientific, Fair Lawn, NJ) were used to treat coupons. Free chlorine solutions were prepared from 6% sodium hypochlorite (Fisher Scientific, Fair Lawn, NJ) to $8000 \text{ mg Cl}_2\cdot\text{L}^{-1}$ as stock solution, then reduced to the target concentration in the 4-liter bulk synthetic water solution for the experiments. HCl and NaOH (Fisher Scientific, Fair Lawn, NJ) were used for pH adjustments. The bulk water was air-saturated before the pH adjustment and free chlorine addition. The synthetic water was then drove by peristaltic pump (Cole-Palmer, Vernon Hills, IL) under $2 \text{ ml}\cdot\text{min}^{-1}$ through the flow cell for the experiment. Fresh coupon will be pretreated under flow condition for one hour before the actual measurement.

Table 5. Experimental conditions for microprofiling and 2D mapping of galvanic joint coupons in synthetic drinking water.

Experiment groups	Flow Condition	pH	Free Chlorine (mg Cl ₂ L ⁻¹)	DIC (mg C L ⁻¹)
Ex1 - Control	Ex1.1 - flow	7	2	10
	Ex1.2 - stagnation	7	2	10
Ex2 - DIC	Ex2.1 - flow	7	2	50
	Ex2.2 - stagnation	7	2	50
Ex3 - Free Chlorine	Ex3.1 - flow	7	4	10
	Ex3.2 - stagnation	7	4	10
Ex4 - pH	Ex4.1 - flow	9	2	10
	Ex4.2 - stagnation	9	2	10
Ex5 - pH + DIC	Ex5.1 - flow	9	2	50
	Ex5.2 - stagnation	9	2	50
Ex6 - pH + Free Chlorine	Ex6.1 - flow	9	4	10
	Ex6.2 - stagnation	9	4	10
Ex7 Non-continuous stagnation	Ex7 - stagnation	7	2	10

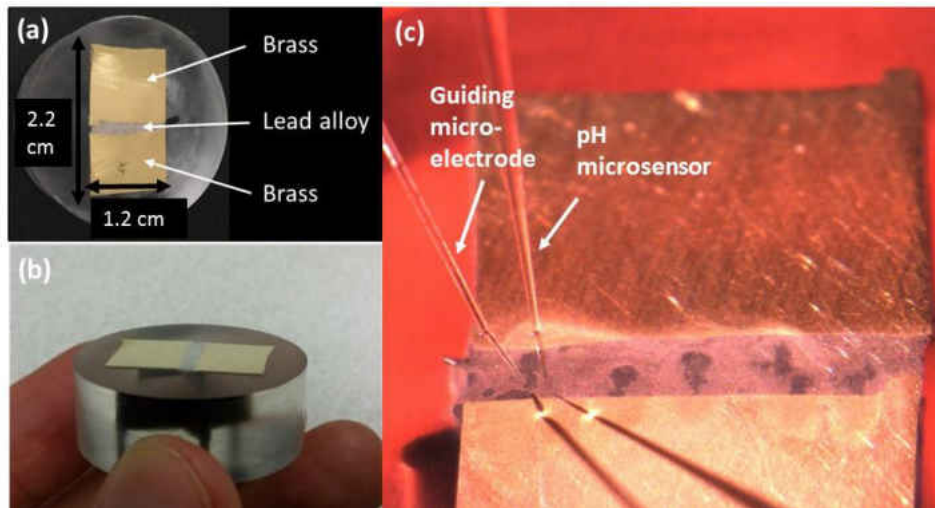


Figure 21. Galvanic joint coupons and microprofiling. (a) Vertical view of an epoxy specimen mounted galvanic joint coupon with scale specification, (b) Smoothness of the coupon by horizontal view, and (c) In-situ pH microprofiling near the coupon surface (100 μm) from the surface) using microelectrodes.

5.2.2. Micro-profile and 2D mapping setups

Multiple parameters were measured using different microelectrodes, including pH microelectrode (pH-10, 10 μm tip diameter, UNISENSE A/S, Denmark), free chlorine microelectrode (10 μm tip diameter, self-made), and oxygen microelectrode (O₂-50, 50 μm tip diameter, UNISENSE A/S, Denmark). Microelectrodes used in this research were mentioned in different researching fields and their performances have been validated in numerous experiments.^{70, 81-83, 94, 105} Each fresh coupon was placed in a transparent flow cell with desired water condition from Table 5 (i.e., pH 7.0, 100 mg Cl⁻·L⁻¹, 100 mg SO₄²⁻·L⁻¹, 10 mg C·L⁻¹ DIC, and 4.0 mg Cl₂·L⁻¹ free chlorine). The coupon was then pretreated in the synthetic drinking water for 1 hour under flow before the mapping process. During the pretreatment time, a well-calibrated microelectrode was connected along with a dip-type Ag/AgCl reference electrode (MI-401, Microelectrodes Inc., Bedford, NH) and the sensor tip was positioned by controlling 3D manipulator (UNISENSE A/S, Denmark) through microscope (World Precision Instruments, Sarasota, FL), which were operated by computer software.

In microprofile measurement, microelectrode tip was positioned 2,000 μm above the coupon surface, and stopped at 50 μm above the surface with 50 μm step for every measurement. The 3D manipulator was able to adjust the microelectrode at the exact height with precision of 1 μm . Due to the nature of different microelectrodes, there was a 15-second waiting time before the stabilization of the pH/Oxygen microelectrode and 5 seconds for free chlorine microelectrode in between each step. Every micro-profile was measured duplicate to ensure profiles were representable and reproducible.

In 2D mapping measurement, microelectrode tip was stationed 100 μm above the metal surface, and only moving horizontally across the coupon. As it can be seen from picture, a surface

area of 8400 μm (W) \times 20000 μm (L) was measured using microelectrode with distance intervals of 1200 μm (W) \times 2000 μm (L). The movement of the microelectrode was controlled by 3D manipulator with precision level to 1 μm , which helped to create uniform mapping after the data collection. A total of 112 data points was obtained for each 2D mapping image, which providing high resolution of chemistry profiles across the coupon surface. During each point measurement, there was a 15-second waiting time before the stabilization of the pH microelectrode and 5 seconds for free chlorine microelectrode. The mapping of pH and free chlorine concentration across the metal surface reflects the chemistry change over spatial and temporal perspective.

After the surface scanning using microelectrodes, data was imported and constructed using an advanced programming language (Python 2.7.10, Python software). And for quality control, free chlorine microelectrode calibration curve was pre- and post-calibrated with comparison to colorimetric test (HACH-8021) using DR 5000 spectrophotometer (HACH Co.). Also, pH microelectrode was pre- and post-calibrated in pH standard solution (Fisher Scientific, Fair Lawn, NJ).

5.2.3. Metal surface characterization

A ZEISS ULTRA 55 FEG SEM machine was used for galvanic coupon surface characterization purpose. During experiments, one of the coupon was conditioned in Table 5. (Ex1) environment and sacrificed for analysis. SEM images, BSE images, and EDS analysis were used for the element distribution under different magnification, which can provide surface morphology of the coupon, chemical elements distribution and identification. These results will be reflecting the lead particles migration and deposition during the experiment.

5.3. Results and Discussion

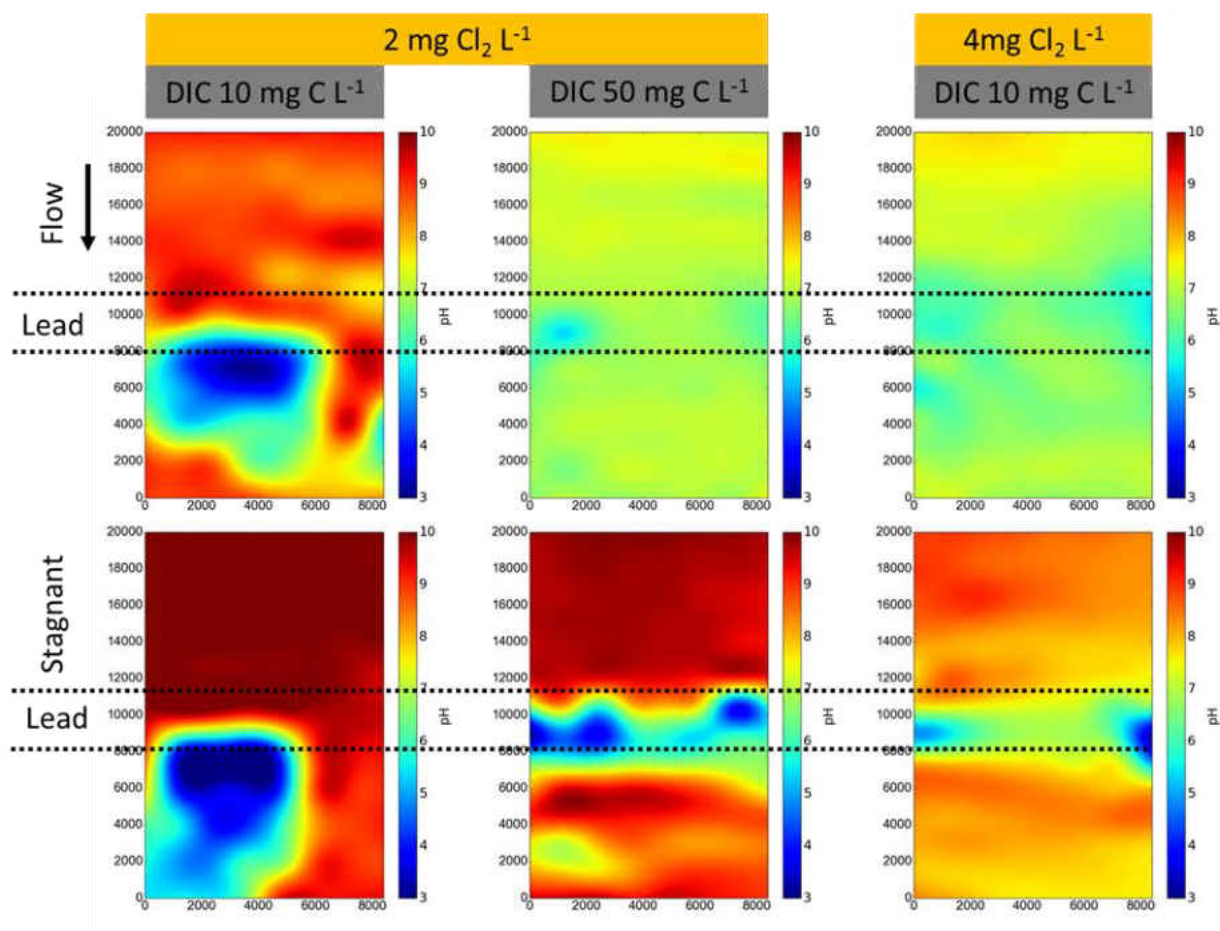


Figure 22. 2D mapping of pH on galvanic coupons surface under different flow, DIC, and free chlorine concentration (pH 7, $100 \text{ mg Cl}^- \text{ L}^{-1}$, $100 \text{ mg SO}_4^{2-} \text{ L}^{-1}$).

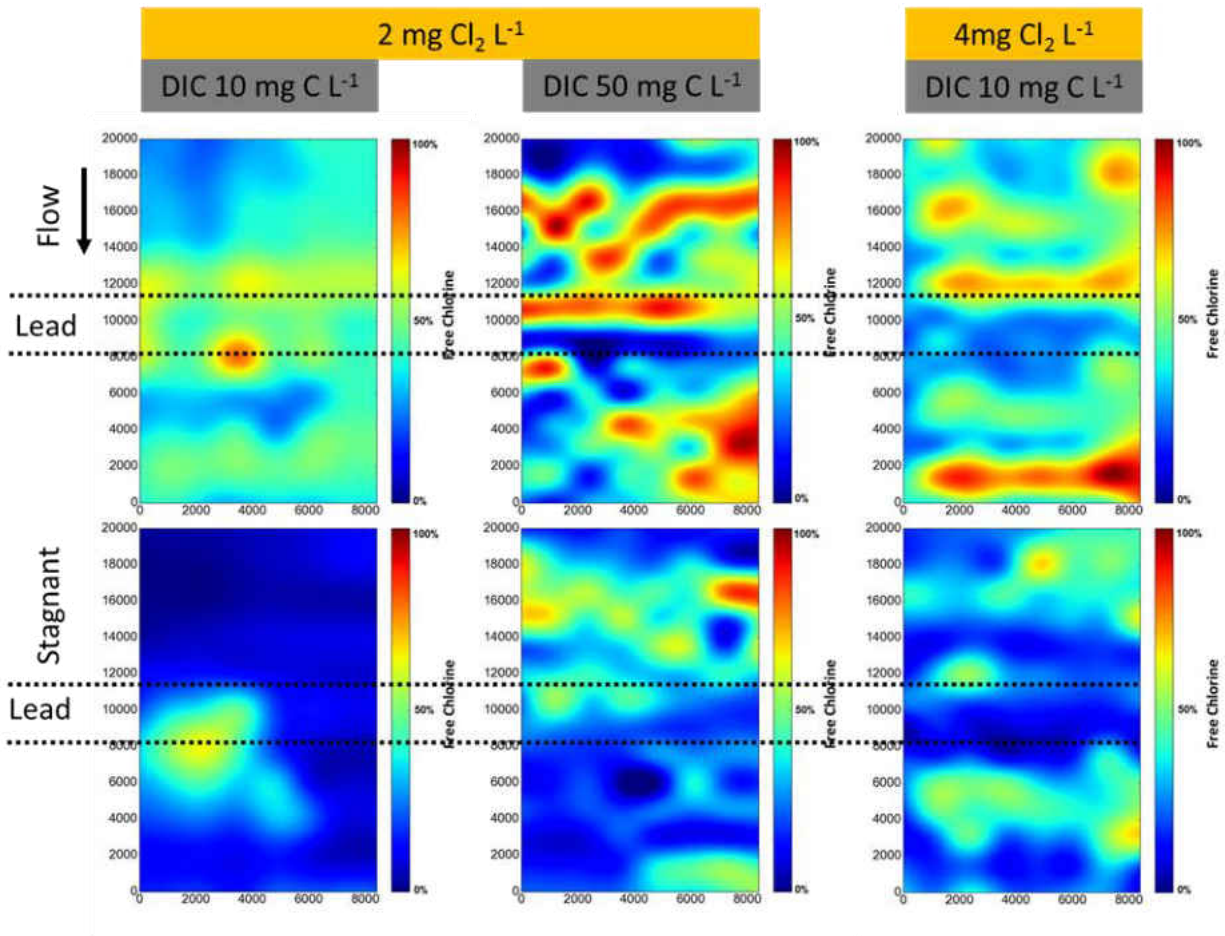


Figure 23. 2D mapping of free chlorine concentration on galvanic coupons surface under different flow, DIC, and free chlorine concentration ($\text{pH } 7$, $100 \text{ mg Cl}^- \text{ L}^{-1}$, $100 \text{ mg SO}_4^{2-} \text{ L}^{-1}$).

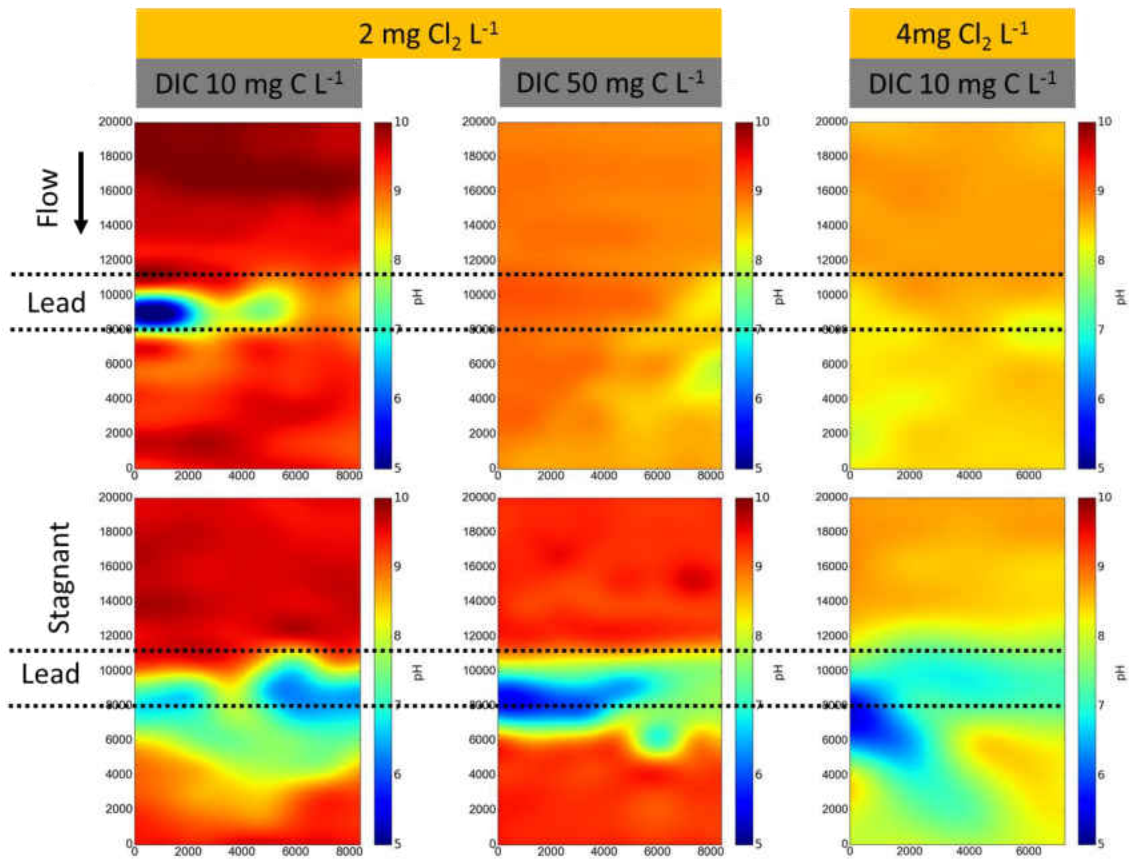


Figure 24. 2D mapping of pH on galvanic coupons surface under different flow, DIC, and free chlorine concentration (pH 9, $100 \text{ mg Cl}^- \text{ L}^{-1}$, $100 \text{ mg SO}_4^{2-} \text{ L}^{-1}$).

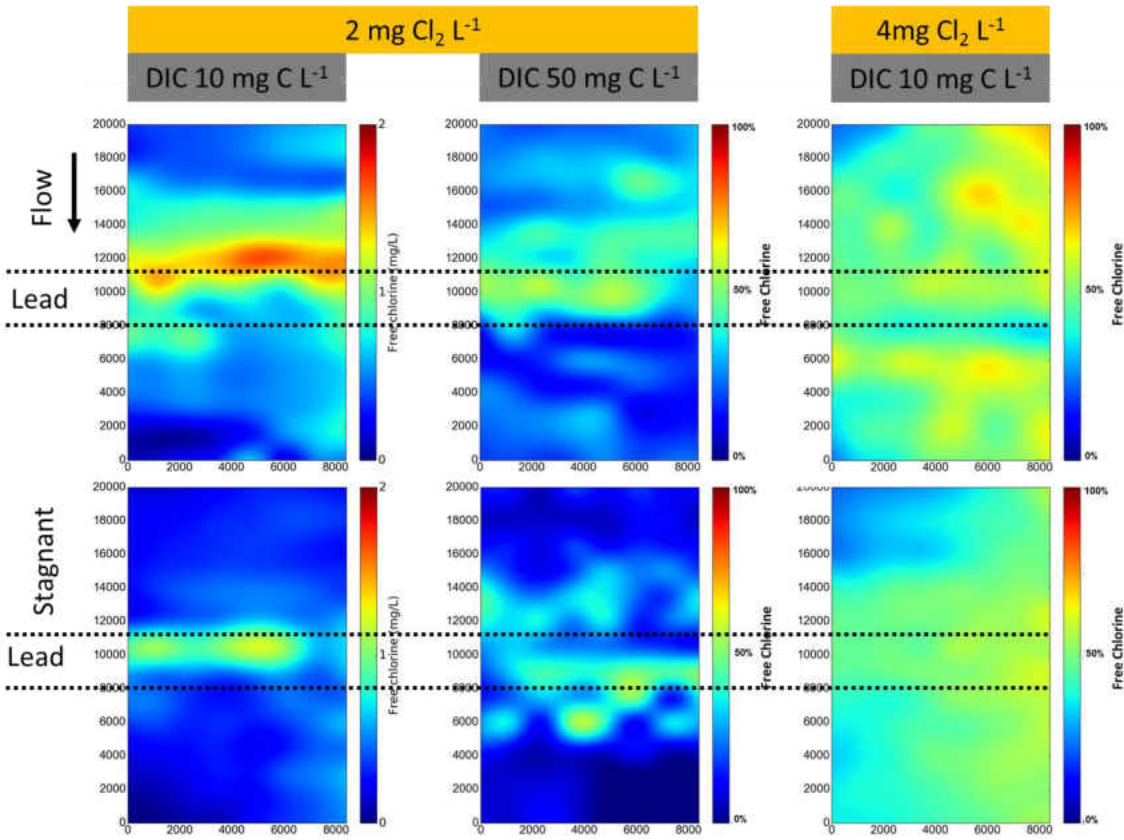


Figure 25. 2D mapping of free chlorine concentration on galvanic coupons surface under different flow, DIC, and free chlorine concentration (pH 9, $100 \text{ mg Cl}^- \text{ L}^{-1}$, $100 \text{ mg SO}_4^{2-} \text{ L}^{-1}$).

As it can be seen from Figure 22 - 25, two major parameters (pH and free chlorine concentration) were measured along with oxygen concentration (data not shown). Each label in Figure 22 is accordingly to Figure 24 with same back ground condition except for the pH difference. For example, Figure 22 & 23 showed pH and free chlorine concentration 2D mapping in both flow and stagnation under initial condition at pH 7, free chlorine at $2 \text{ mg Cl}_2 \cdot \text{L}^{-1}$, DIC at $10 \text{ mg C} \cdot \text{L}^{-1}$, with saturated oxygen and background chloride and sulfate ions, while the only difference for initial condition in Figure 24 & 25 was the pH adjustment from 7 to 9. This pH difference is applied to Figure 22 - 25 comparison.

5.3.1. pH effect

pH change is one of the most important factors in this galvanic corrosion study. Under pH 7 condition, low DIC (10 mg C·L⁻¹) and low free chlorine concentration (2 mg Cl₂·L⁻¹) showed dramatic pH variance under both flow and stagnant condition (Figure 22). The pH changes from 9.3 (inflow brass end) to 3.8 (outflow brass and lead interface) under flow condition. This pH difference increased under stagnation, with highest pH at 10.3 (inflow brass end) and lowest 2.8 (lead end). This 7.5 pH unit change occurred on a 2 cm × 0.84 cm area under 8 hours of experiment time. Similar pH diversity was found under pH 9 condition (Figure 24). The highest pH point reached 10 under both flow and stagnation on the brass ends of the coupon, similar to pH 7 condition, while the lowest pH was found at 4.7 under flow and 6.3 under stagnation. Even though the pH measurement at pH 9 stagnation condition was higher comparing to pH 7, reductions from the original pH were similar under different conditions. After increasing the alkalinity from DIC 10 mg C·L⁻¹ to 50 mg C·L⁻¹ and free chlorine concentration from 2 mg Cl₂·L⁻¹ to 4 mg Cl₂·L⁻¹ respectively, 2D mapping under flow showed that surface pH distribution was similar to the buffer pH in both conditions, while stagnation still resulted in localized pH drop on the galvanic joint with high pH increase on the brass end. Even though at different pH under stagnant condition, pH 2D mapping on the galvanic joint showed relatively similar pH unit drop from the original buffer, with averaging pH 3.1 from pH 7 condition and pH 5.9 from pH 9 condition. Free chlorine consumption in different pH appears to be more randomly across the coupon surface. In pH 7 conditions, free chlorine concentration depleted over 90% in some locations (Figure 23), which were similar to most conditions in pH 9 solution. However, in pH 9, DIC 10 mg C·L⁻¹, and 4 mg Cl₂·L⁻¹ solution, about 46% of free chlorine residual was remained at the coupon surface (Figure 25). Similar observations interfacial pH studies on galvanic metals were made in previous research.

Kuhn and Chan (1984) stressed the importance of studying interfacial pH change between liquid and solid phase.¹⁰³ Several works have been conducted to achieve the *in situ* measurement of pH at the interfacial area. Tada et al. (2004) measured pH distribution on zinc (Zn)/steel samples with potential method.¹⁰⁴ This research found drastic pH change across the coupled slide at about 1.5 mm above the surface. Katsounaros et al. (2012) used electrochemical method (Cyclic Voltammetry) to identify the effect of solid-liquid interfacial pH difference in buffered and unbuffered solutions.¹⁰⁹ Nguyen et al. (2010) performed micro-environment experiment regarding to galvanic corrosion between lead solder with copper pipe. Even though the microelectrode used in the study was 800 μm and the height was unclear, it indicated that much lower pH can be generated near the lead surface than in the bulk solution under the stagnation process in a very short period. The article mentioned that away from lead solder, pH tends to arise close to the metal surface.⁹ The dramatic difference of pH distribution between the lead joint and brass end can accelerate the galvanic corrosion process, which leads to more severe lead leaching in drinking water system. As Figure 22 showed, the leaching of lead could also result in pH drop at the outflow end due to the possible lead deposition from the flow condition.

5.3.2. Alkalinity effect

Sodium bicarbonate was used to control the alkalinity in this synthetic water system. In pH 7 condition under flow, it appears with higher alkalinity, the more evenly distribution of pH can be observed. Compared to DIC 10 $\text{mg C}\cdot\text{L}^{-1}$, DIC 50 $\text{mg C}\cdot\text{L}^{-1}$ showed a much less diversified surface from pH perspective, and free chlorine was much less consumed under flow condition (Figure 22 & 3). Yet after 2 hours, high pH difference and free chlorine consumption from brass end to galvanic joint end was observed from different DIC solution. Unlike DIC (10) condition,

DIC(50) localized pH drop was able to maintained only on the surface of lead-tin solder, with minimum effect on the brass end (Figure 22). This similar pH observation was also found in pH 9 different DIC comparison (Figure 24). Results showed that with increased alkalinity in the water, pH at the surface tends to be more uniformed under flow, and less drift effect under stagnation. Arnold Jr. (2011) reported that with higher alkalinity resulted less pH decrease near galvanic joint surface in a similar setup.¹¹⁰ Even though higher buffer capacity (50 mg C L^{-1}) still showed great pH decrease at the lead joint, the mitigation of low pH was restricted in the center compared to low alkalinity condition ($10 \text{ mg C}\cdot\text{L}^{-1}$).

5.3.3. Free chlorine residual effect

Free chlorine is used as one of main disinfectants in United States. It has a stronger oxidation ability compared to DO in the drinking water system. In this research, different free chlorine residual effects on galvanic corrosion were evaluated using the 2D mapping techniques. In pH 7 with low DIC ($10 \text{ mg C}\cdot\text{L}^{-1}$) in synthetic water, free chlorine consumption at the coupon surface in high free chlorine initial concentration ($4 \text{ mg Cl}_2\cdot\text{L}^{-1}$) was less compared to low free chlorine initial concentration ($2 \text{ mg Cl}_2\cdot\text{L}^{-1}$) from percentage viewpoint under both flow and stagnation (Figure 23). This observation in pH 9 condition was clearer (Figure 25). And with less free chlorine consumption at the surface, pH distribution difference between brass and galvanic joint was much less. Also, DO (DO) profiles were measured through the whole experiments (data not shown). There was no obvious DO decrease ($<1\%$) at the coupon surface, which indicate that free chlorine was the main oxidant for galvanic corrosion in these simulations. This result was consistent with previous work.⁹⁴

5.3.4. Flow effect

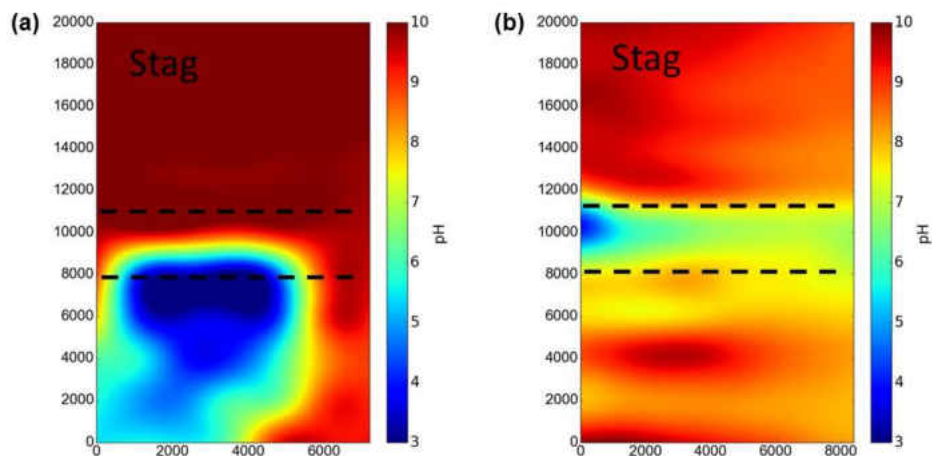


Figure 26. 2D pH mapping of (a) consecutive stagnation after initial flow condition vs. (b) stagnation without flow under pH 7, free chlorine $2 \text{ mg Cl}_2 \text{ L}^{-1}$, and DIC 10 mg C L^{-1} .

As it was mentioned in materials and methods section, stagnation measurements in this chapter were mainly conducted consecutively after the flow. *In situ* pH microprofiles showed more intense pH drop and more free chlorine consumption at the metal surface under stagnation compared to flow condition (Figure 22 & 24), providing insightful view for the pH change at the metal-liquid surface level of galvanic corrosion. During data analysis, another interesting point was found, at pH 7, observed low pH and free chlorine concentration distribution shifted from galvanic joints to downstream brass end (Figure 22) under low initial free chlorine and DIC concentration ($2 \text{ mg Cl}_2 \cdot \text{L}^{-1}$, $10 \text{ mg C} \cdot \text{L}^{-1}$). This comparable phenomenon was also found in 2D mapping at pH 9 under stagnation after the consecutive flow (Figure 24). Even though in the work by Tada et al. (2004), it was mentioned that in galvanic connections the pH distribution across two dissimilar metals may overlay in both surfaces under stagnation,¹⁰⁴ the 2D maps at both pH 7 and

9 conditions showed that this could also be affected by the flow (Figure 22 and 23) according to the deposition corrosion theory.^{107, 111} After suspecting this could be the impact from the flow, an additional control experiment was done for comparison. In Figure 26, it was shown that pH distribution under stagnation after consecutive flow (left), and pH distribution under stagnation without initial flow action. It was shown that without continuous flow, the pH reduction was localized mostly in the galvanic joint area, while coupon with initial flow, pH decreased not only on the galvanic joint as well as on the outflow end of the brass. These pH mappings gave direct evidence for the deposit corrosion theory that was mentioned before.

Surface characterization was performed on a coupon under flow condition at 2 ml/min for 2 hours (pH 7, DIC 10 mg C L⁻¹, and free chlorine 2 mg Cl₂·L⁻¹). After 2 hours of flow, the surface of lead joint already showed dissolution of the surface area with expansion of the white particles (Figure 27a), while brass surface stayed the same. However, after examined location i&ii in Figure 27a under SEM, noticeable white stripes and points can be observed in SEM images (Figure 27b), and with BSE images (Figure 27c), these figures indicated that different elements with high differential atom numbers were located on the outflow end of the brass surface. An EDS analysis was performed to identify these elements (Figure 27e). After increasing a random location in Figure 27c, EDS scanning results showed that high concentration of lead contained particles, along with copper, zinc and oxygen located in the targeting area. This implied that for deposit corrosion in galvanic corrosion, not only can copper deposit on lead pipe,¹⁰⁷ the deposit of lead particles could also result in the downstream of brass end, which can lead to localized pH drop in the downstream brass.

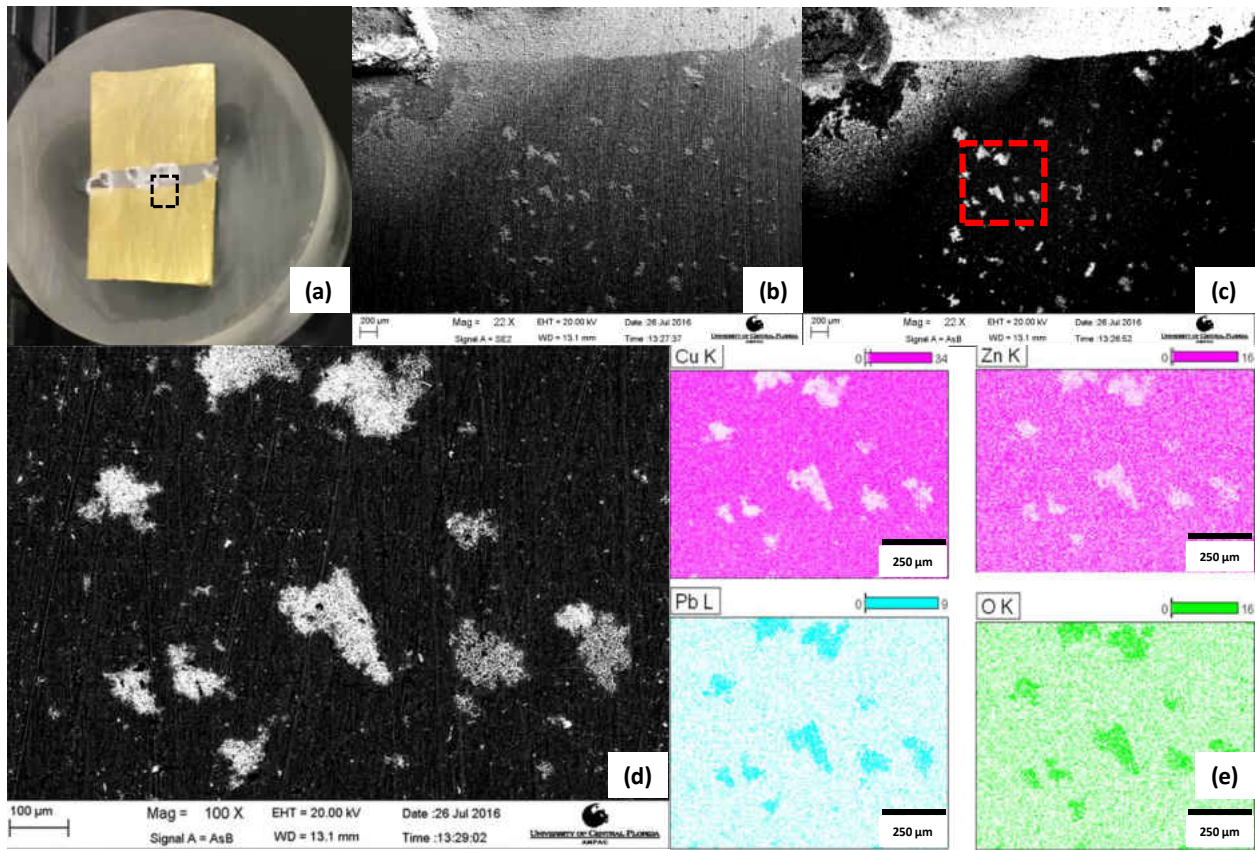


Figure 27. Surface characterization of galvanized coupon (after two hours of flow under pH 7, free chlorine 2 mg Cl₂ L⁻¹, and DIC 10 mg C L⁻¹, 100 mg Cl⁻ L⁻¹, 100 mg SO₄²⁻ L⁻¹). (a) Observation of corroded coupon and location for surface characterization; (b) SEM image of the selected location with magnification (×22); (c) Backscattered electrons (BSE) image of location with magnification (×22); (d) Magnification (×100) of BSE image of selected location in Figure 7c; (e) and element distribution using EDS.

5.3.5. Cross-sectional image

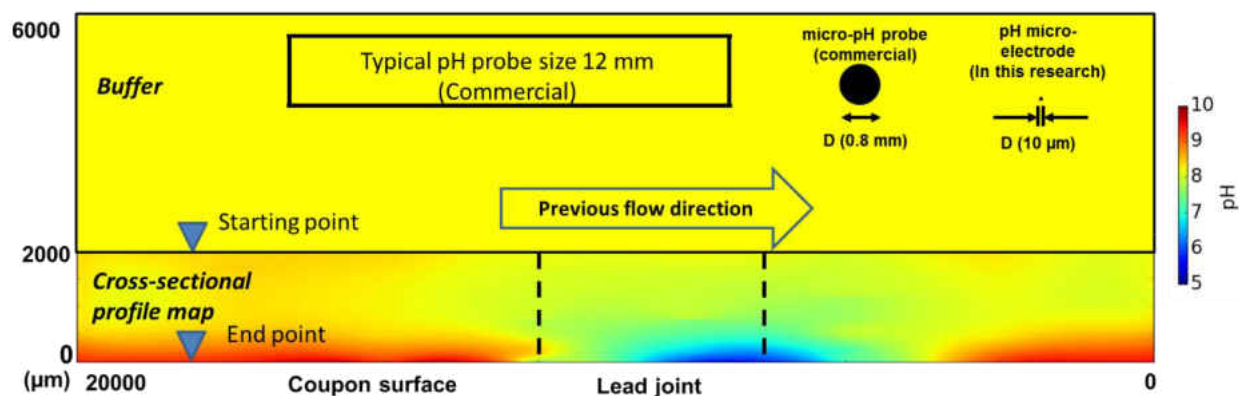


Figure 28. Cross-sectional 2D mapping view of pH profiles under stagnation ($\text{pH } 9$, free chlorine $2 \text{ mg Cl}_2 \text{ L}^{-1}$, DIC 50 mg C L^{-1}), with comparison among commercialized pH sensor tip size and this research pH tip size.

Kuhn and Chan (1984), and Tada et al. (2004) stressed the importance of studying interfacial chemistry change between liquid and solid phase, and how it differentiated from the bulk measurement.^{103,104} The dramatic change of pH from buffer to surface is one of the most important factors inspiring the production of this chapter. Visualization has always been an important illustration in environmental studies, and 2D mapping showed an innovative and organized technique of direct presentation of chemistry changes in the area which was under appreciated. As it was shown in Figure 28, comparison among commercialized pH probe, micro probe, and microelectrode was presented in the buffer solution. The commercialized probe was designed for the purpose of buffer monitoring with a diameter about 12 mm. The micro-probe, which is 0.8 mm tip pH meter (Microelectrode, INC), was used in Nguyen et al. (2010) research to study the micro-environment in galvanic corrosion.⁹ It was shown that pH distribution along the surface and comparison to the buffer, which was moderately close to “micro-environment” as it described in the manuscript. As for this research, a $10 \mu\text{m}$ pH microelectrode was used for the

2D mapping experiments, which was able to provide high resolution results for the micro-environment investigations. Thus, a multi-profiling experiment was done to present the difference between micro-environment *in situ* measurement to bulk monitoring. Twelve profiles from 2,000 μm above the surface to 50 μm above the metal surface were measured with 50 μm intervals during each measurement under Figure 23f condition (pH 9, free chlorine 2 $\text{mg Cl}_2\cdot\text{L}^{-1}$, DIC 50 $\text{mg C}\cdot\text{L}^{-1}$). With about 500 data points, high resolution image of pH distribution on a cross-sectional area above the metal surface was presented in Figure 26. It was visualized the diffusion boundary layer of pH, which was approximately 600 μm (extract from the profiles, data not shown) from brass end to galvanic joint end. While assuming 2,000 μm above the metal surface can be considered as the buffer pH, Figure 28 showed that micro-environment at the galvanic coupled surface varies dramatically from the original pH. Another important advantage of using microelectrode for the direct measuring is no disruption of the diffusion boundary layer, especially under stagnation, which is essential for micro-environments study. In Nguyen et al. (2010) research, it was found that pH can drop quickly near the galvanic surface in an hour, which also confirmed in this research.

In summary, the results in this chapter showed that galvanic coupons in pH 7 synthetic water with low DIC and low free chlorine concentration had the largest pH difference across the surface. With the presence of free chlorine, oxygen was not a main factor for galvanic corrosion process. The dramatic pH difference across the coupon size of 2 $\text{cm} \times 1 \text{ cm}$ was precisely recorded under hours of operation, it showed great advantages of using microelectrode to study galvanic corrosion mechanisms in micro-environment, separating itself from macro-environment investigation and buffer monitoring. This research showed systematic evaluations of galvanic corrosion in micro-environment under different situations/parameters. The results showed direct

evidence for previous works and theories with *in situ* measurements, the mitigation of lead particles with flow can result in dramatic pH drop in downstream of pipelines, which can cause further micro-cell galvanic corrosion or general corrosion in drinking water. This technique expanded the view of galvanic corrosion process and future corrosion studies.

CHAPTER 6: IN-SITU MONITORING OF Pb^{2+} LEACHING FROM THE GALVANIC JOINT SURFACE IN A SIMULATED CHLORINATED DRINKING WATER

6.1. Introduction

Due to its durability and flexibility, lead (Pb) has been widely used in drinking water delivery pipelines, premise plumbing systems, various fittings, and has been added to solder for making pipe connections.¹¹² However, from general corrosion and galvanic corrosion processes, and dissolution of lead minerals, lead can leach out of lead-containing materials into the drinking water resulting in elevated Pb^{2+} levels in drinking water, which may be correlated lead levels in blood.³⁹ Chronic exposure of lead can cause serious health issues related to brain development, liver, kidney, and bones, especially to children.³⁹ After establishing amendments of the Safe Drinking Water Act (SDWA) in 1986, United State Environmental Protection Agency (USEPA) proposed the use of “lead free” in drinking water pipelines, fittings, and solders, which were related to water for human consumptions under Section 1417.¹¹³ In 1991, Lead and Copper Rule (LCR) was issued by USEPA, regulating lead concentration in drinking water at taps should not exceeding 0.015 mg L^{-1} and copper concentration action level not exceeding 1.3 mg L^{-1} .¹¹⁴ Development and implementation of effective corrosion control is important to mitigate lead leaching from the source in household plumbing systems. Galvanic corrosion, however, is a complicated process and our understanding on the mechanism(s) related to lead leaching in chlorinated drinking water has largely been based on theory, bulk water analysis and forensic metal surface characterization. For example, inductively coupled plasma mass spectrometry (ICP-MS) analysis were used for lead measurement in many studies on galvanic corrosion in drinking water.^{10, 42-44, 76} Although ICP-MS

provide information of accurate lead concentrations, it is limited to the bulk concentration of soluble lead. For better understanding of the lead leaching and its transport from lead-containing metal surface, it is required to directly monitor the lead concentrations at the interface where corrosion occurs.

Potentiometric ion-selective electrodes (ISEs) have been known as an attractive, sensitive, and easily miniaturized tool for the analysis of heavy metal ions in aqueous samples¹¹⁵ and have been used for a variety of applications including clinical, food, environment, and industrial analyses.¹¹⁶⁻¹¹⁹ ISEs are often the preferred analytical tool due their high degree of sensitivity and selectivity, and are able to reach nanomolar and sub-nanomolar limits of detection (LOD), competing with other well-established and sophisticated analytical tools (e.g. ICP-MS and high-performance liquid chromatography mass spectrometry (HPLC-MS)).^{115, 120, 121} Particularly, polymeric-based ISEs offer the versatility to analyze a variety of ions by simple manipulation of the polymer membrane composition. A polymeric membrane is typically composed of three compounds: 1) an ionophore, which selectively binds the target ion, 2) an ion-exchanger, which maintains electroneutrality within the matrix and allows for permselectivity of ions and 3) a polymer matrix, which yields the support and mechanical stability of the membrane.¹²² The response mechanism does not require an external input of energy, as the resulting potential, or electromotive force (EMF) response is directly related to the potential difference across the hydrophobic and sample phase boundary of the ISE.¹²²

In this study, a micro-scale needle-type ion-selective electrode (micro-ISE) was developed using lead-selective liquid ion exchange (LIX) membrane for *in situ* monitoring of Pb²⁺ concentrations near the metal surface of galvanic joints in a simulated chlorinated drinking water environment. The miniaturization of the polymeric-based ISE's tip size to micrometer level (50–

100 μm) will not only make *in situ* monitoring possible in a small amount of sample volume, but can also provide real-time dynamic information about liquid-metal interfacial chemistry with high spatio-temporal resolution, which can be further interpreted by determining diffusion boundary layer (DBL), reaction rate, and flux of the ion species of interest. As soluble lead (Pb^{2+}) is pH-dependent, two-dimensional (2D) surface pH mapping was also performed using a pH microelectrode. It is expected that the direct measurement of lead concentrations near metal surface at micro-scale will expand the knowledge of galvanic corrosion and lead leaching mechanisms in drinking water distribution systems.

6.2. Materials and Methods

6.2.1. Reagents and Materials

Chemicals used in this study were in analytical reagent grade. Tert-Butylcalix-4 arene-tetrakis (N,N-dimethylthioacetamide) (Pb ionophore IV), sodium tetrakis 3,5-bis-(trifluoromethyl)phenyl borate (NaTFPB), 2-nitrophenyl octyl, high molecular weight polyvinyl chloride (PVC) and tetrahydrofuran (THF) were purchased from Sigma-Aldrich (Milwaukee, WI). The Pb^{2+} ISE cocktail was prepared by adding 5 mmol/kg of NaTFPB, 12 mmol/kg of Pb IV, o-NPOE (66.6 w%) and PVC (33.3 w%), dissolved in 1mL of THF and vortexed for 1 hour. Synthetic chlorinated drinking water solutions were prepared in distilled (DI) water with serial dilutions from the stock solution containing dissolved inorganic carbon (DIC), chloride (Cl^-), sulfate (SO_4^{2-}), and free chlorine (Cl_2) (see APPENDIX A for details).

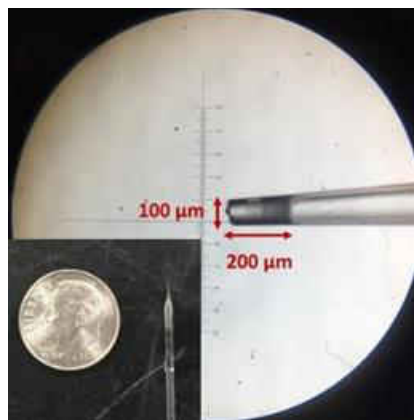


Figure 29. A finished Pb^{2+} micro-ISE with a tip size of $100\ \mu\text{m}$ and membrane length of $200\ \mu\text{m}$. (nickel for scale).

6.2.2. Fabrication, preparation and calibration of a lead micro-ISE

A flaming/brown micropipette puller (Model P-1000, Sutter Instrument Co., Novato, CA) was used to pull the glass micropipette (640815, O.D.: 1.5 mm, I.D.: 1.1 mm, 10 cm length, Warner Instruments, Hamden, CT). After opening the tip by a surgical grade tweezer (Sigma-Aldrich, Milwaukee, WI), the tip was silanized with N-N Dimethyltrimethyl-silyamine (Sigma-Aldrich, Milwaukee, WI) and the micropipettes were stationed at the glass micropipette holder (custom-made) and baked in the oven (Quincy Lab, Chicago, IL) at $180\ ^\circ\text{C}$ for 4 hours. After removing them from the oven, the micropipettes were kept in the dark in a desiccator for 1.5–2 hours. The silanized micropipette was then back-filled with an internal solution ($1\ \text{mM}\ \text{Pb}(\text{NO}_3)_2$ and $1\ \text{mM}\ \text{KCl}$) using fine injection needles (World precision instruments, MF28G-5) and the lead cocktail was inserted into the front tip by capillary force (2 min). An internal Ag/AgCl coated wire was prepared (see APPENDIX A for details) and inserted from the electrode back and immersed in the internal solution with 1 cm distance between LIX membrane and the internal reference electrode. The fully-assembled lead micro-ISE was then pretreated in $1.0 \times 10^{-3}\ \text{M}\ \text{Pb}(\text{NO}_3)_2$ solution at $25\ ^\circ\text{C}$ for overnight to achieve the equilibrium of the sensor. A commercial Ag/AgCl milli-electrode was

used as an external reference electrode. During profiling, the order of the lead micro-ISE assembly was followed by:

Internal Ag/AgCl | internal solution (1 mM Pb(NO₃)₂ and 1 mM KCl) | PVC membrane | test solution | 3.0 M KCl | external Ag/AgCl.

Finally, the finished Pb²⁺ micro-ISE was calibrated in the lead standard solution (Pb(NO₃)₂) with different lead concentrations (1.0×10⁻⁷–1.0×10⁻² M). Interference of different ions¹²³ such as sodium ion (Na⁺) was also evaluated during the calibration. Calibrations were conducted at pH 4.8 and 23 °C.

6.2.3. Microprofiling of lead concentrations using a lead micro-ISE

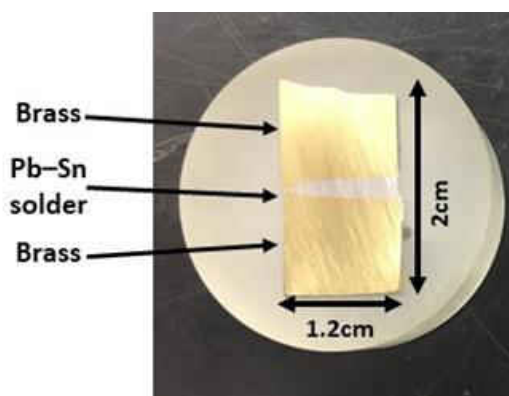


Figure 30. A specifically designed brass-lead galvanic coupon (2×1 cm) imbedded using a cold epoxy specimen mounting technique.

For microprofiling of lead concentrations using the fabricated lead micro-ISE, a fresh brass-lead galvanic joint coupon imbedded with cold epoxy specimen mounting technique (Figure 30) was prepared (see Appendix A for details) and immersed in the synthetic chlorinated drinking water solution (pH 7, free chlorine 2 mg Cl₂ L⁻¹, 100 mg L⁻¹ of Cl⁻ and SO₄²⁻, and DIC 10 mg C L⁻¹) for 1 hour before microprofiling. Microprofiles were measured under stagnation where pH

changes are found to be more significant compared to the flow condition⁹⁴ and thus more lead leaching was expected during the experiments. During the lead concentration microprofiling, the Pb micro-ISE tip was positioned at 2,000 μm above the lead joint surface in the synthetic chlorinated drinking water (Figure 31). After a steady electric signal (mV vs. Ag/AgCl) was obtained, the tip of the micro-ISE was positioned perpendicular to the metal surface area of interest using a three-dimensional (3D) manipulator (UNISENSE A/S, Denmark) and electronic signals were recorded at 50 μm interval from the bulk (2,000 μm) to the metal surface with every 15 seconds of electrode signal stabilization (total 10 minutes of duration for one profile). Profile measurements were duplicated to investigate whether the measured profile was reproducible and representable. Two consecutive profiles were measured at 1 hour and 2 hours after the coupon was immersed in the synthetic chlorinated drinking water. After lead microprofilings, surface pH at 50 μm above the metal's surface was measured at total 96 points (8×12) across the galvanic coupon (Figure 31a) and a 2D pH spatial map was constructed to investigate the correlation between pH and lead concentrations. The details on microprofile measurements using a microelectrode and the construction of 2D pH spatial map were described elsewhere.⁹⁴

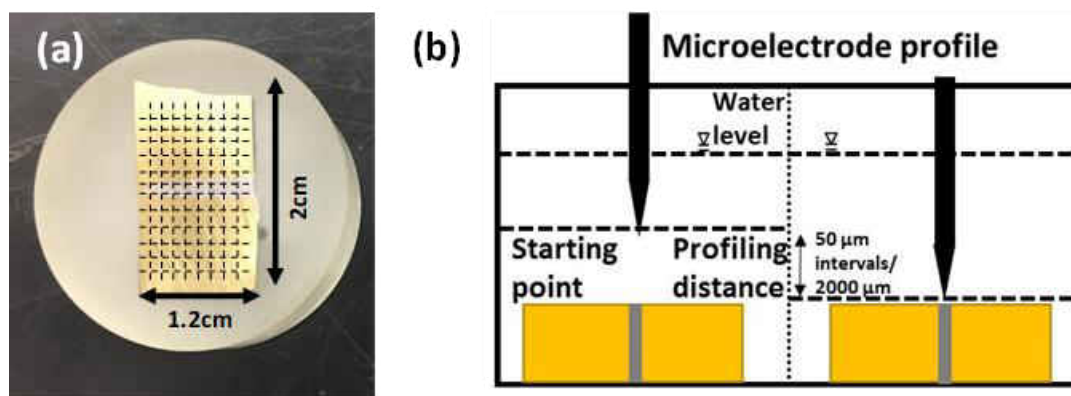


Figure 31. (a) 2D map grid (total 96 points: 8×12) with scale on the brass-lead galvanic coupon (2×1 cm) and (b) a schematic of microprofiling using a Pb^{2+} micro-ISE in a flow cell.

Continuous monitoring of Pb^{2+} leaching from the galvanic joint for 16 hours was also performed using the lead micro-ISE to evaluate long-term sensor performance. MINEQL+ (Environmental Research Software, Hallowell, ME) chemical equilibrium modeling system software was used to identify soluble lead ions depending on pH in various aqueous solutions. Bulk monitoring including free chlorine and Pb^{2+} concentrations, and pH was also performed over time. Lead (Pb^{2+}) concentrations in the synthetic water were validated using a Atomic Absorption Spectrometer (AAS) (Perkin Elmer AAnalyst 400 Flame, Waltham, MA). During the experiment, pre-calibration and post-calibration were performed for the correct measurements of Pb using the Pb micro-ISE. After completion of Pb^{2+} microprofiling, the coupon was sacrificed for the surface characterization using Raman spectroscopy (Renishaw RM 1000B Micro-Raman Spectrometer) to identify corrosion by-products.

6.3. Results and Discussion

6.3.1. Characterization of the developed lead micro-ISE performance

Figure 29 shows the finished lead micro-ISE with tip diameter of 100 μm . When Pb^{2+} cocktail successfully applied to the hydrophobic silanized microelectrode tip, a noticeable dark LIX membrane with a length of 200 μm was observed (Figure 29) The selectivity and sensitivity of Pb^{2+} ISE is greatly influenced (up to 1,000 times variance) by the ratio (w/w) between ionophore and PVC.^{124, 125} In this fabrication, PVC content was adjusted to 33% to optimize the sensitivity of electrode towards soluble Pb^{2+} and sensor life-time (one week). A tip diameter less than 50 μm was found to be difficult to have a sufficient length of LIX membrane for lead detection due to relatively high density of PVC (33%) in the cocktail.

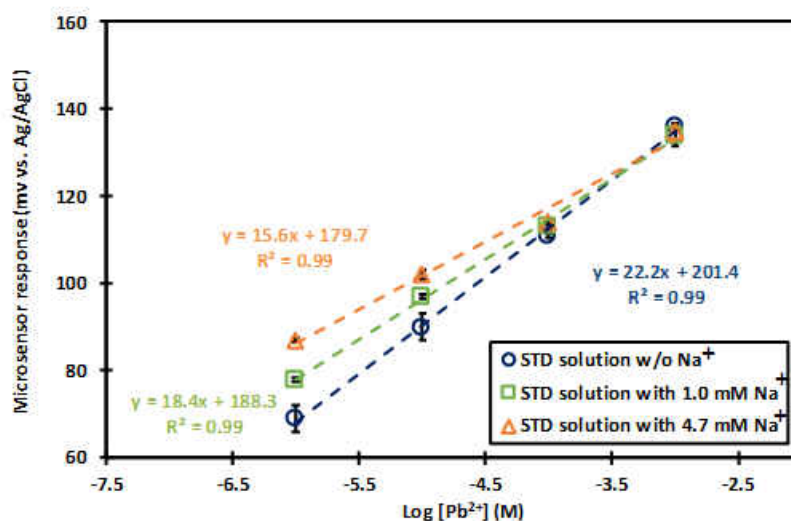


Figure 32. Calibration curves of a developed Pb micro-ISE with different Pb^{2+} concentrations. $\text{Pb}(\text{NO}_3)_2$ was used for preparing Pb standard solutions and NaNO_3 was used for testing ion interference (pH 4.8, 23 °C). The lead concentrations in the x-axis are the measured lead concentration by AAS.

Table 6. Pb^{2+} concentration comparison between AAS method and Pb^{2+} micro-ISE method

Methods	Average concentration (mg L^{-1})	S.D. (n=3)	R.S.D. (%)
AAS	2.06	0.0012	0.06
Pb^{2+} micro-ISE	2.13	0.09	4.23

S.D.: standard deviation; *R.S.D.*: relative standard deviation

The developed Pb^{2+} micro-ISE exhibited excellent linear relationship with various Pb^{2+} concentrations up to $10^{-3.0}$ M with the slope of 22.2 ± 0.5 mV decade $^{-1}$ which is similar with the theoretical value (22.4 ± 0.5 mV decade $^{-1}$) from Nernst equation. The Pb^{2+} micro-ISE showed good calibration curves over the wider working range of lead concentrations between 10^{-6} to 10^{-3} M (0.21 to 210 mg L^{-1}), compared to the previous Pb^{2+} ISEs fabricated using a similar configuration of the LIX membrane where the Pb^{2+} concentration detection range was $1.0 \times 10^{-4.1}$ to 1.0×10^{-2} M.¹²⁵ It was also found that the performance of the developed Pb^{2+} micro-ISE was comparable to AAS (Table 6). The LOD of the Pb^{2+} micro-ISE was 1.22×10^{-6} M (0.25 mg L^{-1}) and response time

of the sensor was less than 10 seconds. It is expected that the solubility of lead would be changed by the presence of other ions (e.g. Cl_2 , Cl^- , and SO_4^{2-}). In the range of pH 2–10 (DI water containing 10^{-5} M), a MINEQL+ simulation showed that Pb^{2+} solubility was soluble below pH 6.0 and the soluble lead species were changed to insoluble lead at pHs above 7.5 (Figure 33a). The developed Pb^{2+} micro-ISE followed the trend of the soluble Pb^{2+} concentrations, confirming that the micro-ISE measures the soluble Pb^{2+} ions in a solution (Figure 33b). The optimal working pH range for lead detection in DI water using Pb^{2+} micro-ISE is 2.0–7.0.^{123, 124}

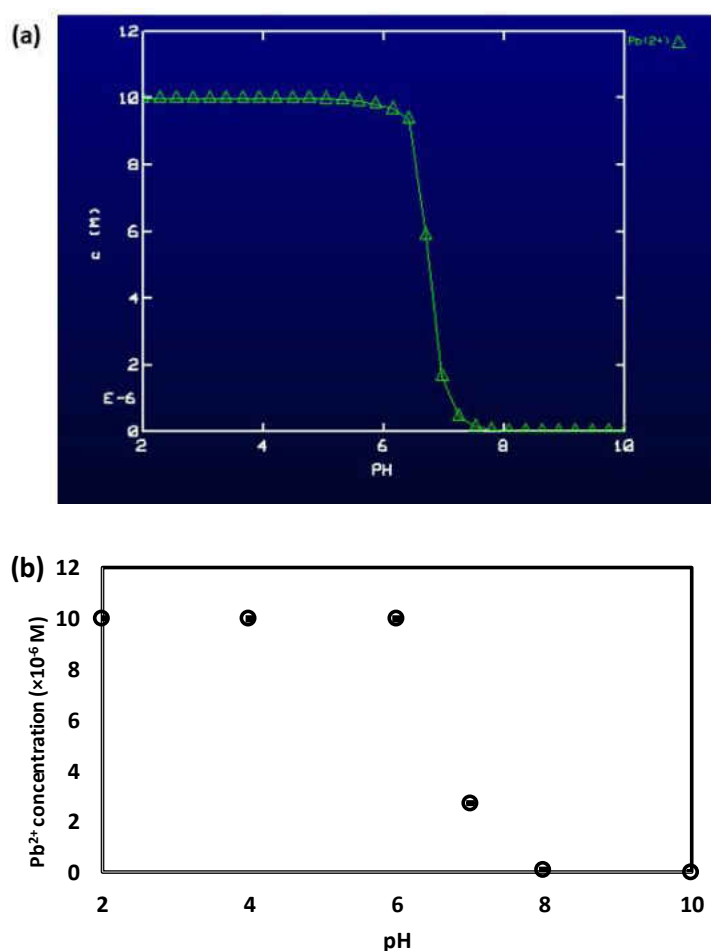


Figure 33. (a) pC-pH diagram simulated using MINEQL software and (b) measured data using a Pb^{2+} micro-ISE. 10^{-5} M Pb^{2+} in DI water was used for both the simulation and the experiment.

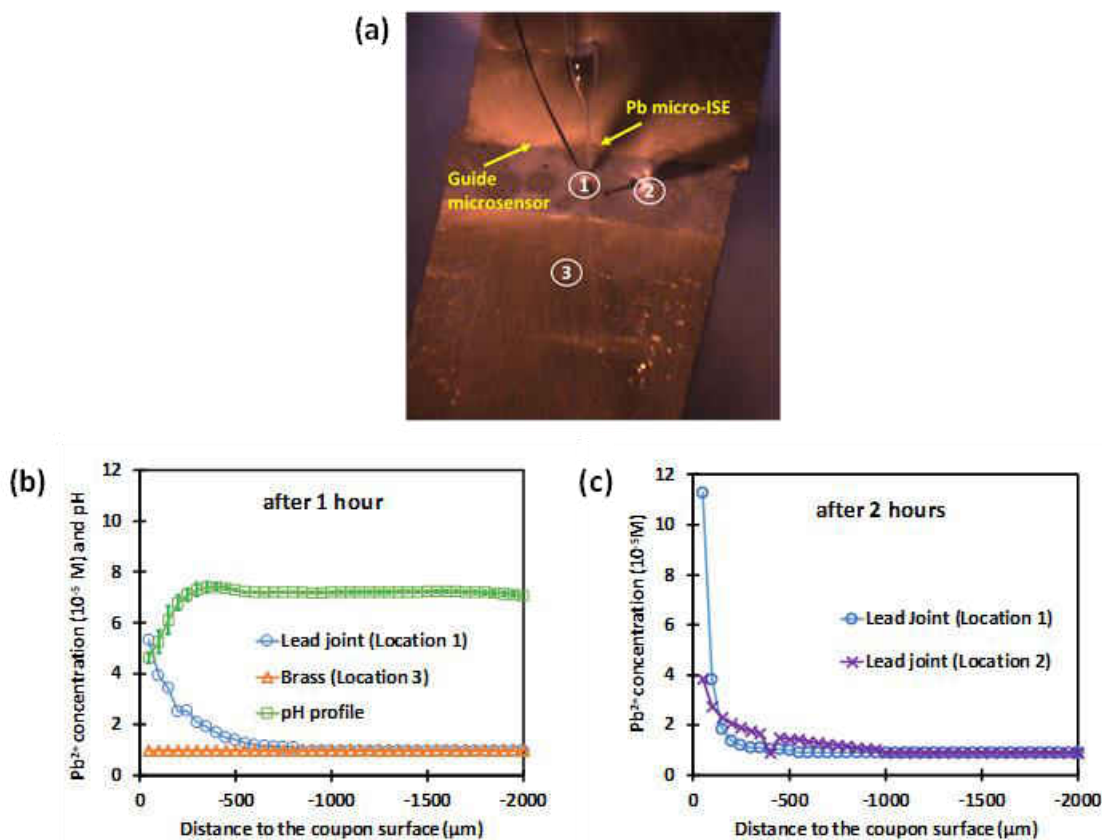


Figure 34. (a) *In situ* Pb²⁺ concentration microprofiling of a lead-brass galvanic joint coupon with three profiling locations, (b) Pb²⁺ concentration and pH microprofiles on location 1 and location 3 after 1 hour of stagnation, and (c) Pb²⁺ concentration microprofiles on location 1 and 2 after 2 hours of stagnation (pH 7, 23 °C, 2.0 mg Cl₂ L⁻¹, 100 mg Cl⁻ L⁻¹, 100 mg SO₄²⁻ L⁻¹, and DIC 10 mg C L⁻¹).

Based on the selectivity coefficient for lead ionophore IV, it seems that mercury (Hg) and silver (Ag) have the highest interference with lead due to their soft character and binding affinity to sulfur atoms.^{126, 127} Among the other possible ions interference, sodium ion (Na⁺) is known as one of the interfering ions for the lead concentration measurements.^{124, 125} As the selectivity coefficients of other positively charged ions (Mg²⁺ and Ca²⁺) are relatively low, only sodium ion interference was evaluated for the sensor performance. In the standard lead solution containing 1 mM Na⁺, the slope of the calibration curve slightly decreased to 18.4 mV decade⁻¹ from the original slope of 22.2 mV decade⁻¹ without Na⁺ (Figure 32) due to the increased ionic strength. Given that

sodium concentration in typical drinking water is approximately 20 mg L⁻¹ (1 mM),¹²⁸ the sensitivity changes was only about 82.9% with a good linear relationship with different Pb concentrations, indicating that the presence of the sodium would not affect the sensor performance. The ion interference is based on the lead ionophore IV used for Pb²⁺ micro-ISE fabrication and thus it is important to test ion interferences in every real environment. Therefore, in this study, a pre- and post-calibration was performed in the same solution of microprofiling for accurate Pb²⁺ measurements.

6.3.2. *Pb²⁺ microprofiles in a galvanic joint*

After the sensor characterization, the developed Pb²⁺ micro-ISE was deployed and measured soluble Pb²⁺ concentrations in the synthetic drinking water environment (pH 7, free chlorine 2 mg Cl₂ L⁻¹, 100 mg L⁻¹ of Cl⁻ and SO₄²⁻, and DIC 10 mg C L⁻¹). Figure 34 shows Pb²⁺ concentration microprofiles from 2,000 μm above to the metal surface at three different locations of the galvanic joint coupon and after one and two hours of stagnation. After 1 hour, Pb²⁺ concentration in the solution between 600 μm and 2,000 μm directly above the surface of location 1 was 9.89×10⁻⁶ M (2.05 mg L⁻¹). From the microprofiling (Figure 34b), the bulk water concentration was relatively constant until the until 600 μm above the lead joint surface and after 600 μm, the concentration of Pb²⁺ was dramatically increased as the micro-ISE moved closer to lead joint surface, indicating the build-up of Pb²⁺ ions from the corroding lead joint surface. DBL was approximately 380 μm. The soluble Pb²⁺ concentration at 50 μm above the lead joint surface (location 1) was 5.31×10⁻⁵ M (11.0 mg L⁻¹), which is 5.4 times greater than the bulk lead concentration. The increase of Pb²⁺ concentration was associated with the corresponding local decrease in pH (Figure 34b, location 1), increasing the solubility of Pb²⁺. The pH at location 1 was as low as 6.4 at a distance of 50 μm from the lead joint. The Pb²⁺ microprofile at the location 3

(3,000 μm downward from location 1) over the brass surface showed that lead levels were consistent throughout the distance from the bulk to the brass surface, indicating that there is no lead leaching from the brass surface (Figure 34b). The relatively low Pb^{2+} in this region was attributed to the minor amount of lead (0.07%) associated with the brass and the negligible change in pH at the metal surface (Figure 37) from the bulk (e.g. pH 7.0). The 2D pH mapping of the coupon surface (Figure 35) also shows that the pH near the cross section of 7,000 μm (Y-axis) and 4,000 μm (X-axis) was approximately 7.6 which was similar to the bulk pH after 1 hour of stagnation (Table 8). After 2 hours of stagnation, the surface Pb^{2+} concentration (50 μm above the surface) in location 1 increased to $1.13 \times 10^{-4} \text{ M}$ (23.4 mg L^{-1}), which is 12.5 times greater than the bulk lead concentration of $9.04 \times 10^{-6} \text{ M}$ (1.87 mg L^{-1}) (Figure 34c). DBL decreased from 380 μm to 220 μm , indicating the surface reaction of lead joint with high concentration of Pb^{2+} . In a different location (location 2) of lead joint, the Pb^{2+} concentration was $3.84 \times 10^{-5} \text{ M}$ (7.95 mg L^{-1}), which was lower than the concentration in location 1 which was attributed largely to the higher local surface pH (Figure 35) of approximately 7.0. The 2D pH mapping of the coupon surface (Figure 35) showed the dramatic pH differences between lead joint and brass surface. The maximum pH difference (ΔpH) between brass (the highest pH was 10) and lead (the lowest pH was 4) was 6 pH units, while the bulk pH was not changed throughout the experiments (Table 8). The pH difference between lead and brass reflected anodic (lead solder) and brass (cathodic) functions in the galvanic cell in the electrolyte (a simulated chlorinated drinking water) and subsequently directly impacted the solubility of lead in the respective regions.

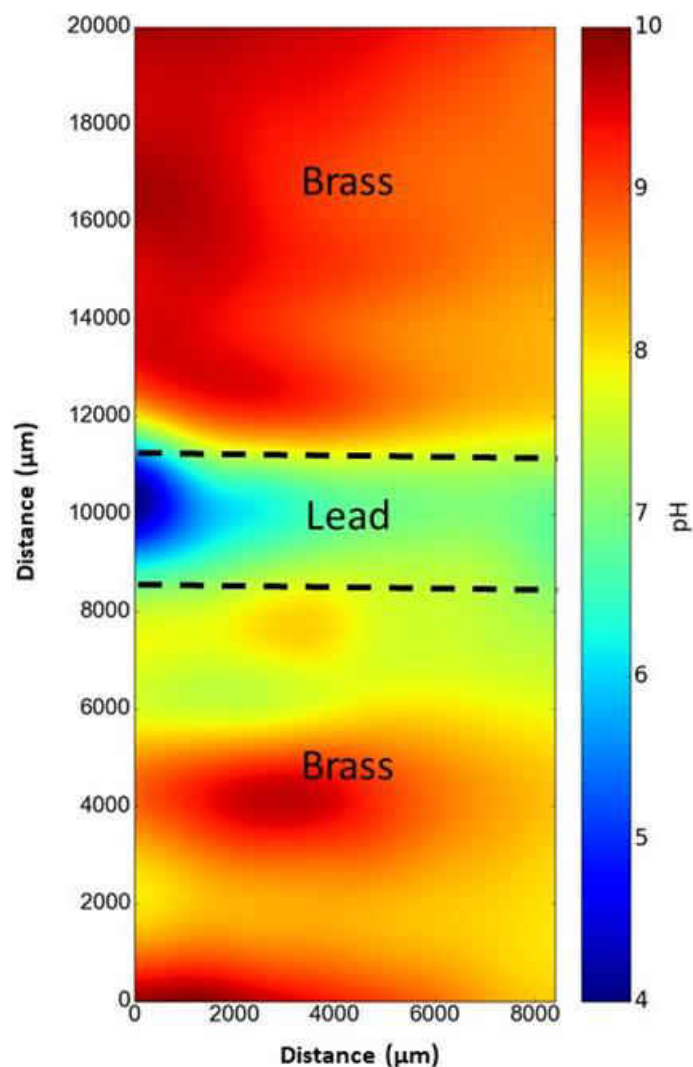


Figure 35. 2D mapping of pH on the galvanic coupon surface (50 μm above the surface) under stagnation (pH 7, 23 °C, stagnation, free chlorine 2 mg L⁻¹, 100 mg L⁻¹ of Cl⁻ and SO₄²⁻, and DIC 10 mg C L⁻¹).

The measured lead concentration profiles were further interpreted to determine reaction rates (k) and flux (J) related to the lead leaching process (Table 7). The reaction rates (k) and flux (J) in location 1 after 1 hour of reaction was $2.46 \times 10^{-4} \text{ cm s}^{-1}$ and $3.7 \times 10^{-6} \text{ mg cm}^{-2} \text{ s}^{-1}$, respectively. After 2 hours, the reaction rates (k) and flux (J) in location 1 was increased to $4.31 \times 10^{-4} \text{ cm s}^{-1}$ and $18.5 \times 10^{-6} \text{ mg cm}^{-2} \text{ s}^{-1}$ with decreased DBL, indicating the increased Pb²⁺ leaching from the lead joint over time and accumulation of lead at the metal surface. The predicted surface

Pb^{2+} concentration at location 1 was 2.8 times increased from 14.86 to 42.93 mg L^{-1} for 1 hour (Table 6). During the profiling, Pb^{2+} concentration in the bulk solution was relatively constant at 2 mg L^{-1} (Table 8).

At the lead joint surface, pH was randomly decreased across the strip, with lowest pH found in the left side at 4.0. ΔpH across the Pb/Sn alloy was 3.1 (pH 4.0–7.1). In contrast, the pHs on both brass sides were increased to maximum pH 10 in some locations. However, the initial and final pH in the bulk (before and after the lead and pH microprofile measurements) was 7.0 and 7.2, respectively. It is practically important to point out that although the pH in the bulk was 7.2 throughout the experiment, over time of the galvanic reaction under stagnation, ΔpH across the brass-lead joint coupon was around 6.0, indicating that there is significant difference of pH. Only at the local level and through the application of truly microelectrode measurement capabilities could this important and informative observation be recognized. This dramatic pH difference would be enough to initiate and continue cathodic-anodic reaction on the galvanic joint coupon. The low pH environment at the lead joint which was created by galvanic corrosion along with Pb^{2+} leaching could intensify the corrosion on both lead and brass surface.⁹ In this experiment, the measured lead concentrations between location 1 and 2 clearly demonstrated the pH effect on lead leaching processes. From the surface pH variance across the Pb/Sn alloy surface (pH 4.0–7.1), it is predicted that left side of the lead material would contribute more to the lead leaching to the bulk, indicating that the lead leaching is a non-uniform process. The mechanism of this randomly selective Pb^{2+} leaching is still unclear; however, the 2D map of pH changes and lead concentration microprofiles with two different locations (Figure 35) clearly showed that lead leaching is highly heterogeneous even in the small area of lead joint, and lower pH leads to higher lead concentration at the lead surface. Although ΔpH was only 0.6 between location 1 (pH 6.4) and 2 (pH 7.0), the

surface lead concentration was 4 times different between location 1 (42.93 mg L⁻¹) and 2 (11.61 mg L⁻¹). The increase in soluble Pb²⁺ concentrations after 2 hours showed the continuous oxidation-reduction reaction between the chlorinated bulk water and the galvanic joint, oxidizing pure solid lead to the soluble Pb²⁺ form before forming any possible complexes with background solution.¹²⁹

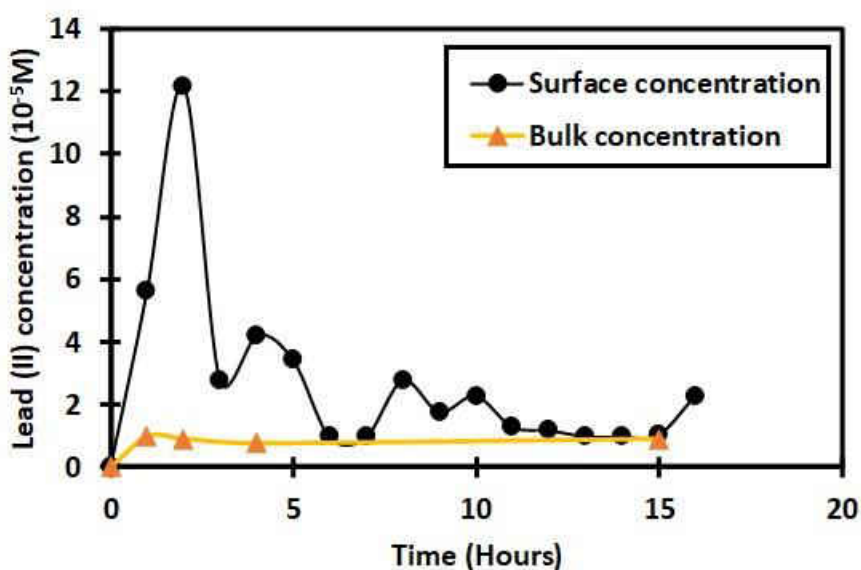


Figure 36. Continuous real-time monitoring of Pb²⁺ leaching from the lead surface (50 μm above the surface) and comparison of Pb²⁺ concentrations between lead joint surface and bulk. Another spike of a feed solution after 15 hours was performed (pH 7, 23 °C, stagnation, free chlorine 2 mg L⁻¹, 100 mg L⁻¹ of Cl⁻ and SO₄²⁻, and DIC 10 mg C L⁻¹).

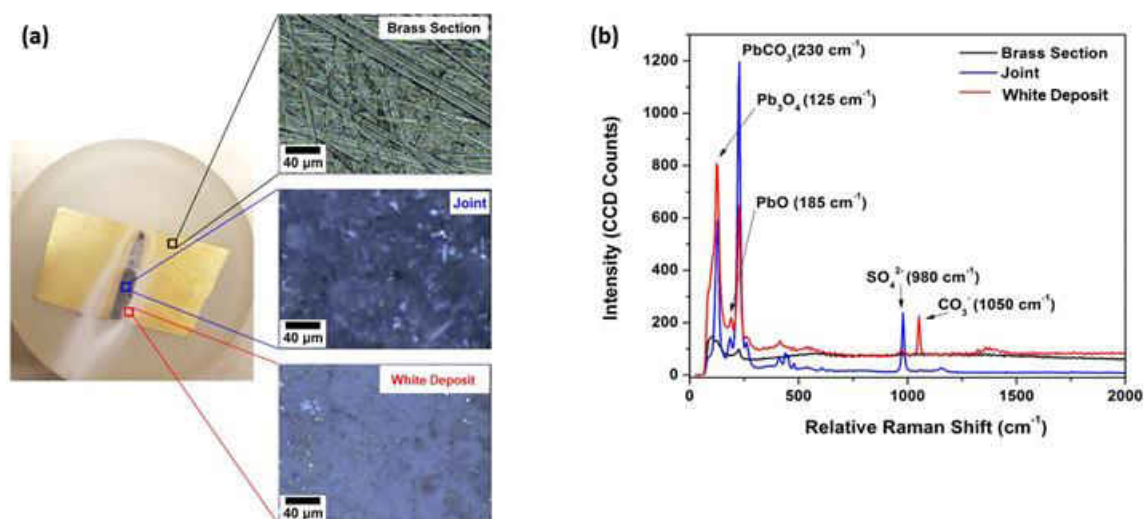


Figure 37. Metal surface characterization using Raman spectroscopy. (a) Optical images of (left) the part and (right) the brass, lead joint and region made of white deposit characterized with Raman spectroscopy. (b) Average Raman spectra obtained in each region described in (a) with bands corresponding to Pb₃O₄ (125 cm⁻¹), PbO (185 cm⁻¹), PbCO₃ (230 cm⁻¹), SO₄²⁻ (980 cm⁻¹) and CO₃⁻ (1050 cm⁻¹).

The continuous real-time monitoring of lead concentrations at 50 μm above the lead joint surface (location 1) was conducted using the developed lead micro-ISE over 18 hours and the surface lead concentrations were compared to the bulk lead concentrations over time (Figure 36). The monitoring result showed that the Pb²⁺ leaching from the lead joint occurs mostly at the first few hours (i.e. 3 hours) under stagnation. During the period, white corrosion by-products were deposited on the lead joint (Figure 38). After 12 hours of stagnation when free chlorine concentration in the solution was zero (measured by Hach method), the soluble Pb²⁺ near the lead joint surface was reduced similar to bulk level (1.58 mg L⁻¹). However, when replacing the feed solution with a freshly prepared synthetic chlorinated drinking water after 15 hours, the Pb²⁺ concentration immediately increased to about 2.28×10⁻⁵ M (4.71 mg L⁻¹) within 1 hour, indicating that free chlorine may be the primary contributor for lead leaching. Throughout the experiment, there was only a slight change of DO (DO) concentrations in the bulk and near the metal surface

(e.g. 8.5 to 8.4 mg O₂ L⁻¹) which were measured using DO microelectrodes.⁹⁴ The galvanic coupon was then sacrificed for surface characterization using Raman spectroscopy. Optical images of the coupon showed that on the brass section where it was protected due to high pH, the structure of the surface remains unchanged, while in the corroded lead joint and white deposit areas crystallized structure was observed (Figure 37a). After scanning these areas with Raman spectroscopy, the average Raman spectra showed peak of PbO, Pb₃O₄, and PbCO₃ formed on the lead joint and white deposit area (Figure 37b).¹³⁰⁻¹³² This observation shows that the consumption of free chlorine is the main contributor to the Pb oxidation in the galvanic corrosion process. The leaching of soluble Pb²⁺ at the liquid-metal interface occurred instantly after placing the fresh coupon in artificial water environment. This fast reaction was able to raise the Pb²⁺ concentration in the bulk solution at the first hour, and maintained at the same level through the entire experiment. Even though after 2 hours of stagnation, the highest Pb²⁺ leaching was observed (Figure 36), the concentration in the bulk was not changed significantly. The Raman analysis of white deposits on the coupon surface directly showed results of soluble Pb²⁺ into the formation of insoluble Pb complexes.

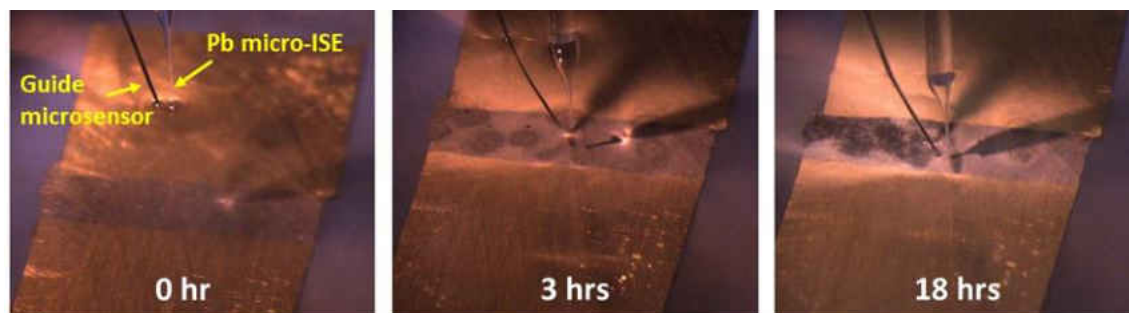


Figure 38. Spatio-temporal microprofiling of *in situ* Pb²⁺ measurements at the brass-lead galvanic coupon surface (pH 7, 23 °C, 2.0 mg Cl₂ L⁻¹, 100 mg Cl⁻ L⁻¹, 100 mg SO₄²⁻ L⁻¹, and DIC 10 mg C L⁻¹).

Table 7. Quantification of Pb leaching from microprofiles after 1 hr and 2 hrs.

Location	Time	DBL (μm)	Reaction rate, k (cm s^{-1})	Flux, J ($\text{mg cm}^{-2} \text{s}^{-1}$)	C_s (ppm)*	C_{bulk} (ppm)
Location 1	after 1 hr	380	2.46×10^{-4}	3.7×10^{-6}	14.86	2.05
	after 2 hrs	220	4.31×10^{-4}	18.5×10^{-6}	42.93	1.87
Location 2	after 2 hrs	320	3.46×10^{-4}	3.5×10^{-6}	11.61	1.87

(* C_s is the predicted surface lead concentration (ppm) at $0 \mu\text{m}$ based on the measured lead concentration at $50 \mu\text{m}$ above the metal surface with the assumption of same flux.)

Table 8. Monitoring of Pb^{2+} concentration, pH, and free chlorine concentration in the experimental solution over 24 hours.

Species/Time	0 hour	1 hour	2 hours	4 hours	24 hours
Pb^{2+} (mg L^{-1})	0	2.05	1.87	1.58	3.68
pH	7.0	7.3	7.2	7.1	7.4
Free chlorine ($\text{mg Cl}_2 \text{L}^{-1}$)	2.00	1.72	1.50	1.14	0.00

Overall, this study successfully developed and demonstrated an innovative tool for *in situ* monitoring of Pb^{2+} concentrations near metal surfaces with high spatial resolutions. This is the first to measure lead concentrations directly near (within $50 \mu\text{m}$) the galvanic joint surface along with corresponding pH measurements at same resolution. Although the continuous monitoring for months may not be possible due to the inherent short life time (1 – 3 days) from evaporation of the liquid membrane,¹³³ the real-time monitoring for a certain duration (e.g. 16 hours) seems to be enough to identify the trend of lead leaching from the galvanic joint under various water/metal conditions with further experimental plans. It is expected that the application of this novel

technique of lead detection using a microelectrode technique will provide better understanding of lead corrosion and leaching in drinking water distribution plumbing systems and elucidate the related galvanic corrosion mechanism along with other microprofiles of DO, pH, free chlorine, oxidation-reduction potential (ORP), and zinc (for brass) for improving corrosion control strategies.

CHAPTER 7. SUMMARY

In the last four years of work, my research has been mainly focused on the corrosion mechanisms investigation using different microelectrodes. Microelectrodes showed steady and dramatic chemistry change on the metal-liquid interface of uniformed corrosion on brass and cement coupon, and heterogeneous corrosion on galvanic joint. Microelectrodes, commercial and self-made, were successfully utilized to fulfill the objectives and assumptions of each experiment.

In the brass and cement corrosion experiment. At initial stage, brass corrosion in free chlorine was slower than brass in monochloramine through observation, with selective leaching of zinc on brass surface observed throughout the experiment. A “Fiber structured” zinc compounds was formed at pH 7. Oxygen at the brass surface showed much greater decrease under the reduced-mass-transfer condition. Cement dissipation was expected at the start of the experiment with pH increased at the surface and weight loss in the end of the experiment.

During the galvanic joint experiment, the methods evolved greatly throughout the entire experiment stage, from 2D mapping on a rough coupon surface to epoxy mounting fabricated surface, and from EXCEL data processing to python code processing. The results showed detail and dramatic chemistry change on the liquid-metal interface. Under both flow and stagnant condition, pH increased to maximum 10 at the both end of the brass. In the galvanic joint, pH decreased under different flow conditions. At pH 7, pH varies from 2.8 to 10.3 across the surface of a single coupon. There was little oxygen consumption observed during the experiment, indicating that free chlorine served the main contributor as the oxidant to the chemistry reaction. The dramatic local pH can be a great concern for the drinking water pipeline corrosion, promoting galvanic corrosion and accelerating pitting corrosion. With this newly introduced methodology, it

can be extended in other important water quality parameters in the drinking water, such as lead, zinc, and phosphate profiling using microelectrodes for corrosion studies.

In the lead micro-ISE experiment, an in-situ lead monitoring method was developed for liquid-metal interface at a brass-lead galvanic joint in a simulated chlorinated drinking water. The developed lead micro-ISE (100 μm tip diameter) showed excellent performance toward soluble lead (Pb^{2+}) with the sensitivity of $22.2 \pm 0.5 \text{ mV decade}^{-1}$ and limit of detection (LOD) of $1.22 \times 10^{-6} \text{ M}$ (0.25 mg L^{-1}). The response time was less than 10 seconds with a working pH range of 2.0–7.0. Using the lead micro-ISE, lead concentration microprofiles were measured from the bulk to the metal surface over time. Combined with two-dimensional (2D) pH map, this work clearly demonstrated that lead leaching at the metal surface is non-uniform and lower surface pH leads to higher lead leaching from the surface. Once significant pH variation (ΔpH : 6.0) was developed across brass-lead joint coupon, even a small pH change (ΔpH : 0.6) within the Pb/Sn alloy resulted in 4 times different surface lead concentrations ($42.93 \text{ vs. } 11.61 \text{ mg L}^{-1}$) and 5 times different fluxes ($18.5 \times 10^{-6} \text{ vs. } 3.5 \times 10^{-6} \text{ mg cm}^{-2} \text{ s}^{-1}$). Continuous surface lead leaching monitoring and surface characterization found that free chlorine is the primary contributor to lead leaching.

CHAPTER 8. FUTURE WORK

The points below are proposed as possible contents for future research:

8.1. Phosphate sensor development

Co based phosphate sensor has been developed by other researchers in previous years, and results showed multiple application of phosphate microelectrode in drinking water system.¹³⁴ Phosphate as an important component in drinking water pipeline corrosion inhibitor has been applied to many drinking water facilities. The development of a phosphate sensor will allow more quantification in corrosion control strategies. Based on fundamental knowledge of electrochemistry, more experiments need to be focused on pH effect, oxygen and ion interference, which can greatly improve the sensor's performance in a complicated drinking water system.

8.2. Chloride to sulfate mass ratio (CSMR) experiment

Chloride to sulfate mass ratio was proposed by other researchers which indicating it as a major part of corrosion mechanism.⁹ However, this theory was mainly focused on the bulk monitoring, along with elemental analysis. The surface chemistry change was not emphasized due to the lack of techniques for investigation. Based on the fundamental knowledge to this specific matter, liquid-metal interface investigation can improve the understanding of corrosion mechanisms under different water environment, which can further improve the theory regarding to the corrosion process. The results of CSMR experiment with microelectrodes can visualize and quantify the chemistry change over the metal surface. The behavior of corrosion in drinking water varies to different conditions, and microelectrodes will be able to help and model pipeline reaction even under extreme environment.

**APPENDIX A: SOLUTION PREPARATION, MICROELECTRODES
FABRICATION, AND CALCULATION**

A chlorinated artificial water solution preparation

Stock solution was prepared with NaCl, NaHCO₃, and Na₂SO₄ (Fisher Scientific, Fair Lawn, NJ) and was diluted proportionally for the lead profile measurements in a 20 L feeding solution with a final concentration of 10 mg C L⁻¹, 100 mg Cl⁻ L⁻¹ and 100 mg SO₄²⁻ L⁻¹. Free chlorine solutions were prepared by diluting 6% sodium hypochlorite (Fisher Scientific, Fair Lawn, NJ) to 8,000 mg Cl₂ L⁻¹ as stock solution, then diluted to the 2 mg Cl₂ L⁻¹ in the bulk test water solution for the experiment. The free chlorine concentration was validated by a colorimetric test kit (Hach-8021) and a DR 5000 spectrophotometer (Hach Co.). HCl and NaOH were used for pH adjustments to pH 7. The bulk water was air-saturated before the pH adjustment and free chlorine addition.

Ag/AgCl internal reference electrode fabrication and preparation

The Ag/AgCl internal reference electrode for the connection of Pb micro-ISE was prepared manually in the laboratory. An 8-cm silver wire (0.25 mm diameter, Sigma-Aldrich, Milwaukee, WI) was cut and connected against graphite rod. The brownish AgCl was formed by electroplating the Ag wire 1 M HCl (Fisher Scientific, Fair Lawn, NJ) at 4.5 V for 10 minutes. The typical distance between the LIX membrane and the Ag/AgCl internal reference electrode is 1 cm.

Brass-lead galvanic joint coupons

Two small pieces of brass coupon (DCA 443, admiralty brass, Metal Samples Co., Munford, AL) were cleaned using a combination of two American Society for Testing and Materials (ASTM) coupon wash procedures: G31-72⁶⁷ and D2688-83⁶⁸ and then connected to each other with 50:50 lead-tin (Pb-Sn) solder (38110, Forney). Then after polishing with 800 grit sandpaper, a cold epoxy specimen mounting technique was applied to the brass-lead soldered galvanic joint coupon to provide a smooth even surface throughout the coupon area for microprofiling.

Mass flux and reaction rate determination

Using measured Pb²⁺ concentration microprofiles, the mass flux (J) and reaction rate (k) were calculated from Fick's first law¹³⁵:

$$J = -D \frac{dC}{dz} = -D \frac{C_1 - C_2}{z_1 - z_2} = kC_s \quad (\text{Eq. 1})$$

where J is the mass flux (mg/cm²·s) of constituent (Pb²⁺), D is the coefficient for the species (9.45×10⁻⁶ cm²/s for Pb²⁺),¹³⁶ dC/dz is the concentration gradient with depth (mg/cm⁴), C₁ and C₂ are two different concentrations at different depth (cm) z₁ and z₂ within the diffusion layer

(mg/cm^3), C_s is the estimated concentration at $0 \mu\text{m}$ on coupon surface (mg/cm^3), and k is the reaction rate (cm/s).

Experiment setups

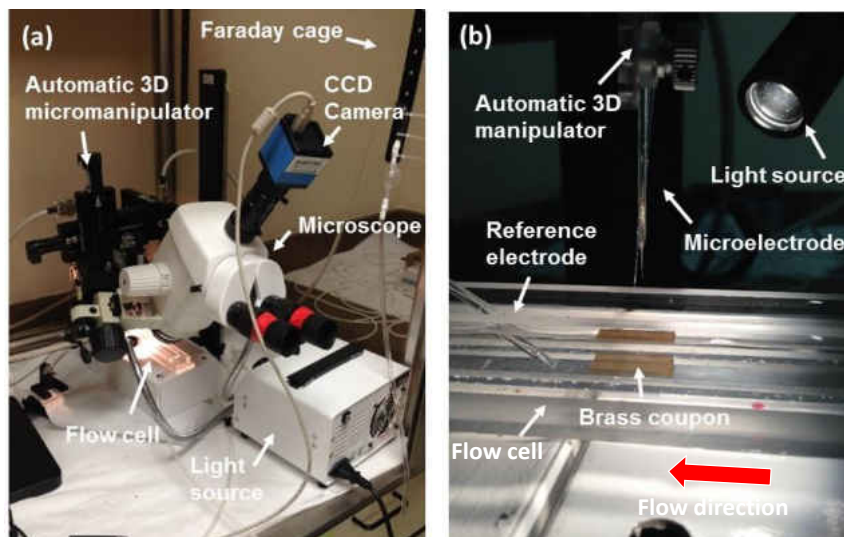


Figure 39. Experiment setups for microprofile system.

Microprofile experiments were conducted in a designated faraday cage in the lab as it displayed in figure 39. A flow cell was connected to a peristaltic pump (Masterflex, Cole-Parmer Instrument Company, Court Vernon Hills, IL) with artificial water flowing at controlled speed and a beaker for waste collection. Light source was used for microelectrodes positioning, and it was turned off during the profile/mapping experiment. The working and guide microelectrodes were controlled by automatic 3D manipulator during the experiment with connected Ag/AgCl reference electrode submerged in the tested water. The faraday cage was closed and properly grounded during the experiment.

APPENDIX B: A SAMPLE CODE FOR PYTHON FIGURES

```

#example code for pH distribution at pH 7, free chlorine 2 mg L-1

# -*- coding: utf-8 -*-

import scipy.interpolate

import matplotlib.pyplot as plt

import numpy as np

from matplotlib.ticker import MultipleLocator

import matplotlib

#pH 9 chlorine

font = {'family' : 'serif',

        'color'  : 'black',

        'weight' : 'bold',

        'size'   : '40',

        }

x = np. array([0, 1200, 2400, 3600, 4800, 6000, 7200, 8400, 0, 1200, 2400, 3600, 4800, 6000,
7200, 8400,0, 1200, 2400, 3600, 4800, 6000, 7200, 8400,
0, 1200, 2400, 3600, 4800, 6000, 7200, 8400,
0, 1200, 2400, 3600, 4800, 6000, 7200, 8400,
0, 1200, 2400, 3600, 4800, 6000, 7200, 8400,

```

0, 1200, 2400, 3600, 4800, 6000, 7200, 8400,

0, 1200, 2400, 3600, 4800, 6000, 7200, 8400,

0, 1200, 2400, 3600, 4800, 6000, 7200, 8400,

0, 1200, 2400, 3600, 4800, 6000, 7200, 8400,

0, 1200, 2400, 3600, 4800, 6000, 7200, 8400,

0, 1200, 2400, 3600, 4800, 6000, 7200, 8400,0, 1200, 2400, 3600, 4800, 6000, 7200, 8400,

0, 1200, 2400, 3600, 4800, 6000, 7200, 8400])

y = np. array([0, 0, 0, 0, 0, 0, 0, 0, 0,

1500, 1500, 1500, 1500, 1500, 1500, 1500, 1500,

3000, 3000, 3000, 3000, 3000, 3000, 3000, 3000,

4500, 4500, 4500, 4500, 4500, 4500, 4500, 4500,

6000, 6000, 6000, 6000, 6000, 6000, 6000, 6000,

7500, 7500, 7500, 7500, 7500, 7500, 7500, 7500,

9000, 9000, 9000, 9000, 9000, 9000, 9000, 9000,

10500, 10500, 10500, 10500, 10500, 10500, 10500, 10500,

12000, 12000, 12000, 12000, 12000, 12000, 12000, 12000,

13500, 13500, 13500, 13500, 13500, 13500, 13500, 13500,

15000, 15000, 15000, 15000, 15000, 15000, 15000, 15000,

```
16500, 16500, 16500, 16500, 16500, 16500, 16500, 16500,
```

```
18000, 18000, 18000, 18000, 18000, 18000, 18000, 18000,
```

```
20000, 20000, 20000, 20000, 20000, 20000, 20000, 20000
```

```
)
```

```
z = np. array([9.5, 9.6, 9.7, 9.3, 9.6, 9.4, 9.2, 9.0, 8.1, 7.7, 7.6, 8.2, 8.8, 9.0, 8.9, 8.8, 7.6, 7.1, 8.1,  
8.7, 8.4, 8.2, 8.3, 8.5, 9.1, 9.4, 9.4, 9.3, 9.2, 9.0, 8.9, 8.8, 8.1, 9.4, 9.3, 9.4, 9.2, 8.8, 8.1, 7.3, 6.1,  
6.0, 6.0, 6.5, 6.5, 6.6, 6.7, 6.7, 3.1, 4.7, 3.7, 5.6, 5.9, 5.4, 5.7, 5.8, 6.7, 8.2, 5.9, 7.9, 8.0, 7.6, 4.0,  
5.8, 9.5, 9.5, 9.4, 9.4, 9.4, 9.2, 9.1, 9.1, 9.6, 9.7, 9.8, 9.8, 9.7, 9.7, 9.5, 9.4, 9.7, 9.8, 9.8, 9.8, 9.7,  
9.7, 9.5, 9.4, 9.7, 9.7, 9.8, 9.8, 9.8, 9.6, 9.5, 9.4, 9.7, 9.8, 9.9, 9.8, 9.8, 9.7, 9.7, 9.6, 9.8, 9.9, 10.0,  
10.0, 10.0, 9.9, 9.9, 9.8])
```

```
# Set up a regular grid of interpolation points
```

```
xi, yi = np.linspace(x.min(), x.max(), 600), np.linspace(y.min(), y.max(), 600)
```

```
xi, yi = np.meshgrid(xi, yi)
```

```
xmajorLocator = MultipleLocator(2000)
```

```
ymajorLocator = MultipleLocator(2000)
```

```
# Interpolate
```

```
rbf = scipy.interpolate.Rbf(x, y, z)
```

```
zi = rbf(xi, yi)
```

```
print(zi)
```

```

plt.imshow(zi, vmin=7, vmax=10, origin='lower',

            #extent=[x.min(), x.max(), y.min(), y.max()])

plt.figure(figsize=(10,18))

ax = plt.subplot(1, 1, 1)

ax.xaxis.set_major_locator(xmajorLocator)

ax.yaxis.set_major_locator(ymajorLocator)

plt.xlim((0,8400))

plt.ylim((0,20000))

for label in (ax.get_xticklabels() + ax.get_yticklabels()):

    label.set_fontname('Arial')

    label.set_fontsize(24)

plt.scatter(x, y, c=z)

cmap = matplotlib.cm.jet

norm = matplotlib.colors.Normalize(vmin=3, vmax=10)

plt.pcolor(xi, yi, zi, cmap=cmap, norm=norm)

cb = plt.colorbar(ticks=[3, 4, 5, 6, 7, 8, 9, 10])

cb.set_label("pH", size=24)

cb.ax.tick_params(labelsize=24)

```

```
#cb.ax.set_xticklabels(['Low', 'Medium', 'High'])
```

```
#plt.show()
```

```
my_dpi=5000
```

```
plt.show()
```

REFERENCES

1. Kimbrough, D. E., Brass Corrosion as a Source of Lead and Copper in Traditional and All-plastic Distribution Systems. *Journal-American Water Works Association* **2007**, *99*, (8), 70-76.
2. American Water Works Association, *Water://Stat 2002 Distribution Survey*. AWWA: Denver, CO, 2004.
3. American Water Works Association, *Distribution System Inventory, Integrity and Water Quality*. 2007.
4. Kirmeyer, G. J.; Richards, W.; Dery Smith, C., *Assessment of water distribution systems and associated research needs, An.* AWWA: 1994.
5. Sarver, E.; Edwards, M., Effects of flow, brass location, tube materials and temperature on corrosion of brass plumbing devices. *Corrosion Science* **2011**, *53*, (5), 1813-1824.
6. Nicholas, D. M. F.; Water, M., *Dezincification of Brass in potable waters*. Urban Water Research Association of Australia: 1994.
7. Zhang, Y.; Edwards, M., Effects of pH, chloride, bicarbonate, and phosphate on brass dezincification. *Journal of American Water Works Association* **2011**, *103*, (4), 90-102.
8. Valcarce, M.; De Sanchez, S.; Vazquez, M., Brass dezincification in a tap water bacterial suspension. *Electrochimica Acta* **2006**, *51*, (18), 3736-3742.
9. Nguyen, C. K.; Stone, K. R.; Dudi, A.; Edwards, M. A., Corrosive microenvironments at lead solder surfaces arising from galvanic corrosion with copper pipe. *Environmental science & technology* **2010**, *44*, (18), 7076-7081.
10. Brown, M. J.; Raymond, J.; Homa, D.; Kennedy, C.; Sinks, T., Association between children's blood lead levels, lead service lines, and water disinfection, Washington, DC, 1998–2006. *Environmental Research* **2011**, *111*, (1), 67-74.
11. Organization, W. H., *Guidelines for drinking-water quality: recommendations*. World Health Organization: 2004; Vol. 1.
12. Edwards, M. M., RAPID: Synergistic Impacts of Corrosive Water and Interrupted Corrosion Control on Chemical/Microbiological Water Quality: Flint, MI. **2015**.
13. Ganim, S.; Tran, L., How tap water became toxic in Flint, Michigan. In CNN: 2016.
14. Gonzalez, S.; Lopez-Roldan, R.; Cortina, J.-L., Presence of metals in drinking water distribution networks due to pipe material leaching: a review. *Toxicological & Environmental Chemistry* **2013**, *95*, (6), 870-889.

15. Rosario-Ortiz, F.; Rose, J.; Speight, V.; Von Gunten, U.; Schnoor, J., How do you like your tap water? *Science* **2016**, *351*, (6276), 912-914.
16. Trueman, B. F.; Camara, E.; Gagnon, G. A., Evaluating the effects of full and partial lead service line replacement on lead levels in drinking water. *Environmental science & technology* **2016**, *50*, (14), 7389-7396.
17. Camara, E.; Montreuil, K. R.; Knowles, A. K.; Gagnon, G. A., Role of the water main in lead service line replacement: A utility case study. *Journal-American Water Works Association* **2013**, *105*, (8), E423-E431.
18. St. Clair, J.; Cartier, C.; Triantafyllidou, S.; Clark, B.; Edwards, M., Long-term behavior of simulated partial lead service line replacements. *Environmental engineering science* **2016**, *33*, (1), 53-64.
19. Schock, M. R.; Hyland, R. N.; Welch, M. M., Occurrence of contaminant accumulation in lead pipe scales from domestic drinking-water distribution systems. *Environmental science & technology* **2008**, *42*, (12), 4285-4291.
20. Yohai, L.; Vázquez, M.; Valcarce, M., Brass corrosion in tap water distribution systems inhibited by phosphate ions. *Corrosion Science* **2011**, *53*, (3), 1130-1136.
21. El-Sherif, R. M.; Ismail, K. M.; Badawy, W. A., Effect of Zn and Pb as alloying elements on the electrochemical behavior of brass in NaCl solutions. *Electrochimica Acta* **2004**, *49*, (28), 5139-5150.
22. Zhang, Y.; Edwards, M., Effects of pH, chloride, bicarbonate, and phosphate on brass dezincification. *Journal American Water Works Association* **2011**, *103*, 90-102.
23. Sarver, E. A. Insights into non-uniform copper and brass corrosion in potable water systems. 2010.
24. Simmonds, M.; Huxley, W., Dezincification of water supply fittings. *Australia Corrosion Engrg* **1967**, *11*, (11), 9.
25. Lytle, D. A.; Nadagouda, M. N., A comprehensive investigation of copper pitting corrosion in a drinking water distribution system. *Corrosion Science* **2010**, *52*, (6), 1927-1938.
26. Edwards, M.; Chock, M.; Travis, E., Alkalinity, pH and Copper. *Corrosion Byproduct Release* **1996**, 81-94.
27. Lagos, G. E.; Cuadrado, C. A.; Letelier, M. V., Aging of copper pipes by drinking water. *Journal (American Water Works Association)* **2001**, 94-103.
28. Craun, G. F.; Hubbs, S. A.; Frost, F.; Calderon, R. L.; Via, S. H., Waterborne outbreaks of cryptosporidiosis. *JOURNAL AWWA* **1998**, *90*, (9), 81-91.

29. Alfantazi, A.; Ahmed, T.; Tromans, D., Corrosion behavior of copper alloys in chloride media. *Materials & Design* **2009**, *30*, (7), 2425-2430.
30. Boulay, N.; Edwards, M., Role of temperature, chlorine, and organic matter in copper corrosion by-product release in soft water. *Water research* **2001**, *35*, (3), 683-690.
31. Xiao, W.; Hong, S.; Tang, Z.; Seal, S.; Taylor, J. S., Effects of blending on surface characteristics of copper corrosion products in drinking water distribution systems. *Corrosion science* **2007**, *49*, (2), 449-468.
32. Parks, J. L.; Kashyap, A.; Atassi, A.; Schneider, O.; Edwards, M., Effect of zinc and orthophosphate corrosion inhibitors on cement-based pipes. *American Water Works Association Journal* **2012**, *104*, (1), 37.
33. AWWA, Internal corrosion control in water distribution systems. *Manual of Water Supply Practices–M58* **2011**.
34. Trussell, R. R.; Morgan, J. J. In *A saturation index for cement surfaces exposed to water*, 2006 Water Quality Technology Conference and Exposition Proceedings, 2006; 2006.
35. Verbeck, G. J., Mechanisms of corrosion of steel in concrete. *ACI Special Publication* **1975**, *49*.
36. Chen, D.; Mahadevan, S., Chloride-induced reinforcement corrosion and concrete cracking simulation. *Cement and Concrete Composites* **2008**, *30*, (3), 227-238.
37. Huet, B.; L'hostis, V.; Santarini, G.; Feron, D.; Idrissi, H., Steel corrosion in concrete: Determinist modeling of cathodic reaction as a function of water saturation degree. *Corrosion science* **2007**, *49*, (4), 1918-1932.
38. Ngueta, G.; Abdous, B.; Tardif, R.; St-Laurent, J.; Levallois, P., Use of a cumulative exposure index to estimate the impact of tap water lead concentration on blood lead levels in 1-to 5-year-old children (Montréal, Canada). *Environmental health perspectives* **2016**, *124*, (3), 388.
39. Edwards, M.; Triantafyllidou, S.; Best, D., Elevated blood lead in young children due to lead-contaminated drinking water: Washington, DC, 2001– 2004. *Environmental science & technology* **2009**, *43*, (5), 1618-1623.
40. Hanna-Attisha, M.; LaChance, J.; Sadler, R. C.; Champney Schnepf, A., Elevated blood lead levels in children associated with the Flint drinking water crisis: a spatial analysis of risk and public health response. *American journal of public health* **2016**, *106*, (2), 283-290.
41. EPA EPA's Safe Drinking Water Information System Federal Reporting Services.
42. Triantafyllidou, S.; Edwards, M., Galvanic corrosion after simulated small-scale partial lead service line replacements. *Journal of American Water Works Association* **2011**, *103*, (9), 85-99.

43. Nguyen, C.; Stone, K.; Clark, B.; Edwards, M.; Gagnon, G.; Knowles, A., Impact of chloride: sulfate mass ratio (CSMR) changes on lead leaching in potable water. *Water Research Foundation, Denver, CO* **2010**.
44. DeSantis, M.; Welch, M.; Schock, M. In *Mineralogical evidence of galvanic corrosion in domestic drinking water pipes*, American Water Works Association Water Quality Technology Conference, Denver, CO, 2009; Denver, CO, 2009.
45. Wang, Y.; Mehta, V.; Welter, G. J.; Giammar, D. E., Effect of connection methods on lead release from galvanic corrosion. *Journal of American Water Works Association* **2013**, *105*, (7), E337-E351.
46. Wang, Z.; Lee, J. H.; Lu, Y., Label-free colorimetric detection of lead ions with a nanomolar detection limit and tunable dynamic range by using gold nanoparticles and DNAzyme. *Advanced Materials* **2008**, *20*, (17), 3263-3267.
47. Li, J.; Lu, Y., A highly sensitive and selective catalytic DNA biosensor for lead ions. *Journal of the American Chemical Society* **2000**, *122*, (42), 10466-10467.
48. Arduini, F.; Calvo, J. Q.; Palleschi, G.; Moscone, D.; Amine, A., Bismuth-modified electrodes for lead detection. *TrAC Trends in Analytical Chemistry* **2010**, *29*, (11), 1295-1304.
49. Wei, Y.; Yang, R.; Zhang, Y.-X.; Wang, L.; Liu, J.-H.; Huang, X.-J., High adsorptive γ -AlOOH (boehmite)@ SiO₂/Fe₃O₄ porous magnetic microspheres for detection of toxic metal ions in drinking water. *Chemical Communications* **2011**, *47*, (39), 11062-11064.
50. Naseri, M. T.; Hemmatkhah, P.; Hosseini, M. R. M.; Assadi, Y., Combination of dispersive liquid-liquid microextraction with flame atomic absorption spectrometry using microsample introduction for determination of lead in water samples. *Analytica Chimica Acta* **2008**, *610*, (1), 135-141.
51. Abbaspour, A.; Mirahmadi, E.; Khalafi-Nejad, A.; Babamohammadi, S., A highly selective and sensitive disposable carbon composite PVC-based membrane for determination of lead ion in environmental samples. *Journal of hazardous materials* **2010**, *174*, (1), 656-661.
52. Mathew, S.; Rajith, L.; Lonappan, L. A.; Jos, T.; Kumar, K. G., A lead (II) selective PVC membrane potentiometric sensor based on a tetraazamacrocyclic ligand. *Journal of Inclusion Phenomena and Macrocyclic Chemistry* **2014**, *78*, (1-4), 171-177.
53. Benjamin, M. M.; Reiber, S. H.; Ferguson, J. F.; Vanderwerff, E., Chemistry of corrosion inhibitors in potable water. *AWWA Rep* **1990**, 127.
54. EPA, Optimal Corrosion Control Treatment Evaluation Technical Recommendations for Primacy Agencies and Public Water System. **2016**.
55. Xie, Y.; Giammar, D. E., Effects of flow and water chemistry on lead release rates from pipe scales. *Water research* **2011**, *45*, (19), 6525-6534.

56. Edwards, M.; Dudi, A., Role of chlorine and chloramine in corrosion of lead-bearing plumbing materials. *Journal (American Water Works Association)* **2004**, *96*, (10), 69-81.
57. Guo, Q.; Toomuluri, P. J.; Eckert Jr, J. O., Leachability. **1998**.
58. Berend, K.; Trouwborst, T., Cement–mortar pipes. **1999**.
59. Sarver, E.; Dodson, K.; Scardina, R. P.; Lattyak-Slabaugh, R.; Edwards, M.; Nguyen, C., Copper pitting in chlorinated, high-pH potable water. *Journal of the American Water Works Association* **2011**, *103*, (3), 86-98.
60. Sarver, E.; Zhang, Y.; Edwards, M., Review of brass dezincification corrosion in potable water systems. *Corrosion Reviews* **2010**, *28*, (3-4), 155-196.
61. Welker, C., Microelectrode delineation of fine grain somatotopic organization of Sml cerebral neocortex in albino rat. *Brain research* **1971**, *26*, (2), 259-275.
62. Ammann, D.; Lanter, F.; Steiner, R. A.; Schulthess, P.; Shijo, Y.; Simon, W., Neutral carrier based hydrogen ion selective microelectrode for extra-and intracellular studies. *Analytical Chemistry* **1981**, *53*, (14), 2267-2269.
63. Silver, I.; Murrills, R.; Etherington, D., Microelectrode studies on the acid microenvironment beneath adherent macrophages and osteoclasts. *Experimental cell research* **1988**, *175*, (2), 266-276.
64. Lee, W.; de Beer, D., Oxygen and pH microprofiles above corroding mild steel covered with a biofilm. *Biofouling* **1995**, *8*, (4), 273-280.
65. Lee, W.; Lewandowski, Z.; Okabe, S.; Characklis, W. G.; Avci, R., Corrosion of mild steel underneath aerobic biofilms containing sulfate-reducing bacteria part I: At low dissolved oxygen concentration. *Biofouling* **1993**, *7*, (3), 197-216.
66. Lee, W.; Characklis, W., Corrosion of mild steel under anaerobic biofilm. *Corrosion* **1993**, *49*, (3), 186-199.
67. ASTM Standard G31-72, Standard Practice for Laboratory Immersion Corrosion Testing of Metals, ASTM International, West Conshohocken, PA, . **1983**.
68. ASTM Method 2688-83 Method B, Coupon Test, ASTM International, West Conshohocken, PA. In American Society for Testing and Materials (ASTM), 1983.
69. Manual, E. G., Alternative disinfectants and oxidants. *Disinfectant Use in Water Treatment, Washington, DC* **1999**.
70. De Beer, D.; Srinivasan, R.; Stewart, P. S., Direct measurement of chlorine penetration into biofilms during disinfection. *Applied and Environmental Microbiology* **1994**, *60*, (12), 4339-4344.

71. Lee, W. H.; Wahman, D. G.; Pressman, J. G., Monochloramine-sensitive amperometric microelectrode: optimization of gold, platinum, and carbon fiber sensing materials for removal of dissolved oxygen interference. *Ionics* **2015**, 1-12.
72. Lee, W. H.; Wahman, D. G.; Lytle, D. A.; Pressman, J. G. In *Evaluating In-Situ Reactions of Chlorine and Chloramines at the Surface of Copper and Iron Pipe Materials using Microelectrodes*, Water Quality Technology Conference and Exhibition, Louisiana, LA, November 16-20, 2014; American Water Work Association: Louisiana, LA, 2014.
73. Murray-Ramos, N. A. Examining aspects of copper and brass corrosion in drinking water, Doctoral dissertation. Virginia Polytechnic Institute and State University, 2006.
74. Zhang, X.; Pehkonen, S. O.; Kocherginsky, N.; Ellis, G. A., Copper corrosion in mildly alkaline water with the disinfectant monochloramine. *Corrosion Science* **2002**, *44*, (11), 2507-2528.
75. Glass, G.; Buenfeld, N., The presentation of the chloride threshold level for corrosion of steel in concrete. *Corrosion Science* **1997**, *39*, (5), 1001-1013.
76. Renner, R., Exposure on tap: drinking water as an overlooked source of lead. *Environ Health Perspect* **2010**, *118*, A68-A74.
77. U.S.EPA, Maximum contaminant level goals and national primary drinking water regulations for lead and copper. Final rule. *Federal Register* **1991**, *56*, p. 26460.
78. Arnold Jr, R. B.; Edwards, M., Potential reversal and the effects of flow pattern on galvanic corrosion of lead. *Environmental science & technology* **2012**, *46*, (20), 10941-10947.
79. Yohai, L.; Vázquez, M.; Valcarce, M. B., Brass corrosion in tap water distribution systems inhibited by phosphate ions. *Corrosion Science* **2011**, *53*, (3), 1130-1136.
80. Wang, Y.; Jing, H.; Mehta, V.; Welter, G. J.; Giammar, D. E., Impact of galvanic corrosion on lead release from aged lead service lines. *Water Research* **2012**, *46*, (16), 5049-5060.
81. Fike, D. A.; Gammon, C. L.; Ziebis, W.; Orphan, V. J., Micron-scale mapping of sulfur cycling across the oxycline of a cyanobacterial mat: a paired nanoSIMS and CARD-FISH approach. *The ISME journal* **2008**, *2*, (7), 749-759.
82. Elberling, B.; Knudsen, K. L.; Kristensen, P. H.; Asmund, G., Applying foraminiferal stratigraphy as a biomarker for heavy metal contamination and mining impact in a fiord in West Greenland. *Marine Environmental Research* **2003**, *55*, (3), 235-256.
83. Hurd, C. L.; Cornwall, C. E.; Currie, K.; Hepburn, C. D.; McGraw, C. M.; Hunter, K. A.; Boyd, P. W., Metabolically induced pH fluctuations by some coastal calcifiers exceed projected 22nd century ocean acidification: a mechanism for differential susceptibility? *Global Change Biology* **2011**, *17*, (10), 3254-3262.

84. Lee, W. H.; Wahman, D. G.; Bishop, P. L.; Pressman, J. G., Free chlorine and monochloramine application to nitrifying biofilm: comparison of biofilm penetration, activity, and viability. *Environmental Science and Technology* **2011**, *45*, 1412-1419.
85. Pressman, J. G.; Lee, W. H.; Bishop, P. L.; Wahman, D. G., Effect of free ammonia concentration on monochloramine penetration within a nitrifying biofilm and its effect on activity, viability, and recovery. *Water Research* **2012**, *46*, 882-894.
86. Oliphant, R., Summary Report on the Contamination of Potable Water by Lead From Soldered Joints. *Water Research Centre* **1983**.
87. Gregory, R., Galvanic corrosion of lead solder in copper pipework. *Water and Environment Journal* **1990**, *4*, (2), 112-118.
88. Nguyen, C. K.; Stone, K. R.; Edwards, M. A., Chloride-to-sulfate mass ratio: Practical studies in galvanic corrosion of lead solder. *Journal of American Water Works Association* **2011**, *103*, (1), 81.
89. Cartier, C.; Arnold, R. B.; Triantafyllidou, S.; Prevost, M.; Edwards, M., Effect of flow rate and lead/copper pipe sequence on lead release from service lines. *Water Research* **2012**, *46*, (13), 4142-4152.
90. *HDR Engineering Inc., An Analysis of the Correlation Between Lead Released from Galvanized Iron Piping and the Contents of Lead in Drinking Water*. Washington, USA, 2009.
91. Dudi, A. Reconsidering lead corrosion in drinking water: product testing, direct chloramine attack and galvanic corrosion, Doctoral dissertation. 2004.
92. Britton, A.; Richards, W., Factors influencing plumbsolvency in Scotland. *Journal of the Institution of Water Engineers and Scientists* **1981**, *35*, 349-64.
93. Edwards, M.; Dudi, A., Role of chlorine and chloramine in corrosion of lead-bearing plumbing materials. *Journal (American Water Works Association)* **2004**, 69-81.
94. Ma, X.; Lee, W. H.; Lytle, D. A., In situ 2D maps of pH shifts across brass–lead galvanic joints using microelectrodes. *Measurement Science and Technology* **2016**, *28*, (2), 025101.
95. Tam, Y.; Elefsiniotis, P., Corrosion control in water supply systems: effect of pH, alkalinity, and orthophosphate on lead and copper leaching from brass plumbing. *Journal of Environmental Science and Health Part A* **2009**, *44*, (12), 1251-1260.
96. Vaccari, D. A., How Not to Get the Lead Out—Lead Service Line Replacement Will Not Solve Our Drinking Water Crisis. *Current Pollution Reports* **2016**, 1-3.
97. EPA, Prohibition on Use of Lead Pipes, Solder, and Flux. *Safe Drinking Water Act* **2015**, Section 1417.

98. Rabin, R., The lead industry and lead water pipes “A modest campaign”. *American journal of public health* **2008**, *98*, (9), 1584-1592.
99. Triantafyllidou, S.; Nguyen, C.; Edwards, M., Contribution of galvanic corrosion to lead (Pb) in water after partial lead service line replacements. *Proc. 2009 AWWA WQTC, Seattle* **2009**.
100. Triantafyllidou, S.; Edwards, M., Galvanic corrosion after simulated small-scale partial lead service line replacements. *American Water Works Association. Journal* **2011**, *103*, (9), 85.
101. Wang, Y.; Mehta, V.; Welter, G. J.; Giammar, D. E., Effect of connection methods on lead release from galvanic corrosion (PDF). *Journal-American Water Works Association* **2013**, *105*, (7), E337-E351.
102. Atlas, D.; Coombs, J.; Zajicek, O., The corrosion of copper by chlorinated drinking waters. *Water Research* **1982**, *16*, (5), 693-698.
103. Kuhn, A.; Chan, C., pH changes at near-electrode surfaces. *Journal of Applied Electrochemistry* **1983**, *13*, (2), 189-207.
104. Tada, E.; Sugawara, K.; Kaneko, H., Distribution of pH during galvanic corrosion of a Zn/steel couple. *Electrochimica acta* **2004**, *49*, (7), 1019-1026.
105. Lee, W. H.; Wahman, D. G.; Bishop, P. L.; Pressman, J. G., Free chlorine and monochloramine application to nitrifying biofilm: comparison of biofilm penetration, activity, and viability. *Environmental science & technology* **2011**, *45*, (4), 1412-1419.
106. Church, J., Park, Y.J., Lee, W.H., Wahman, D. G, and Pressman, J. G. In *In-situ Spatial Chemical Reactions of Copper Pitting Corrosion in a Household Plumbing System*, American Water Work Association, Water Quality Technology Conference and Exhibition, Salt lake City, Utah, 2015; Salt lake City, Utah, 2015.
107. Hu, J.; Gan, F.; Triantafyllidou, S.; Nguyen, C.; Edwards, M., Copper-induced metal release from lead pipe into drinking water. *Corrosion* **2012**, *68*, (11), 1037-1048.
108. Clark, B.; St Clair, J.; Edwards, M., Copper Deposition Corrosion Elevates Lead Release to Potable Water (PDF). *Journal-American Water Works Association* **2015**, *107*, (11), E627-E637.
109. Katsounaros, I.; Dortsiou, M.; Polatides, C.; Preston, S.; Kypraios, T.; Kyriacou, G., Reaction pathways in the electrochemical reduction of nitrate on tin. *Electrochimica Acta* **2012**, *71*, 270-276.
110. Arnold Jr, R. B. New insights into lead and copper corrosion: Impacts of galvanic corrosion, flow pattern, potential reversal, and natural organic matter. Virginia Polytechnic Institute and State University, 2011.

111. Richards, W.; Britton, A.; Cochrane, A., Reducing Plumbosolvency- The Effect of Added Lime on the Loch Katrine Supply to Glasgow. *Journal of the Institution of Water Engineers and Scientists* **1980**, *34*, (4).
112. Vaccari, D. A., How Not to Get the Lead Out—Lead Service Line Replacement Will Not Solve Our Drinking Water Crisis. *Current Pollution Reports* **2016**, *2*, (3), 200-202.
113. Calabrese, E. J., *Safe Drinking Water Act*. CRC Press: 1989.
114. EPA, U., 40 CFR Part 141 Subpart I Control of Lead and Copper. *National Primary Drinking Water Regulations* **2012**.
115. Lai, C.-Z.; Joyer, M. M.; Fierke, M. A.; Petkovich, N. D.; Stein, A.; Bühlmann, P., Subnanomolar detection limit application of ion-selective electrodes with three-dimensionally ordered macroporous (3DOM) carbon solid contacts. *Journal of Solid State Electrochemistry* **2009**, *13*, (1), 123.
116. Dimeski, G.; Badrick, T.; St John, A., Ion selective electrodes (ISEs) and interferences—a review. *Clinica Chimica Acta* **2010**, *411*, (5), 309-317.
117. Nery, E. W.; Kubota, L. T., Integrated, paper-based potentiometric electronic tongue for the analysis of beer and wine. *Analytica chimica acta* **2016**, *918*, 60-68.
118. Fucskó, J.; Tóth, K.; Pungor, E.; Kunovits, J.; Puxbaum, H., Application of ion-selective electrodes in environmental analysis: determination of acid and fluoride concentrations in rain-water with a flow-injection system. *Analytica chimica acta* **1987**, *194*, 163-170.
119. Light, T. S., Industrial use and applications of ion selective electrodes. *J. Chem. Educ* **1997**, *74*, (2), 171.
120. Mensah, S. T.; Gonzalez, Y.; Calvo-Marzal, P.; Chumbimuni-Torres, K. Y., Nanomolar detection limits of Cd²⁺, Ag⁺, and K⁺ using paper-strip ion-selective electrodes. *Analytical chemistry* **2014**, *86*, (15), 7269-7273.
121. Ceresa, A.; Bakker, E.; Hattendorf, B.; Günther, D.; Pretsch, E., Potentiometric polymeric membrane electrodes for measurement of environmental samples at trace levels: New requirements for selectivities and measuring protocols, and comparison with ICPMS. *Analytical chemistry* **2001**, *73*, (2), 343-351.
122. Bakker, E.; Bühlmann, P.; Pretsch, E., Carrier-Based Ion-Selective Electrodes and Bulk Optodes. 1. General Characteristics. *Chemical Reviews* **1997**, *97*, (8), 3083-3132.
123. Rouhollahi, A.; Ganjali, M. R.; Shamsipur, M., Lead ion selective PVC membrane electrode based on 5, 5'-dithiobis-(2-nitrobenzoic acid). *Talanta* **1998**, *46*, (6), 1341-1346.

124. Rahmani, A.; Barzegar, M.; Shamsipur, M.; Sharghi, H.; Mousavi, M., New potentiometric membrane sensors responsive to Pb (II) based on some recently synthesized 9, 10-anthraquinone derivatives. **2000**.
125. Mathew, S.; Rajith, L.; Lonappan, L. A.; Jos, T.; Kumar, K. G., A lead (II) selective PVC membrane potentiometric sensor based on a tetraazamacrocyclic ligand. *Journal of Inclusion Phenomena and Macrocyclic Chemistry* **2014**, *1*, (78), 171-177.
126. Malinowska, E.; Brzózka, Z.; Kasiura, K.; Egberink, R. J.; Reinhoudt, D. N., Lead selective electrodes based on thioamide functionalized calix [4] arenes as ionophores. *Analytica chimica acta* **1994**, *298*, (2), 253-258.
127. McGraw, C. M.; Radu, T.; Radu, A.; Diamond, D., Evaluation of Liquid-and Solid-Contact, Pb²⁺-Selective Polymer-Membrane Electrodes for Soil Analysis. *Electroanalysis* **2008**, *20*, (3), 340-346.
128. Bradshaw, M. H.; Powell, G. M., Sodium in drinking water. **1994**.
129. Triantafyllidou, S.; Schock, M. R.; DeSantis, M. K.; White, C., Low contribution of PbO₂-coated lead service lines to water lead contamination at the tap. *Environmental science & technology* **2015**, *49*, (6), 3746-3754.
130. Hedoux, A.; Le Bellac, D.; Guinet, Y.; Kiat, J.; Noiret, I.; Garnier, P., Raman spectroscopy and X-ray diffraction studies on PbO and (PbO) 1-x (TiO₂) x. *Journal of Physics: Condensed Matter* **1995**, *7*, (45), 8547.
131. Burgio, L.; Clark, R. J.; Firth, S., Raman spectroscopy as a means for the identification of plattnerite (PbO₂), of lead pigments and of their degradation products. *Analyst* **2001**, *126*, (2), 222-227.
132. Socrates, G., *Infrared and Raman characteristic group frequencies: tables and charts*. John Wiley & Sons: 2004.
133. Lee, W. H.; Lee, J. H.; Choi, W. H.; Hosni, A. A.; Papautsky, I.; Bishop, P. L., Needle-type environmental microsensors: design, construction and uses of microelectrodes and multi-analyte MEMS sensor arrays. *Measurement Science and Technology* **2011**, *22*, 042001.
134. Lee, W. H.; Seo, Y.; Bishop, P. L., Characteristics of a cobalt-based phosphate microelectrode for in situ monitoring of phosphate and its biological application. *Sensors and Actuators B: Chemical* **2009**, *137*, (1), 121-128.
135. Okabe, S.; Satoh, H.; Watanabe, Y., In situ analysis of nitrifying biofilms as determined by in situ hybridization and the use of microelectrodes. *Applied and Environmental Microbiology* **1999**, *65*, (7), 3182-3191.

136. Sato, H.; Yui, M.; Yoshikawa, H., Ionic Diffusion Coefficients of Cs⁺, Pb²⁺, Sm³⁺, Ni²⁺, SeO₄²⁻ and TcO₄⁻ in Free Water Determined from Conductivity Measurements. *Journal of Nuclear Science and Technology* **1996**, 33, (12), 950-955.